DEVELOPMENT OF A REGRESSION MODEL FOR THE FATIGUE LIFE ASSESSMENT OF OPEN-HOLE SPECIMENS WITH DOUBLE THROUGH THE THICKNESS CRACKS

A THESIS SUBMITTED TO
THE GRADUATE SCHOOL OF NATURAL AND APPLIED SCIENCES
OF
MIDDLE EAST TECHNICAL UNIVERSITY

BY

SEYED SOHRAB HEIDARI SHABESTARI

IN PARTIAL FULFILLMENT OF THE REQUIREMENTS
FOR
THE DEGREE OF MASTER OF SCIENCE
IN
AEROSPACE ENGINEERING

JULY 2019

Approval of the thesis:

DEVELOPMENT OF A REGRESSION MODEL FOR THE FATIGUE LIFE ASSESSMENT OF OPEN-HOLE SPECIMENS WITH DOUBLE THROUGH THE THICKNESS CRACKS

submitted by **SEYED SOHRAB HEIDARI SHABESTARI** in partial fulfillment of the requirements for the degree of **Master of Science in Aerospace Engineering Department, Middle East Technical University** by,

Prof. Dr. Halil Kalıpçılar

Dean, Graduate School of **Natural and Applied Sciences** _____

Prof. Dr. İsmail. H. Tüncer

Head of Department, **Aerospace Engineering** _____

Prof. Dr. Altan Kayran

Supervisor, **Aerospace Engineering, METU** _____

Examining Committee Members:

Prof. Dr. Demirkan Çöker

Aerospace Engineering, METU _____

Prof. Dr. Altan Kayran

Aerospace Engineering, METU _____

Assoc. Prof. Dr. Ercan Gürses

Aerospace Engineering, METU _____

Assist. Prof. Dr. Tuncay Yalçınkaya

Aerospace Engineering, METU _____

Prof. Dr. Levend Kemal Parnas

Mechanical Engineering, TED University _____

Date: 16.07.2019

I hereby declare that all information in this document has been obtained and presented in accordance with academic rules and ethical conduct. I also declare that, as required by these rules and conduct, I have fully cited and referenced all material and results that are not original to this work.

Name, Surname: Seyed Sohrab Heidari Shabestari

Signature:

ABSTRACT

DEVELOPMENT OF A REGRESSION MODEL FOR THE FATIGUE LIFE ASSESSMENT OF OPEN-HOLE SPECIMENS WITH DOUBLE THROUGH THE THICKNESS CRACKS

Heidari Shabestari, Seyed Sohrab
Master of Science, Aerospace Engineering
Supervisor: Prof. Dr. Altan Kayran

July 2019, 126 pages

This thesis mainly deals with the investigation of the fatigue crack growth characteristics of open rivet holes in aluminum 2024-T3 material. In this respect, most commonly observed type of cracks emanating from rivet holes, namely, double through the thickness edge cracks with centered configurations has been considered. Stress intensity factors and the fatigue lifes are calculated analytically and also with the Extended Finite Element Method (XFEM).Analytical calculations have been carried out using the conformal mapping technique whereas the extended finite element simulation for crack growth and determination of stress intensity factors are performed using a developed code for the desired cracks of interest in Ansys Parametric Design Language APDL. The objective of the analytical part of the study is to verify the calculated stress intensity factors using XFEM method. Nevertheless, XFEM results are also compared with results of AFGROW which is a Damage Tolerance Analysis (DTA) framework that allows users to analyze crack initiation, fatigue crack growth and fracture to predict the life of metallic structures. The effect of geometry in terms of initial crack length (c) and also radius (r) of the open rivet hole and the applied stress on the stress intensity factor and the fatigue life under constant amplitude loading has been studied.

Finally, the statistical analysis is carried out using the Response Surface of experiments and Analysis of Variance (ANOVA) to investigate the effects of the parameters to fatigue life and a regression model to predict the fatigue life of open-hole specimens with double through the thickness cracks is developed.

Keywords: Stress Intensity Factor, Fatigue Life, XFEM Method, Crack Growth, Double Through the Thickness Crack, Response Surface, Regression Model

ÖZ

KALINLIK BOYUNCA ÇIFT ÇATLAKLI DELIKLI NUMUNELERIN YORULMA ÖMRÜNÜN DEĞERLENDIRMESI IÇIN BIR REGRESYON MODELININ GELIŞTIRILMESI

Heidari Shabestari, Seyed Sohrab
Yüksek Lisans, Havacılık ve Uzay Mühendisliği
Tez Danışmanı: Prof. Dr. Altan Kayran

Temmuz 2019, 126 sayfa

Bu tez ana olarak perçin delikli aluminyum 2024-T3 malzemesinin yorulma kaynaklı çatlak uzamasının incelenmesi ile ilgilidir. Bu itibarla bu çalışmada, merkezi perçin delik kenarlarında oluşan ve yaygın olarak görülen çatlak tipi olan kalınlık boyunca çift çatlak konfigürasyonu ele alınmıştır. Gerilme şiddeti faktörleri ve yorulma ömürleri analitik olarak ve genişletilmiş sonlu elemanlar yöntemi (XFEM) ile hesaplanmıştır. Analitik hesaplamalar konform dönüşüm tekniği ile, çatlak uzamasının ve gerilim şiddet faktörlerinin genişletilmiş sonlu elemanlar yöntemi ile belirlenmesi ise istenen çatlak tipleri için Ansys Parametrik Tasarım Dili (APDL) kullanılarak geliştirilmiş olan bir kod ile gerçekleştirilmiştir. Çalışmanın analitik kısmının amacı XFEM yöntemi ile hesaplanmış olan gerilim şiddeti faktörlerinin doğrulanmasıdır. Bununla birlikte XFEM sonuçları kullanıcıların çatlak oluşum, yorulmaya dayalı çatlak büyümesi ve kırılma analizlerinin yapmasını sağlayan ve metalik yapıların ömrünü tahmin eden Hasar Tolerans Analiz (DTA) yazılımı olan AFGROW sonuçları ile de kıyaslanmıştır. Geometrik açıdan ilk çatlak uzunluğu (c), perçin delik çapı (r) ve uygulanan gerilmenin gerilim şiddet faktörü ve sabit büyüklükteki yük altında yorulma ömrü üzerindeki etkileri çalışılmıştır.

En sonunda, Yanıt Yüzeyi deneylerini kullanarak istatiksel analiz yapılmış ve Varyans Analiz (ANOVA) yöntemi ile parametrelerin yorulma ömrüne olan etkileri incelenmiş ve kalınlık boyunca çift çatlaklı delikli numunelerin yorulma ömrünün tahmin eden bir regresyon modeli geliştirilmiştir.

Anahtar Kelimeler: Gerilme şiddet faktörü, Yorulma ömrü, XFEM metodu, Çatlak büyümesi, Kalınlık

I would like to dedicate my thesis to my beloved family; my parents, sister and my wonderful wife.

ACKNOWLEDGEMENTS

Foremost, I would like to express my sincere gratitude to my advisor Prof. Altan Kayran for the continuous support of my Masters study, for his patience, motivation, enthusiasm, and immense knowledge. His guidance helped me in all the time of research and writing of this thesis. I could not have imagined having a better advisor and mentor for my Masters study.

I would like to thank my parents, whose love and guidance are with me in whatever I pursue. Most importantly, I wish to thank my loving and supportive wife, Asal, who provide unending inspiration.

TABLE OF CONTENTS

LIST OF TABLES

TABLES

LIST OF FIGURES

FIGURES

CHAPTER 1

INTRODUCTION

1.1. Motivation of the Study

Modern aircraft structures are designed using the damage tolerance design philosophy. This design philosophy envisions sufficient strength and structural integrity of the aircraft to sustain major damage and to avoid catastrophic failure. However, structural aging of the aircraft may significantly reduce the strength below an acceptable level. This raises many important safety issues. The most likely places for crack initiation and development are the rivet holes due to the high-stress concentration in this area. Such cracks may grow in time, leading to a loss of strength and the reduction of the lifetime of the structure. If the structure is subjected to different loading, the crack behavior must be assessed in order to avoid catastrophic failures. For this, the knowledge of the crack size, service stress, material properties, and Stress Intensity Factor (SIF) are required.

The aircraft fuselage structure is a good example of a structure that is based largely on a slow crack growth rate design. The United States Air Force reviewed a great number of malfunction reports from a variety of aircraft. The reports showed that the preponderance of structural failures occurred from

1. Built-in preload stresses,

2. Material flaws and

3. Flaw caused by in-service usage.

These facts led to a design approach that required the damage tolerance analysis to assume a material flaw exists in the worst orientation and at the most undesirable location. The analysis helps to ensure that structures are designed that will support

slow stable crack growth until the crack reaches a length during which it can reliably be detected using non-destructive tests as part of maintenance programs. The reason for desiring the slow crack growth is that, as the crack moves slower, the flight cycles between inspection intervals which are determined considering the crack growth rate is allowed to be longer. The best design is the design for which the inspection intervals are the longest, and the crack moves the slowest. Longer inspection intervals will reduce the maintenance cost and the risk of failure significantly. One of the early catastrophic crashes due to fatigue failure of an airplane fuselage goes back to late ’80s (Figure 1.1). ALOHA airlines suffered from multiple site fatigue cracking of the skin adjacent to rivet holes [1].

Figure 1.1. The Aloha Airways Boeing 737 which lost part of its top skin over Hawaii in 1988 showing convergent tears in the fuselage skin below floor level [1].

According to the Federal Aviation Administration (FAA) maintenance technician handbook, common rivet holes in aviation purposes range from 3/32-inch to 3/8-inch in diameter and rivets smaller than 3/32-inch in diameter are never used on any structural part that carry stress [2]. Stress intensity factor is a powerful and important tool used in linear elastic fracture mechanics. Stress intensity factor can be used for

life prediction, but in the case of complex geometries and complex loading, determination of stress intensity factor is very difficult by analytical methods, therefore the only way to determine the SIFs is by using computational methods. This thesis is mainly dedicated to developing reliable methodologies for determining stress intensity factors and fatigue life assessment for cracked panels emanating from rivet holes using the XFEM method and developing a regression model for fast estimation of fatigue life.

1.2. Background and Literature Survey

Fracture mechanics and fatigue crack growth analysis of flawed components, which are used in aerospace structures, oil industries, civil engineering structures etc. are subjects that have been studied vastly in the literature over the decades. In this part, some of the backbone studies in the realm of fracture mechanics are highlighted to give an insight into the background of the subject.

Fracture mechanics theory commenced with A. A. Griffith (1893-1963) at the Royal Aircraft Establishment (RAE) in the United Kingdom with cooperation of the mathematical work of Professor C. E. Inglis [3][4], but the principal development formed in the United States at the Naval Research Laboratory (NRL) in 1950 by George R. Irwin [5]. Griffith's theory is applicable to brittle materials. For brittle materials, under normal rates of loading (monotonically increasing tensile loads) and at the room temperature, materials do not show plastic deformation behavior before fracture under a tensile load. As stated in the study "The Phenomenon of Rupture and Flow in Solids" by Griffith [6], in Griffith theory it is assumed that material contains crack-like defects and that work must be performed on the material to provide the energy necessary to propagate the crack by creating two new crack surfaces. For brittle materials (such as high-strength steels), the Griffith theory predicts the right relationship between the fracture strength, σ_F and the critical flaw size, c. However, this theory is not effective for determining the fracture strength of the ductile material, because cracked structural metals undergo considerable plastic

deformations at the crack tip before fracture. Three decades after Griffith's theory, Irwin and Orowan [7][8] declared that for a ductile material to fracture, the stored strain energy is consumed for both the formation of the two new cracked surfaces and the work done in plastic deformation.

One of the earliest and most famous relations between the crack growth rate *(da/ dN)* and the fatigue life was given by Paris, Gomez, and Anderson [9][10]. The Paris "law", which is an empirical relation obtained through experimental laboratory tests, was later modified to account for other fracture parameters, such as the maximum to minimum load ratio (stress ratio (R)), threshold and critical stress intensity factors, retardation effect due to the plastic zone. Over the years, many studies have been carried out to formulate the analytical solution for different fracture problems, among them Bowie was the first to find an analytical solution for cracks emanating from the hole (Figure 1.2) by employing the technique of conformal mapping [11][12]. Bowie presented the stress intensity factor(K) solution for radial through the thickness cracks emanating from unloaded open holes [11]. The stress intensity factor is given as:

$$K = \sigma\sqrt{\pi a} \cdot f_b(\frac{a}{D}) \qquad (1.2.1)$$

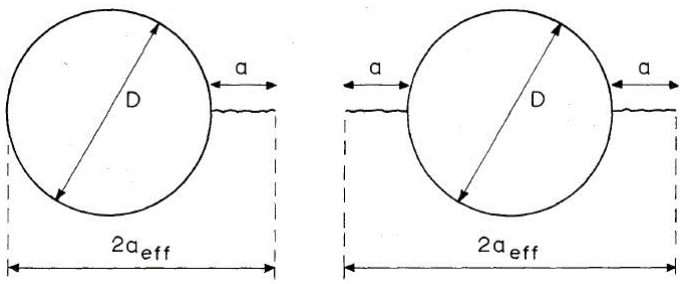

Figure 1.2. geometry definition of single and double through the thickness cracks in Bowie's work

Probably one of the most useful crack growth rate equations is given in the NASA/FLAGRO (NASGRO) computer program [13]. The NASA/FLAGRO

(NASGRO) computer program was developed for fracture analysis of space structural components and is currently the major computer code in NASA, the U.S. Air Force, and the European Agency (ESA) for this purpose. The most significant characteristics of the NASGRO program are the capability of numerous crack case solutions and improved growth rate equation features. To support the National Aging Aircraft Research Program (NAARP), improvements have been made in NASGRO to include the advanced capability for damage tolerance and fatigue crack growth analyses of aeronautical hardware problems. This computer program is currently effectively used by NASA, FAA, and ESA. The primary goal of these developments is the integration of advanced methodology for crack growth retardation. Lastly, Newman's crack closure phenomenon approach [14] was implemented to NASGRO to account for various stress ratios, (R) under constant amplitude loading (CAL). Another well-known computer program to determine the fatigue crack growth characteristics and life assessment in mainly aerospace applications is AFGROW. AFGROW is a Damage Tolerance Analysis (DTA) program which provides the users to model and perform analysis of crack initiation, fatigue crack growth, and fracture to predict the life of metallic structures. AFGROW (Air Force Grow), was originally developed by The Air Force Research Laboratory [15]. Besides the analytical methods, there is still a need for conducting experimental setups to observe the real behavior of crack especially in complex geometries and crack configurations for which there is no analytical solution. Furthermore, life assessment predictive tools and software also rely on collected experimental data to predict the fatigue life and crack nucleation and propagation based on different theories and models developed. In this thesis, aluminum alloy of 2024-T3 is studied. There are many fatigue experiments available for this aluminum alloy as it has a vast application in load carrying hardware of the aerospace industry. FAA, U.S national laboratory for materials, AFGROW DT database, U.S naval research laboratory and many researchers (e.g. J.C. Newman [16]) provide huge experimental data for a broad range of conditions for this alloy. In order to overcome geometry complexity to solve crack problems, a numerical approach may be employed.

Developed primitive crack tip element CRAC2D and CRAC3D [17] in MSC/NASTRAN can be used in 2D and 3D problems for obtaining the stress intensity factors. There are some disadvantages using these elements for crack problems. The main problem about the crack element is that it has to be created directly from the input file, and all the nodes around the crack should be considered precisely. Furthermore, the output is very mesh sensitive, therefore SIF extraction for a crack length is not practical, and tracking SIF for a propagating crack is a hard task. Franc2D/L is a two-dimensional finite element based program for simulating crack propagation for planar structures [18]. This program is a handy software which is very popular among engineers. It is capable of simulating the planar structures for the plain stress and the plain strain cases, moreover, it has simple rivet and cohesive elements which only considers the shear stiffness. The biggest advantage of Franc2D/L is that it can automatically propagate the crack. Therefore, in a model, there is a chance to extract SIF for different crack lengths. The major shortcoming of Franc2D/L is that it has a very simple pre-processor CASCA, and there are many limitations in preparing the model by CASCA. Moreover, Franc2D/L is incapable of simulating structures with many numbers of layers [18]. Nevertheless, there are some commercial open source codes for translating the FEM input files such as ANSYS, ABAQUS, PATRAN... etc. to Franc2D/L [19], but it is not very easy to do this.

ABAQUS finite element analysis program is a powerful software for the analysis of crack problems. Simulating a stationary crack in 2D or 3D structures is practical in ABAQUS [20]. Simulating the crack problems with FEM is tedious such that the solution is dependent on the mesh size. Therefore, the crack tip should be meshed carefully. Moreover, for every single crack length, new crack surfaces should be modeled and prepared because ABAQUS is incapable of propagating the crack. Although XFEM module of the ABAQUS enables a crack growth independent of the mesh, it has some shortcomings [20][21][22][23]. These shortcomings are listed as:

1. Only the STATIC analysis procedure is allowed; 2. The domain must contain single or non-interacting cracks; 3. Only one crack may exist within a particular

element; 4. Only linear continuum elements are allowed (CPE4, CPS4, C3D4, C3D8) with or without reduced integration; 5.Progressive fatigue cracks growth is not supported; Also, contour integrals for cracks cannot be calculated while crack grows. (available in ABAQUS 6.9-EF6 and later for linear brick and tetrahedron elements); 6. A crack may not branch; a crack may not turn more than 90 degrees within a particular element.

One of the most well-known finite element analysis packages is ANSYS. In this study, all SIF and life calculations are performed using APDL. ANSYS does not have an interface for XFEM crack analysis but, it has the capability to do so using predefined fatigue crack growth function groups. APDL features the following:

1. Extends the conventional FEM to account for cracks based on the concept of partition of unity [24,25,26,27].
2. Offers a way to model the cracks without explicitly meshing the crack surfaces.
3. Allows for arbitrary crack growth within the existing mesh. No morphing or re-meshing is needed.
4. Initial crack(s) must be present in the model and can be modeled as traction free or with cohesive zone behavior.
5. Assumes that the discontinuities cut the element fully. Crack tip singularity functions are not included in the displacement formulation.
7. As the crack grows, the newly introduced crack segments are always assumed to have cohesive zone behavior [25,26,27].
8. It is fully aligned with the crack-growth framework in Mechanical APDL.

By means of Ansys parametric design language, one may access the very powerful and versatile XFEM definition and solution of the problem of interest in fracture mechanics, but it should be mentioned that it requires intensive programming as there is no any interface defined inside the software.

Bergara et.al [28] investigate the geometric discontinuities and sharp edges using ABAQUS for fatigue crack propagation at aeronautic engine vane guides. Marques, J.B., et.al.[29] analyzed mode II and mixed mode I-II stress intensity factors using numerical and experimental methods. Numerical methods shows a good correlation

with that of experimental results. Dirik and Yalcinkaya [30], evaluate the crack path and life prediction under mixed mode cyclic variable amplitude loading through XFEM and experimental studies. They developed an algorithm using ABAQUS to compare XFEM solutions with experimental data. Good agreement is observed between numerical and experimental results. Kastratovic, G. et.al.[31] studied stress intensity factors for multi-site damaged problem with 11 holes and 22 cracks emanating from holes using XFEM and approximate method based on superposition. Dirik and yalcinkaya [32] compared the overload and overload-underload effects on life cycles using XFEM with NASGRO. Their developed ABAQUS algorithm for XFEM solution resulted in good correlation with NASGRO predictions.

1.3. Loading on Riveted Joints in AERO-Structures

As the result of cabin pressurization, cyclic stresses occur in the fuselage sheets. Circumferential stresses, which are about two times greater than the longitudinal stresses, are the major loading for the joints in fuselage panels (Figure 1.3). Hence, in most theoretical and experimental studies uniaxial cyclic loading on the lap joints, representing circumferential stress variations in the skin, with a close to zero positive stress ratio are applied [33][34].

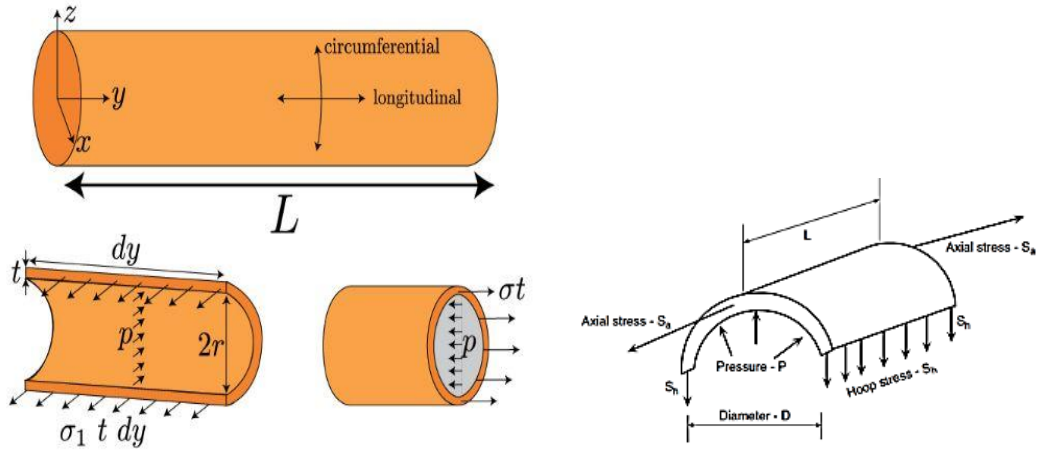

Figure 1.3. Illustration of implied stresses due to cabin pressurization on fuselage panels

1.4. Crack Growth Direction

Pure fracture failures may occur in one of the three primary cases, namely mode I, mode II and mode III as shown in Figure1.4. Considering circumferential loads on riveted lap joints, under uniaxial loading the most possible crack growth direction would be the parallel plane to the crack surface when the crack is not inclined. In this configuration ($\theta=0^o$ and uniaxial loading, Figure 1.5), governing fracture mode is mode I and K2 and K3 stress intensity factors are negligible .

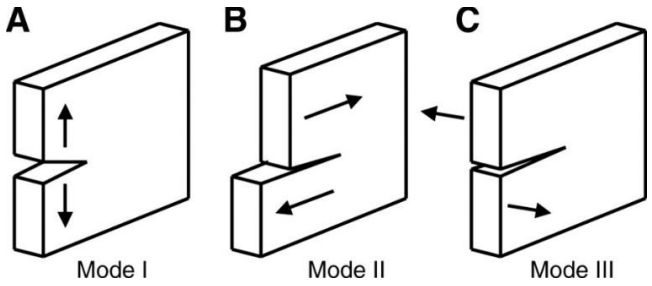

Figure 1.4. Representation of pure fracture failures. A: Mode I (opening mode). B: Mode II (Shearing mode). C: Mode III (Tearing mode)

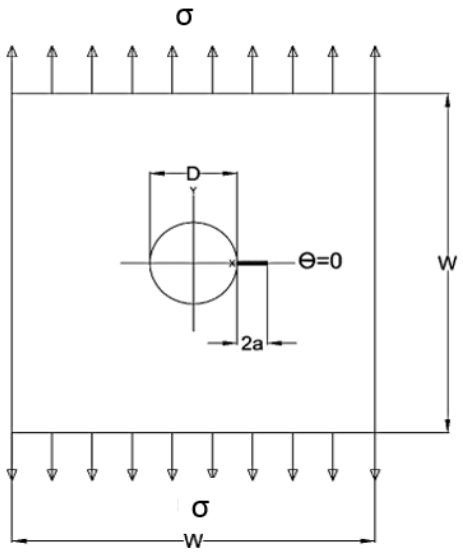

Figure 1.5. Single through the thickness crack emanating from the rivet hole

1.5. Main Accomplishments of the Thesis

1. A robust finite element method based on XFEM for double through the thickness cracks emanating from riveted holes has been developed using APDL.

2. A comparative study of FEM analyses and AFGROW results has been carried out which turned out to be in good agreement with AFGROW.

3. A comparative study has been carried out on the stress intensity factors calculated by the XFEM methodology and the analytical solutions of BOWIE and HARTER explained in detail in [35]. A good correlation is found between the results obtained by both methods.

4. Response Surface design of experiments is applied to study the dependencies of fatigue life to the crack parameters, loading and geometrical parameters.

5. Using the Analysis Of Variance (ANOVA), significance level of the understudy parameters on the fatigue life of double through the thickness cracks emanating from open holes are identified.

1.6. Contribution of the Thesis to the Literature

A regression model is proposed for the prediction of fatigue life of open-hole specimens with double through the crack. The proposed model is a handy tool in the design phase and maintenance services to investigate the fatigue life of the cracked open holes. With the developed regression model, very fast evaluation of the fatigue life of fuselage panels having double through the thickness cracks near the rivet holes can be performed.

1.7. Scope of the Thesis

Firstly, the analytical solution given by BOWIE has been used to calculate the stress intensity factors for fatigue life in CREW's report for double through the thickness cracks emanating from a hole under constant remote tensile load. By means of obtained SIFs and using reported fatigue life in CREW's report, the material

parameters of FORMAN model are obtained. Afterwards, the method of response surface is applied to design approximation experiments.

In the second stage of this study, designed experiments using the Response Surface Methodology (RSM) are modeled in the AFGROW program to predict the life of the modeled geometry under specific levels of considered parameters.

Afterwards, this study is devoted to studying the fatigue crack growth simulation using the XFEM method. All of the RS cases investigated are modeled in the APDL environment and then a code is developed to simulate crack growth and extract the related ΔK and da/dN data and also mode I, stress intensity factors.

Prior to the final stage, obtained fatigue life results within XFEM method are compared to those calculated by AFGROW and analytical results. Significance level of crack growth parameters and dependencies of the parameters are studied using the MINITAB statistical package.

Finally, ANOVA analysis is conducted to develop a regression model for the prediction of fatigue life of specimens with open rivet holes having double through the thickness cracks.

CHAPTER 2

EXPERIMENTAL FATIGUE TESTS

2.1. Specimens Geometry and the Test Procedure

In this study, the required experimental test data for the fatigue life of open-hole metallic specimens with double through the thickness cracks is extracted from Crews' report [36] published in Nasa Technical Report Server (NTRS).

In Crews' report [36], results of fatigue life experiments conducted for open-hole specimens with double through the thickness cracks are reported (Figure 2.1). Specimens of 2024-T3 aluminum alloy are subjected to 115 MPa constant fatigue loading with zero load ratio (R) (Figure2.2).

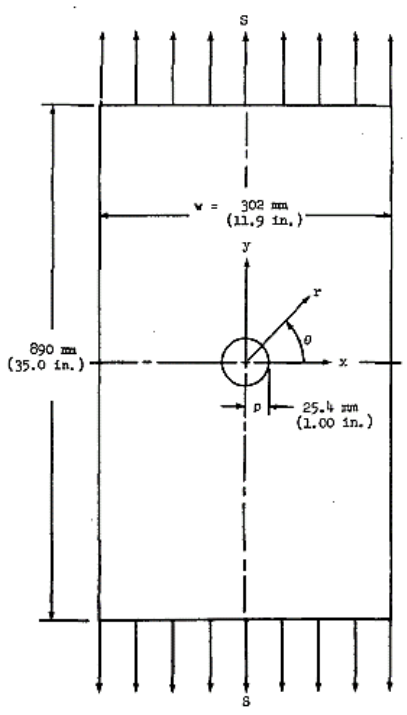

Figure 2.1. Specimen configuration and dimensions. Material, 2024-T3 aluminum; Thickness, 3.96 mm (0.156in.) [35]

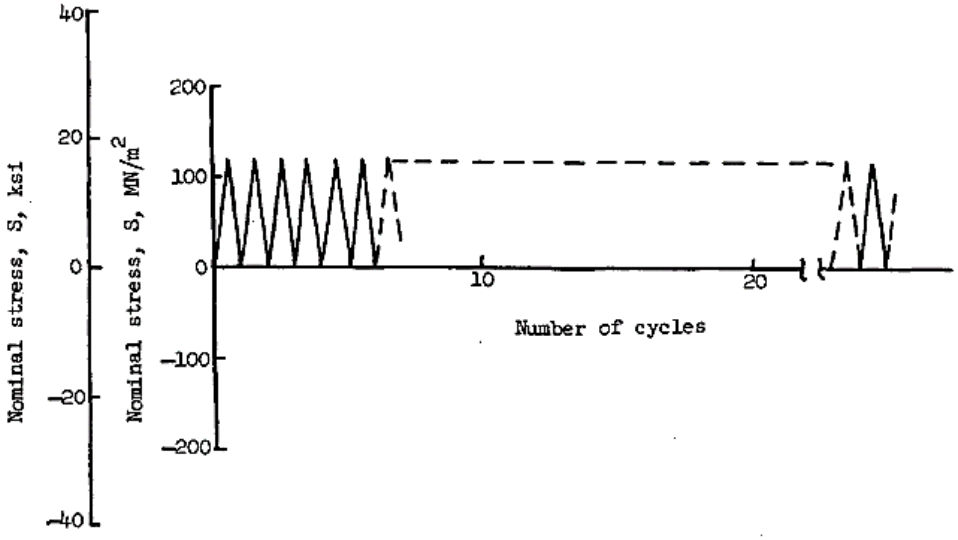

Figure 2.2. Loading Condition in the Experimental Tests [35]

For the single-level loading, fatigue cracks started at the boundary of the hole after 120,000 cycles. These cracks are detected and measured by a 10-power microscope. A scale was taped to the specimen for a reference. As shown in Figure 2.3, the crack length was referenced to the center of the hole by the length "a" or to the edge of the hole by the length "L".

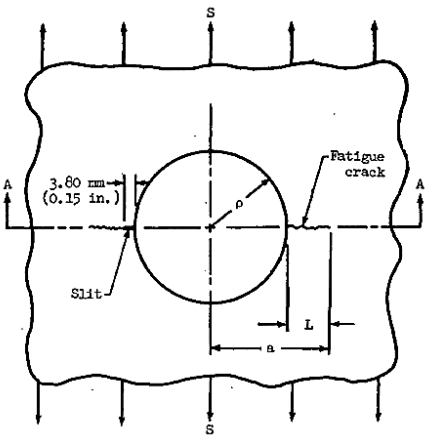

Figure 2.3. Fatigue crack length reference and saw-cut slit [35]

An initial crack length of L = 0.76 mm (0.03 in.) was defined as the beginning of the crack-propagation period and crack-growth data was recorded beyond this initial length. Tests were repeated three times. To simplify the analysis, symmetrical crack growth was desired, but in every test, a fatigue crack started only on one side of the hole. Inasmuch as the difference between stress-intensity factors for a single crack from the edge of a hole and symmetrical cracks is less than 5%when the cracks are shorter than L = 3.8 mm (0.15 in.) [11], the crack was allowed to grow to this length before the opposite side of the hole was slit to the same length to promote symmetrical crack growth. During the execution of the tests, a crack quickly appeared at the end of the slit and both cracks grew symmetrically.

2.2. Test Results

Observation of fracture surfaces revealed that in all tests the cracks started at the intersection of the sheet face and the hole and then the cracks extended radially as shown in Figure 2.4. This so-called corner-crack configuration was maintained until the crack extended through the thickness. A similar crack-growth sequence was reported in [37]. Test data are presented in Table 2.2 which gives crack length (L) and crack-propagation cycles (N) information.

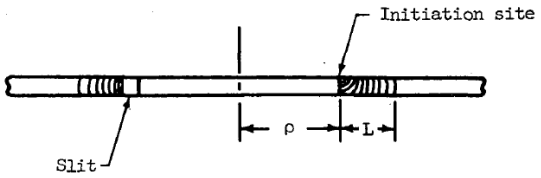

Figure 2.4. Sketch of the Fracture Surface

Table 2.1. *Experimental Fatigue Data Test Results*

Crack Length (L)		Crack Propagation Cycles , N		
mm	in.	Specimen #1	Specimen #2	Specimen #3
0.76	0.03	0	0	0
1.02	0.04	978	1003	452
1.27	0.05	1310	1675	1060
1.52	0.06	1660	2185	1787
1.78	0.07	1832	2550	2425
2.03	0.08	1932	2760	2557
2.29	0.09	2009	3012	2891
2.54	0.1	2069	3214	3545
3.05	0.12	2172	3424	3910
3.56	0.14	2246	3574	4083
4.06	0.16	2300	3664	4369
4.57	0.18	_	3730	4499
5.08	0.2	2416	3790	4595
5.59	0.22	2444	3860	_
6.1	0.24	2499	3937	_
6.6	0.26	2556	3983	_
7.11	0.28	2601	4033	_
7.62	0.3	2647	4073	4873
10.15	0.4	2827	4251	5051
12.7	0.5	2973	4407	5189
15.24	0.6	3116	4538	5312
17.78	0.7	3222	4652	5438
20.32	0.8	3323	4758	5541
22.86	0.9	3410	4850	5634
25.4	1	3491	4923	5711
30.48	1.2	3611	5055	_
35.56	1.4	3704	5153	_
40.64	1.6	3776	5225	_
45.72	1.8	3826	5274	_
50.8	2	3858	5313	6162
55.88	2.2	3880	5338	_
60.96	2.4	3897	5354	_
66.04	2.6	3905	5364	_
71.12	2.8	_	5367	_
76.2	3	_	_	6263

CHAPTER 3

FUNDAMENTALS OF THE STRESS INTENSITY CALCULATIONS USING ANALYTICAL METHOD

3.1. Analytical Study

The calculation of stress intensity factors was conducted using the BOWIE conformal mapping technique. Despite the meticulous designs of structures, practically most of the load carrying structures contain stress concentrations due to discontinuities of the structures such as holes. Bolt and rivet holes are inevitable necessities at joints, and structural holes *(e.g.* connection holes for pipes, access holes, *etc.)* are usually required. It is not surprising that perhaps the majority of service cracks nucleate in the area of stress concentration at the edge of a hole [35].

3.2. Bowie Solution

The knowledge of stress intensity factor for the application of fracture mechanics is a major prerequisite. By using a technique of conformal mapping, Bowie [11][12] has presented the *K* solution for through the thickness cracks emanating from the open hole edges. The stress intensity factor is given as in equation (3.2.1).

$$K = \sigma\sqrt{\pi a} \cdot f_b\left(\frac{a}{D}\right) \tag{3.2.1}$$

where the crack length *a* is measured from the edge of the hole, and *D* is the hole diameter. The function *f (a/D)* is usually given in tabular or graphical form. For small crack lengths compared to the hole diameter, it can be assumed that the combination behaves as if the hole were part of the crack (Figure 3.1a**)**. The effective crack length then equals to the physical length of the crack plus the diameter of the

hole. The effective crack length for the asymmetric case with $2a_{eff} = D + a$ is shown in (Figure 3.1b):

a.

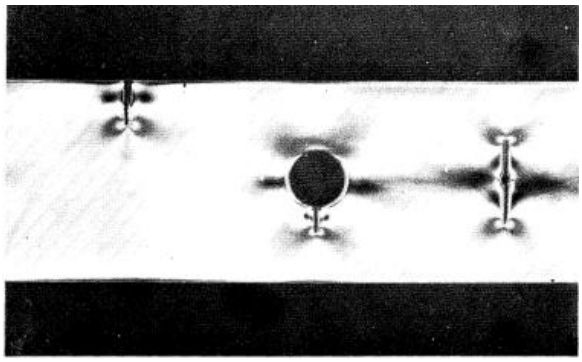

b.

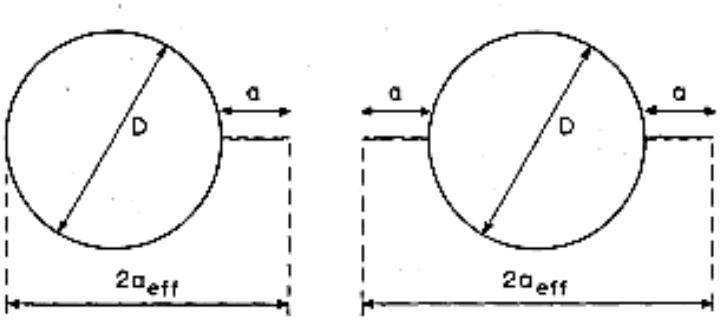

Figure 3.1. Cracks emanating from holes [34] a. Photo-elastic fringe pattern for the crack emanating from the hole is similar to that at the central crack of the same total size (right) and also similar to that of the edge crack of half the size (left) b. Effective crack size

For the symmetric case, the effective crack length is $2a_{eff} = D + 2a$, therefore, for asymmetric and symmetric cases, stress intensity factor can be written as in Eqns. (3.2.2) and (3.2.3), respectively.

$$K = \sigma\sqrt{\pi a_{eff}} = \sigma\sqrt{\pi a}\sqrt{\frac{D}{2a} + \frac{1}{2}} = \sigma\sqrt{\pi a}\, f_{B1}\left(\frac{a}{D}\right) \qquad (3.2.2)$$

$$K = \sigma\sqrt{\pi a_{eff}} = \sigma\sqrt{\pi a}\sqrt{\frac{D}{2a} + 1} = \sigma\sqrt{\pi a}\, f_{B2}\left(\frac{a}{D}\right) \tag{3.2.3}$$

Approximate solutions in equations (3.2.2) and (3.2.3) are be compared to Bowie solution by considering the functions f_{B1} and f_{B2} with $f_{B1} = \sqrt{\frac{D}{2a} + \frac{1}{2}}$ and $f_{B2} = \sqrt{\frac{D}{2a} + 1}$ respectively. Especially for long cracks, the engineering method is very useful. In engineering solution, the crack is considered as the part of the hole as illustrated in Figure 3.2 and K is calculated by equation (3.2.4).

$$K = \sigma\sqrt{\pi a_{eff}} \tag{3.2.4}$$

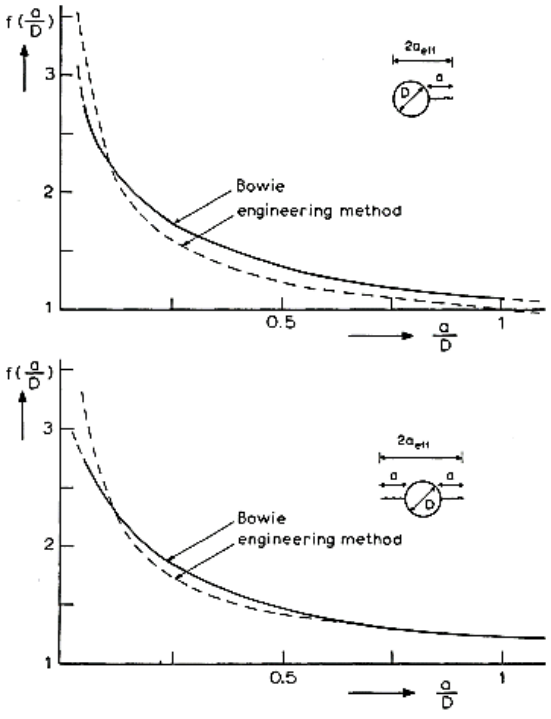

Figure 3.2. Comparison of Bowie solution with the engineering method

As shown in Figure3.2, for small $\frac{a}{D}$ ratios, the accuracy of the engineering method is low. In conclusion, the applicability of equations (3.2.2) and (3.2.3) can be shown with test data of through cracks emanating from holes. Holes can be considered as part of the crack and the growth curves for the cracks at holes coincide with that of a normal through the thickness cracks. The function $f_b\left(\frac{a}{D}\right)$ [38] established in Bowie solution is presented in equations (3.2.5) and (3.2.6). Figure 3.3 shows the variation of Bowie stress intensity geometry correction factor for double through the thickness cracks emanating from hole edges as a function of $s = \frac{c}{r+c}$ for different types of loading in which, c is the crack length and r is the radius of the hole. In case there exist only σ, geometry undergoes pure mode I fracture criterion and mode I stress intensity factor becomes as a function of equation (3.2.6).

$$f_b = 0.5(3 - s)[1 + 1.243(1 - s)^3] \tag{3.2.5}$$

or in terms of c and r, equation (3.2.5) may be re-written as:

$$f_b = 0.5\left(3 - \frac{c}{r+c}\right)[1 + 1.243(1 - \frac{c}{r+c})^3] \tag{3.2.6}$$

3.3. Finite Body Correction Factor

In order to consider the finite body effect in Bowie solution for the stress intensity factor, equation (3.3.1) is used [39]. In this equation r represents the radius of the hole and c accounts for crack length. Moreover, W is the width of the crack embedded specimen.

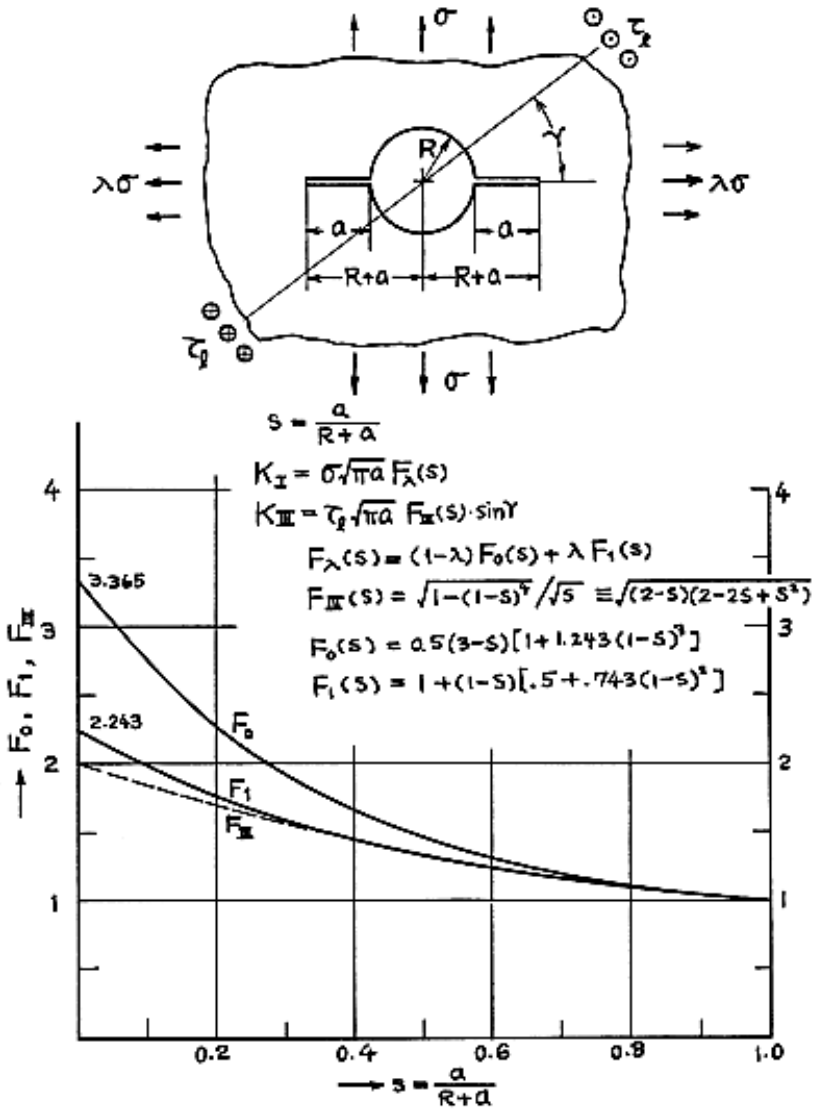

Figure 3.3. Variation of geometry factor function in Bowie solution [38]

$$F_W = \sqrt{\sec\left(\frac{\pi r}{W}\right)\sec\left(\frac{\pi(r+c)}{W}\right)} \tag{3.3.1}$$

By correcting equation (3.2.6) using the finite width correction factor to consider finite width effect, the f_b function can be written as in equation (3.3.2).

$$f_b = [0.5\left(3 - \frac{c}{r+c}\right)\left[1 + 1.243\left(1 - \frac{c}{r+c}\right)^3\right]$$
$$* \sqrt{\sec\left(\frac{\pi r}{W}\right)\sec\left(\frac{\pi(r+c)}{W}\right)} \qquad (3.3.2)$$

3.4. Forman Crack Growth Model

FORMAN crack growth model [40] is an extension of the Paris model to account for region III of the fatigue curve. Forman equation (equation 3.4.1) models the asymptotic increases in the crack growth rate as K_{max} approaches K_c. A weakness of the Forman equation lies in a lack of flexibility in modeling data shifting as a function of the stress ratio (R) [41]. There is no parameter to adjust the R shift directly. Instead, the amount of shifting is controlled by the plane stress fracture toughness (K_c) of a given material. In this equation, $\frac{da}{dN}$ or the rate of crack growth per cycle is related to stress ratio (R) and difference of stress intensity factor (ΔK) through Forman constants *C* and *m* of the specific material of under-study. Forman constants, are obtained through experiments in the laboratory for each material.

$$\frac{da}{dN} = \frac{C\Delta K^m}{((1-R)K_c - \Delta K)} \qquad (3.4.1)$$

3.5. Acquiring Forman Constants

In order to obtain the Forman constants, first, stress intensity factors related to the experimental data is calculated according to the Bowie solution [11] and utilizing finite width correction factor; then, for each specimen, da/dN ($K_C - \Delta K$) versus calculated ΔK curve is plotted in a log-log graph. Then, using equations (3.5.1) , (3.5.2), (3.5.3) and a least square linear regression fit, desired constants are obtained. In order to use constants as input to life calculation of XFEM method and AFGROW, averaged constants are used.

$$\frac{da}{dN}(K_c - \Delta K) = C\Delta K^m \tag{3.5.1}$$

$$Log(\frac{da}{dN}(K_c - \Delta K)) = Log(C\Delta K^m) \tag{3.5.2}$$

$$Log\left(\frac{da}{dN}(K_c - \Delta K)\right) = Log(C) + m\,Log(\Delta K) \tag{3.5.3}$$

The plane stress intensity factor K_c is a function of geometry and is not constant. K_c should be evaluated according to the specimen of the study using some specific tests addressed in the ASME test procedures [42][43]. K_c determined by this test method characterizes the resistance of a material to fracture in a neutral environment in the presence of a sharp crack under essentially linear-elastic stress and severe tensile constraint, such that: 1. The state of stress near the crack front approaches the tri-tensile plane strain, and 2. The crack-tip plastic zone is small compared to the crack size, specimen thickness, and the ligament ahead of the crack. Variation in the K_c can be expected within the allowable range of specimen proportions. K_c may also be expected to rise with increasing ligament size. In this study, $K_c = 110\ \frac{MN}{m^{\frac{3}{2}}}$ is taken from Crews' [36] report from where the fatigue test data is also taken. Figure 3.4 gives the da/dN $(K_C - \Delta K)$ versus the calculated ΔK curve for each specimen and also the related linear fits. Calculated Forman constants for different specimens and also the averaged constants are given in Table 3.1. An example on calculation of the Forman constants via experimental data is given in Appendix A.

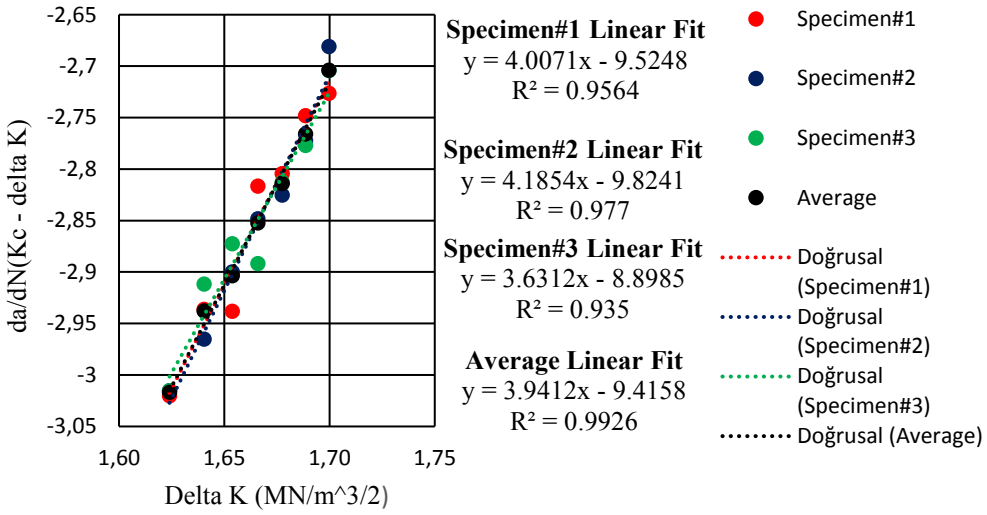

Figure 3.4. da/dN (K_c -ΔK) curve versus calculated ΔK

Table 3.1. *Calculated Forman constants for different specimens*

Specimen #	**C** $\frac{m/cycle}{(MPa\sqrt{m})^m}$	**m (Unit-less Constant)**	K_C $MPa\sqrt{m}$
1	2.986E-10	4	110
2	1.499E-10	4.18	110
3	1.263E-9	3.63	110
Average	3.838E-10	3.94	110

CHAPTER 4

FUNDAMENTALS OF XFEM

4.1. XFEM OVERVIEW

Prior to XFEM in conventional finite element method (FEM), cracks are modeled explicitly as part of the understudy geometry definition. When the crack grows (based on some fracture criterion), the mesh must be suitably updated using features such as morphing and re-meshing so that the analysis can continue. The extended finite element method (XFEM), introduced by Belytschko and Black [44], overcomes the requirements of updating the mesh as the crack grows. XFEM is based on the partition of unity concepts outlined in Melenk and Babuska [45].

4.2. XFEM-Based Crack Analysis and Crack-Growth Simulation

The eXtended Finite Element Method (XFEM) models cracks and other discontinuities by enriching the degrees of freedom in the model with additional displacement functions that account for the jump in displacements across the discontinuity. XFEM is a good engineering approach for modeling both stationary crack problems and crack-growth simulation. The method eliminates the need to re-mesh the crack-tip regions.

The method offers the following features:

•Extends the conventional finite element method to account for cracks based on the concept of partition of unity [45][46][47][48].

•Offers a way to model the cracks without explicitly meshing the crack surfaces.

•Enables 2-D analysis of stationary crack problems with linear elastic isotropic material behavior. (The displacement formulation can account for the presence of singularity.)

•Allows for arbitrary crack growth within the existing mesh. No morphing or re-meshing is needed.

•For a growing crack, the method assumes that the discontinuities cut the element fully. (In this case, displacement formulation does not account for the presence of singularity.)

•As the crack grows, the newly introduced crack segments are always assumed to have cohesive zone behavior [46][47][48].

•Is fully aligned with the crack-growth framework in Mechanical APDL.

4.3. XFEM Analysis Methods

The techniques used in XFEM can be broadly classified into the following methods.

4.3.1. Phantom-Node Method

The phantom-node method accounts for jumps in the displacements across the crack surfaces. Crack-tip singularity is not taken into account. The crack terminates at the edge (or face) of a finite element (Figure 4.1 and Figure 4.2). The phantom-node method [47][48][49][50] considers only the displacement jump across the crack faces and ignores the crack-tip singularity contributions. Thus, the displacement formulation becomes:

$$u(x) = N_1(x)u_1 + H(x)N_1(x)a_1 \tag{4.3.1}$$

By introducing phantom nodes superposed on the parent element nodes, as shown in Figure 4.1, the displacement function can be rewritten in terms of the displacements of the real nodes and the phantom nodes as, [47]

$$u(x,t) = u_I^1(t)N_1(x)H\big(-f(x)\big) + u_I^2(t)N_1(x)H(f(x)) \qquad (4.3.1)$$

which leads to a superposed element formulation that essentially splits the parent element into two sub-elements. In equation (4.3.1),

$u_I^1(t)$ = Displacement vector in sub-element 1

$N_1(x)$= Conventional nodal shape function

$u_I^2(t)$= Displacement vector in sub-element 2

$f(x) =$ Crack surface definition (f(x)=0)

$H\big(-f(x)\big) =$ Heaviside step function

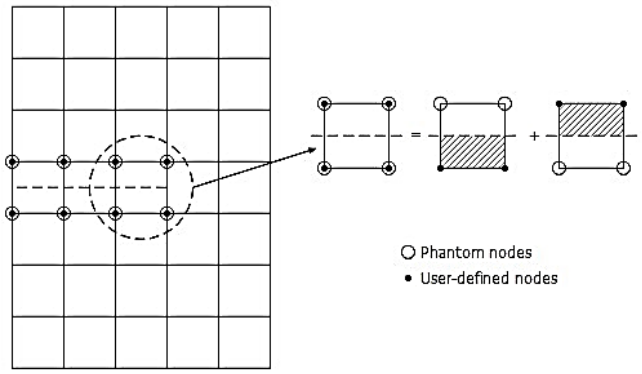

Figure *4.1.* Phantom node illustration within an element

4.3.2. Singularity-Based Method

In the singularity-based method, the crack is allowed to terminate inside an element (Figure 4.2). The displacement functions in the FEM formulation are enhanced by

introducing additional enrichment functions that capture the jump in displacement across the crack surface and also the crack-tip singularities:

$$u(x) = N_1(x)u_1 + H(x)N_1(x)a_1 + N_1(x)\sum_j F_j(x)b_l^j \qquad (4.3.2.1)$$

where:

$u(x) =$ Displacement Vector

$N_1(x) =$ Conventional nodal shape function

$u_1 =$ Nodal displacement vectors

$H(x) =$ Heaviside step function

$a_1 =$ Enriched nodal degrees of freedom accounting for the crack tip singularity

$F_j(x) =$ Crack tip element functions

$b_l^j =$ Nodal degrees of freedom accounting for the crack tip singularity

The functions $F_j(x)$ differ according to the material [10][11][12].

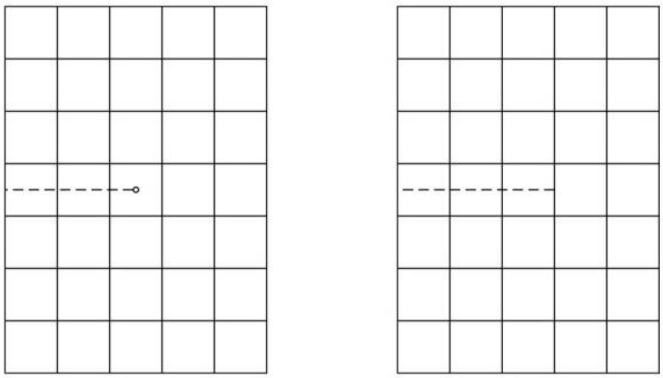

Figure 4.2. Representation of a crack in XFEM; crack terminates inside an element in singularity method (Left) and cracks terminate on the edge of an element in phantom-node method (Right)

4.4. XFEM-Based Fatigue Crack-Growth Assumptions

In the XFEM analysis of fatigue crack growth, following restrictions apply. Fatigue crack growth needs to be conducted with the singularity-based XFEM as a requirement of APDL and also material characteristic is only limited to the linearly elastic isotropic material. Non-linearity of material behavior such as plasticity, non-linear geometry effects, and crack tip closure attributes are not considered during the fatigue crack growth analysis. Crack length ahead of the crack tip is the governing factor in maximum allowable crack growth increment, however, minimum permissible crack increment must be smaller than the size of the element ahead of the crack tip. Nevertheless, in case minimum increment is larger than the length of the element ahead of the crack tip, the crack increment is limited to the length of the element ahead of the crack tip. Deviation of the crack path would only occur at element edges or surfaces. Moreover, crack growth within an element follows a constant path, without any deviation from the direction. Because the crack-tip singularity effects are not incorporated into the analysis, the stress and deformation fields around the crack tip are only approximate. This assumption may result in approximate crack direction prediction during the subsequent crack growth. Crack direction prediction may also be affected by the boundaries, other discontinuities, and the local stress and deformation fields due to the discretization. A fracture criterion is evaluated after the sub-step has converged. If the time stepping is large, the fracture criterion ratio may be exceeded. Limiting the incremental time step for the sub-steps results in a better approximation to the fracture criterion ratio.

4.5. Fatigue Crack Growth

The XFEM-based crack-growth simulation technique can also be used to simulate fatigue crack growth in engineering structures. The method offers a convenient engineering approach for simulating cracks and fatigue crack propagation without resorting to modeling the cracks or re-meshing the crack-tip regions as the crack propagates. Following are characteristics of the XFEM-based approach to simulating

fatigue crack growth: 1.) Uses singularity-based XFEM. 2.) Supports 2-D fatigue crack-growth simulation and linear elastic isotropic materials only. 3.) Ignores large-deflection and finite-rotation effects, crack-tip plasticity effects, and crack-tip closure or compression effects.

4.6. Fatigue Crack Growth in Mechanical APDL

Mechanical APDL analyzes crack growth in structural components subject to repeated or cyclic loading using the linear elastic fracture mechanics (LEFM) concepts.

4.6.1. Valid Loading Types

Only cyclic loadings of constant amplitudes are allowed, as shown in Fig. 4.3.

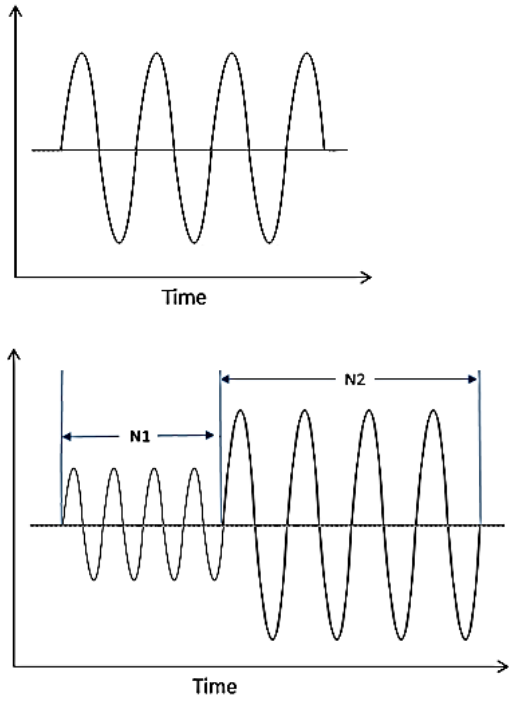

Figure 4.3. Valid loading types in APDL fatigue crack growth using XFEM method; up: constant amplitude cyclic loading; down: variable amplitude cyclic loading

If the cyclical loading is such that the amplitude changes after some number of cycles, then each set of cycles with the same load amplitude should be modeled separately as a load step. Overloading can also be modeled in a similar manner.

4.6.2. Fatigue Crack Growth Analysis Methods in APDL

In a typical fatigue crack-growth calculation in APDL, it is required to follow the steps below:

- Calculation of K_{max} at the maximum load
- Calculation of K_{min} at the minimum load (or using the stress/load ratio (R))
- Calculation of the crack increment Δa

or

- Calculation of the incremental number of cycles ΔN
- Stopping the analysis if the specified maximum crack extension is reached

It should be noted that the calculation of K_{max} or K_{min} (via the stress ratio (R)) is performed numerically during the analysis. The determination of Δa or ΔN depends on the fatigue crack-growth method.

A fatigue crack growth can be modeled via either of these methods:

Life-Cycle (LC) Method

Cycle-by-Cycle (CBC) Method

4.6.3. Life-Cycle (LC) Method

The LC method is typically used with constant-amplitude cyclic loads. The crack-extension increment Δa is user-specified, and a number of incremental cycles ΔN is calculated by the program based on the fatigue crack-growth law. In XFEM-based fatigue crack growth using this method, the crack-extension increment Δa is restricted to the length of the element ahead of the crack tip. Crack extension using the LC method always propagates the crack one element at a time. The initial crack

specification must result in fully-cut elements and the LC method does not support partially cut elements.

4.6.4. Cycle-by-Cycle (CBC) Method

The CBC method is suitable for variable-amplitude cyclic loadings and overload simulations. The incremental cycles ΔN are user-specified, and the crack-extension increment Δa is calculated by the program based on the fatigue crack-growth law. In XFEM-based fatigue crack growth using this method, the calculated Δa can result in partially cut elements. If at any instant the calculated Δa exceeds the element boundaries, the program sets the crack extension length Δa to the remaining uncut portion of the element, and recalculates ΔN to grow the crack by that Δa . The program does not modify the crack-propagation angle until the element is fully cut.

4.7. Performing XFEM-Based Fatigue Crack-Growth Analysis

This type of analysis is assumed to be quasi static and can be performed using the singularity-based method. The general procedure to perform this analysis in APDL is as follows. Firstly, initial crack is defined prior to setting up the solution procedure, then fracture parameters of LEFM are evaluated and finally, crack growth parameters are calculated.

Defining an initial crack: In order to define an initial crack using the singularity-based XFEM approach for fatigue crack-growth analysis in APDL, the following considerations should be taken into account. 1.) The initial crack must cut the element(s) fully. 2.) Only PLANE182 elements can be used. 3.) Only linear elastic isotropic material behavior is allowed.

Setting up the Solution Procedure: To commence the solution procedures, it is important to note that a fatigue crack-growth analysis uses the static analysis procedure only; hence, the static analysis (*ANTYPE,STATIC*) should be declared as the analysis type.

The loading in APDL is assumed to be step-applied by default. Furthermore, the total time of the applied loading specified (*TIME*) has no direct effect on the loading or the boundary conditions. Applied load step at each sub-step of the analysis, results in crack propagation and construction of a finite element formulation to calculate he solution parameters. In order to control the crack, the extent of crack propagation in a load step APDL commands *DELTIM* or *NSUBST* are the two useful commands. DELTIM may be used to define new time steps and NSUBST may be used to divide an already defined time-step to smaller time-steps. Notwithstanding, automatic time stepping also may be used instead of DELTIM and NSUBST commands without accelerating or decelerating the crack propagation rate. In the LC method, the program takes care of the crack growth increment during a loading sub-step, while the CBC method needs a user-specified value (*CGROW,FCG,DN*) to control the incremental number of cycles during a sub-step.

Evaluation of the Fracture Parameters: In APDL, *CINT* command is used to initiate a SIF calculation. A new domain for integral calculation with specific ID should be assigned for each crack while the *CINT* command issues *(CINT,NEW,ID).* Afterwards, desired fracture parameters should be addressed inside the CINT command *(CINT,TYPE,SIFS).* Eventually, crack front containing element set are specified under the element component name *(CINT,CFXE,CompName)* and also the required number of contours for j-integral calculations are defined *(CINT,NCON,n).* The program automatically calculates the average of SIF from contour three to contour n.

Setting up the Crack-Growth Calculation Parameters: The crack-growth calculations occur in the solution phase after the solution has converged. In this phase of the analysis, crack growth set is initialized *(CGROW,NEW,SETNUM)* (where SETNUM is the crack-growth set number). By using the same numerical identifier used for the SIF calculation in the *CINT* command, crack growth ID also is specified *(CGROW,CID,ID).* Moreover, the desired method of the analysis should be declared in the crack growth set *(CGROW,METHOD,XFEM).* In order to stop the

simulation, a specific amount of propagation of crack can be defined to cease the crack extension *(CGROW,STOP,CEMX,Value).*

4.8. Defining the Model in the XFEM Analysis

4.8.1. Elements Used in the XFEM Analysis

For 2D fatigue crack growth analysis PLANE182 element (Figure 4.4) type is supported in ANSYS. PLANE182 is used to model 2-D solid structures. It can be used as either a plane element (plane stress, plane strain or generalized plane strain) or an axisymmetric element with or without torsion. In most cases, the element is defined by four nodes with two degrees of freedom at each node; translations in the nodal x and y directions. For the axisymmetric option with torsion, it is still defined by four nodes, but with three degrees of freedom at each node; translations in the nodal x and y directions, and rotation in the nodal y-direction. The element has plasticity, hyper-elasticity, stress stiffening, large deflection, and large strain capabilities. It has a mixed-formulation capability for simulating deformations of nearly incompressible elastoplastic materials, and fully incompressible hyper-elastic materials.

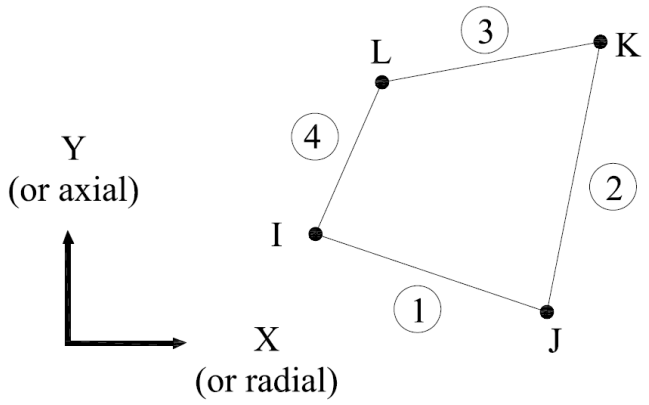

Figure 4.4. Representation of the PLANE182 element used for 2D XFEM fatigue crack growth

Shape functions for the 2-D 4-node and axisymmetric quadrilateral elements of PLANE182 are given in equations (4.8.1) and (4.8.2);

$$u = \frac{1}{4}(u_I(1-s)(1-t) + u_J(1+s)(1-t) + u_k(1+s)(1+t) + u_L(1-s)(1+t)) \quad (4.8.1)$$

$$v = \frac{1}{4}(v_I(1-s)(1-t) + v_J(1+s)(1-t) + v_k(1+s)(1+t) + v_L(1-s)(1+t)) \quad (4.8..2)$$

where, s and t are the coordinates of nodes in transformed (local) coordinate system.

It should be noted that only linear elastic isotropic material behavior is allowed in the XFEM analysis.

4.8.2. Defining the Crack and Associated Parameters

In finite element analysis, the crack is identified as a line for 2D and as a surface for 3D geometries. To define the initial crack in ANSYS, it is necessary to define four important features described below.

- Definition of the Crack-Enrichment Parameters
- Definition of the Enhancement Radius to Account for Crack-Tip Singularity Effects
- Definition of the Snap Tolerance to Snap Crack Tip to Element Face
- Definition of the Initial Crack

Definition of the Crack-Enrichment Parameters: To establish a region, which is enhanced with additional internal nodes necessary to support the enriching displacement functions as required for the crack growth, it is needed to identify the enrichment parameters (Figure 4.5). Multiple cracks may be introduced to a defined region. Care should be taken in the selection of the enrichment field. Enrichment region should be chosen conservatively to cover probable crack growth region. In case multiple cracks exist in the enrichment region, more intensive computation will

be conducted and as a result computation time will be longer. To manage different internal cracks, the enriched region can be associated with a name for identification *(XFENRICH,EnrichmentID)* where *EnrichmentID* is the name assigned for identifying the enrichment region. In addition, an element set, containing initial cracks should be defined inside an enrichment region *(XFENRICH,EnrichmentID,CompName)* where *CompName* is the name of the element set; moreover, the method of crack propagation for the crack defined inside enrichment region should also be defined. Two methods are available for which one may be selected for the analysis of crack growth in XFEM.

1.Phantom-node method:

XFENRICH,EnrichmentID,CompName,,PHAN (default)

2.Singularity-based method:

XFENRICH,EnrichmentID,CompName,,SIN

Definition of the Enhancement Radius to Account for Crack-Tip Singularity Effects: The enhancement radius (Figure 4.5) is applicable to the singularity-based XFEM analysis. By default, the singularity functions apply to crack tip element(s) only and neighboring un-cracked elements surrounding the crack tip are not influenced from crack tip singularity effect. By introducing enhancement radius to the enrichment region, it is possible to account for the effects of the crack tip singularity in a region around the crack tip to include in the element formulation. *(XFENRICH,EnrichmentID,CompName,,SING,RADIUS).*

Definition of the Snap Tolerance to Snap Crack Tip to Element Face: The snap tolerance characteristics are applicable only in the singularity-based XFEM. It is a good practice to position the crack tip close to the mid-element. Snap tolerance enables to snap the crack tip to the closest element edge or face (Figure 4.6). *(XFENRICH, EnrichmentID, CompName, ,SING,RADIUS,SNAPTOLER).* ANSYS utilizes the tolerance value and the average element length to determine if the crack

tip should be snapped to the element edge or to the face or not. The default snap tolerance is 1.E-6.

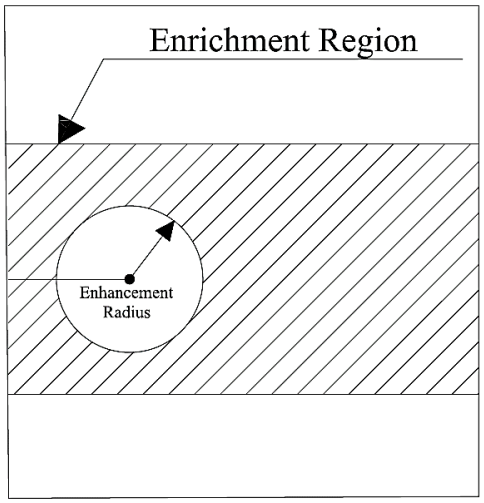

Figure 4.5. Representation of the Enrichment Region and the Enhancement Radius

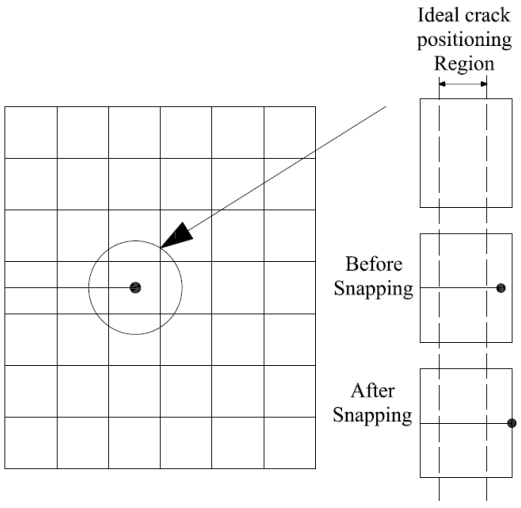

Figure 4.6. representation of snap tolerance

Definition of the Initial Crack: Location of the crack in a finite element model is defined by a level set method (LSM) [51][52]. In order to define a crack in the FE model, the crack geometry is defined by introducing two signed distance functions at the nodes of an element containing the crack. These functions define the position of the nodes from the crack plane and from the crack front. To calculate the value of these functions (also called level set values (PSI and PHI)), crack front containing element number and also crack front node number(s) should be defined in XFEM parameters. *(XFDATA, LSM, ELEMNUM, NODENUM, PHI, PSI).* Figure 4.7 illustrates PHI level set function.

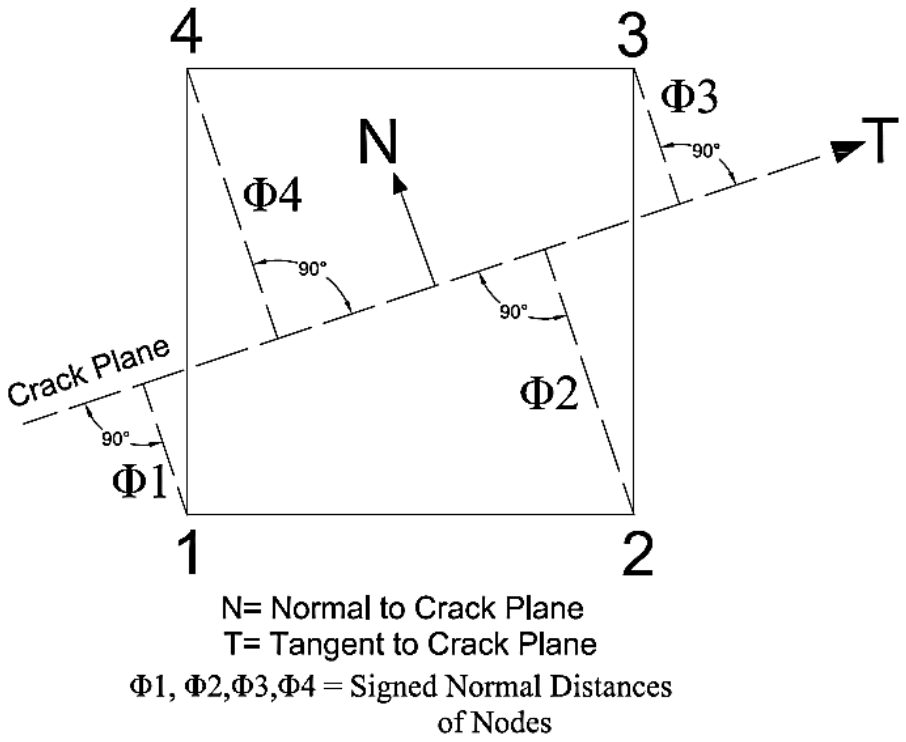

Figure 4.7. Illustration of the PHI level set function

It should be noted that the value of PHI must be > 0 or < 0 and PHI = 0 is invalid; in other words, the crack plane cannot coincide with the element edge or the face. On

the other hand, while the PHI level set value is only calculated for one element where the crack front exists, the PSI level set value is calculated for all of the elements through which the crack passes. Figure 4.8 illustrates the PSI level set function in detail.

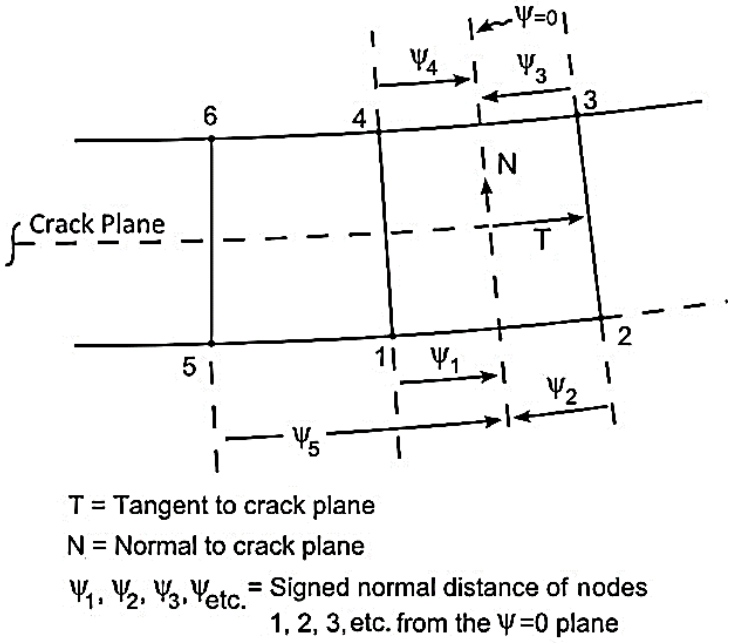

Figure 4.8. Illustration of the PSI level set function

It should be noted that the Ψ=0 plane is assumed to be perpendicular to the crack plane at the crack tip.

4.9. Calculation of Stress Intensity Factors

J-integral Calculation: The concept of J-integral is developed by Cherepanov [53] in 1967 and in 1968 by Jim Rice [54] independently. Cherepanov and Rice showed that calculated strain energy release rate using the path integral (also called the J-integral) is independent of the path around the crack tip. Method of J-integral uses the

calculation of strain energy release rate or work per unit fracture surface area in a material. Afterwards, developed experimental methods allowed measuring the critical fracture properties utilizing small scale laboratory specimens for which the LEFM does not hold [55] and to calculate critical value of fracture energy J_{Ic}. The quantity J_{Ic} defines the point at which large-scale plastic yielding during the crack propagation takes place under mode one loading. In monotonic loadings, the J-integral is a measure for strain energy rate for a crack in a body [56];However, this is generally true only for linear elastic materials with quasi-static conditions. Under special circumstances, J-integral can be used to calculate the energy release rate in case small-scale yielding exists at the crack tip such as monotonic loading in shear mode (mode III or the anti-plane shear). Furthermore, the J-integral method is also applicable to materials undergoing small-scale yielding at the crack tip for pure power law hardening plastic materials. It should be noted that, the path-integral quantity for elastic-plastic materials in monotonic mode I and mode II loading does not conform to path independency, hence, it is valid only in the contour close to the crack tip. Nevertheless, Rice showed that, whenever a non-proportional load is applied in plastic materials, J integral is path independent. Developed method by Shih [57] is the infrastructure for the evaluation of the J-integral based on the domain integral method. In the domain integral method, area integration for 2D problems and volume integration for 3D problems are applied to integration formulations inasmuch area and volume integrations are easier to be applied numerically with reasonable accuracy.

Understanding the Domain Integral Representation of the J-integral:

For a 2-D problem, equation (4.9.1) represents the domain integral of the J-integral:

$$J = \int_A \left[\sigma_{ij}\frac{\partial u_j}{\partial x_1} - W\delta_{1i}\right]\frac{\partial q}{\partial x_i}dA + \int_A \alpha\sigma_{ii}\frac{\partial \theta}{\partial x_1}q_1 dA - \int_A \sigma_{ij}\frac{\partial \varepsilon_{ij}^0}{\partial x_1}q_1 dA - \int_C t_j u_{j,1} q_1 dS \quad (4.9.1)$$

where,

σ_{ij} = stress tensor

u_j = displacement vector

W = strain energy density

δ_{ij} = kronecker delta

x_i = local coordinate axis

q = crack-extension vector

α = coefficient of thermal expansion

ε_{ij}^0 = initial strain tensor

t_j = crack face traction

A = integration domain

C = crack faces upon which tractions act

The direction of the x-axis in the crack tip local coordinate system is the direction of the crack extension vector (q). Crack extension vector at the nodes along the contour Γ is chosen to be zero. Notwithstanding, except the mid-side nodes inside the contour Γ, q vector becomes a unit vector for all nodes inside the Γ region, if there exist any directly connected nodes to Γ. Directly connected nodes to Γ (unit crack extension vector) are referred to as virtual crack extension nodes in ANSYS. A typical crack tip region with Γ contour and the local coordinate system at the crack tip is illustrated in Figure 4.9.

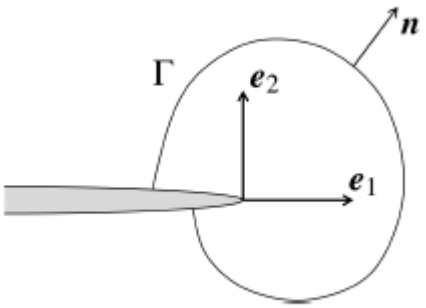

Figure 4.9. Illustration of the contour Γ and the local coordinate system at the crack tip

Virtual Crack-Extension Nodes and J-integral Contours: Virtual nodes are of crucial importance for the input required for the evaluation of J-integrals. In FE applications these nodes are also referred to as crack-tip component. In 2D problems, crack-tip component usually consists of one node which is called the crack tip node. In the evaluation of the J-integral, the first contour of the area integration is evaluated over the associated elements with the crack tip and the second contour is evaluated over the elements associated to adjacent elements of the first contour elements and the procedure of area integration continues for all contours. To assure correct results for the area integration, the last contour should not exceed the boundary of the geometry of the model. In 3D problems, crack tip component consists of a set of nodes along the crack front. A similar procedure for the area integration for J-integral applies for 3D geometry problems as in 2D problems. Figure 4.10 illustrates the first three J-integral contours in a 2D finite element model.

Performing the J-integral Calculation: ANSYS program calculates the J-integral at the solution phase of the analysis after a sub-step has converged, then stores the value to the results file. The *CINT* command initiates the J-integral calculation and also specifies the parameters necessary for the calculation. Following steps are applied in a calculation process of the J-integral.

- Initiation of a new J-integral calculation
- Definition of the crack information
- Specification of the number of contours to calculate the J-integral
- Definition of the crack symmetry condition
- Specification of the output controls

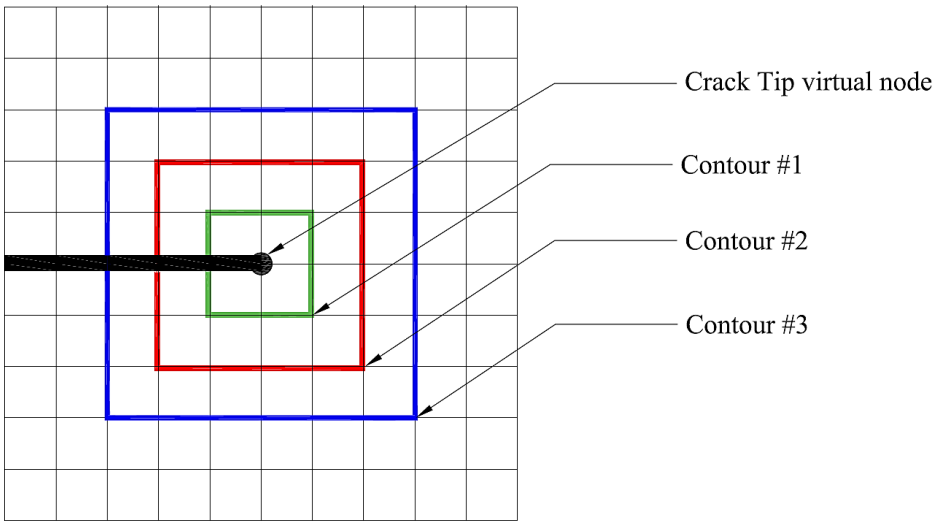

Figure *4.10*. Representation of J-integral contours in a 2D finite element model

CHAPTER 5

FATIGUE CRACK GROWTH USING AFGROW

5.1. AFGROW

In the realm of fracture mechanics, AFGROW is one of the widely used damage tolerance software used in specifically aerospace industry for metallic materials [41]. This software was originally developed by the Air Force Research Laboratory. There are several models of fatigue crack growth defined together with a rich library for well-known problems of fracture mechanics. In this study, AFGROW is used to compare the fatigue life of 2024-T3 aluminum alloy along with the fatigue life predicted by XFEM and experimental [36] methods.

5.2. Modelling of the DTC Problem in AFGROW

In this section, the geometry of the Double through the Thickness Cracks (DTC) used in the experimental tests is modeled using AFGROW (Figure 5.1).

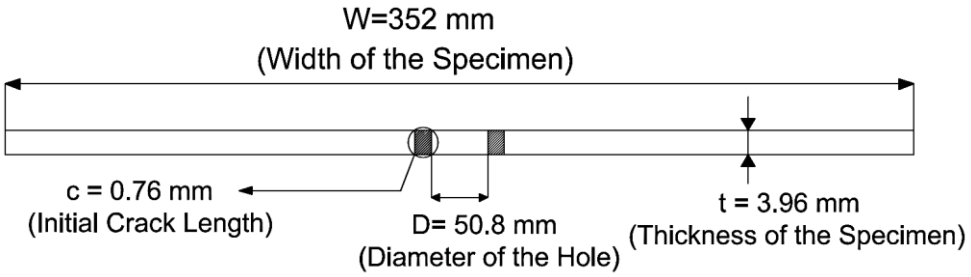

Figure 5.1. Modeled geometry with DTC in AFGROW

DTC problem is a standard available problem in the AFGROW classic model library. After defining the crack geometry in AFGROW, fatigue crack growth model

and loading should also be defined to be able to predict fatigue life. Since the load ratios other than zero are not of interest in this study and experimental fatigue life predictions [36] are conducted using the Forman model (equation 5.2.1), hence in AFGROW Forman model [40] is also chosen to predict fatigue life.

$$\frac{da}{dN} = \frac{C\Delta K^m}{((1-R)K_c - \Delta K)} \tag{5.2.1}$$

As stated earlier in previously, a weakness of the Forman equation lies in a lack of flexibility in modeling data shifting as a function of stress ratio (R). There is no parameter to adjust the R shift directly. Instead, the amount of shifting is controlled by the plane stress fracture toughness of a given material. Nevertheless, as R is not considered as a variable in this study, the efficiency of the Forman model would be sufficient. Required constants in equation (5.2.1) as input for AFGROW are obtained by processing the experimental data as discussed in chapter 3. Forman constants are re-mentioned in Table 5.1.

Table 5.1. *FORMAN constants*

Forman Constants	
C $(\frac{m/cycle}{(MPa\sqrt{m})^m})$	3.838E-10
m (Unit-less Constant)	3.94
K_C $(MPa\sqrt{m})$	110

In order to predict fatigue life including plastic deformation during crack growth in thick materials, AFGROW offers several retardation scenarios to choose from. Plasticity effect usually occurs in thick materials and causes longer fatigue life; however, in this study, no plastic effect is considered. Cyclic constant amplitude load of magnitude 115 MPa, with zero load ratio is applied to the modeled problem in AFGROW. Analysis of the experimental setup in AFGROW for fatigue life

evaluations is conducted and fatigue life versus crack length curve of the AFGROW prediction is shown in Figure 5.2.

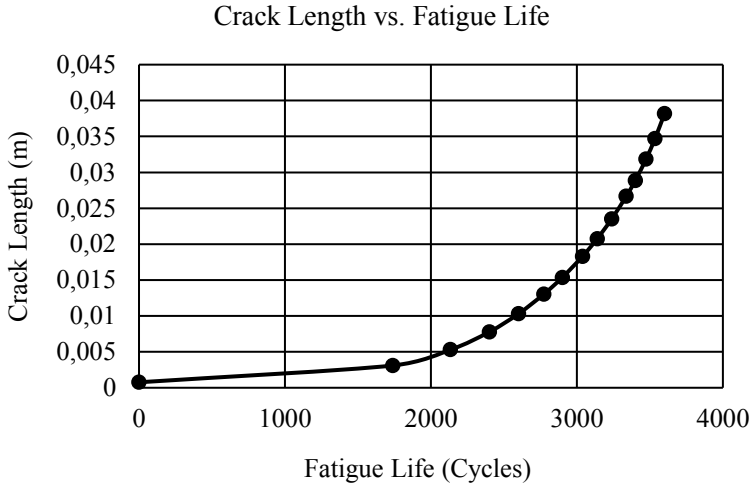

Figure 5.2. Life versus crack length prediction in AFGROW

Comparison of the crack growth rate vs. ΔK for the experimental tests and the AFGROW results is also depicted in Figure 5.3. Figure 5.4 shows the difference in fatigue life due to the plastic effect in experimental tests and the AFGROW prediction. As can be seen from Figure 5.4, the crack growth rate in AFGROW prediction is faster than experimental tests. This behavior can be attributed to the fact that in AFGROW analysis, no plastic effect is considered; However, in the experiments crack tip plasticity accounts for the retardation effect, hence the same crack length as in the AFGROW analysis is reached in higher number of cycles.

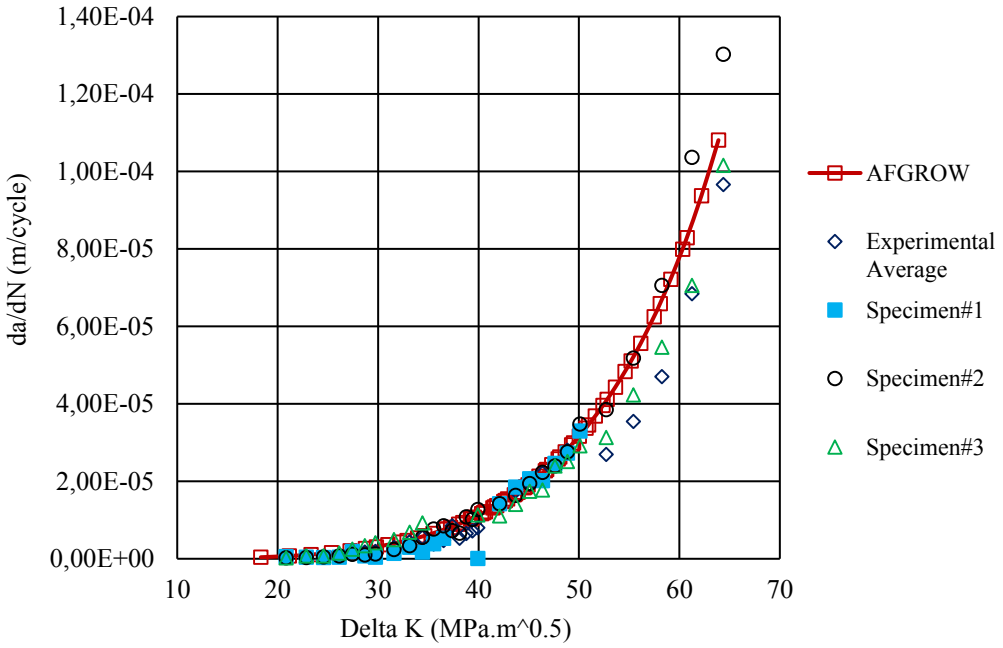

Figure 5.3. Comparison of crack growth rate between experimental results and AFGROW

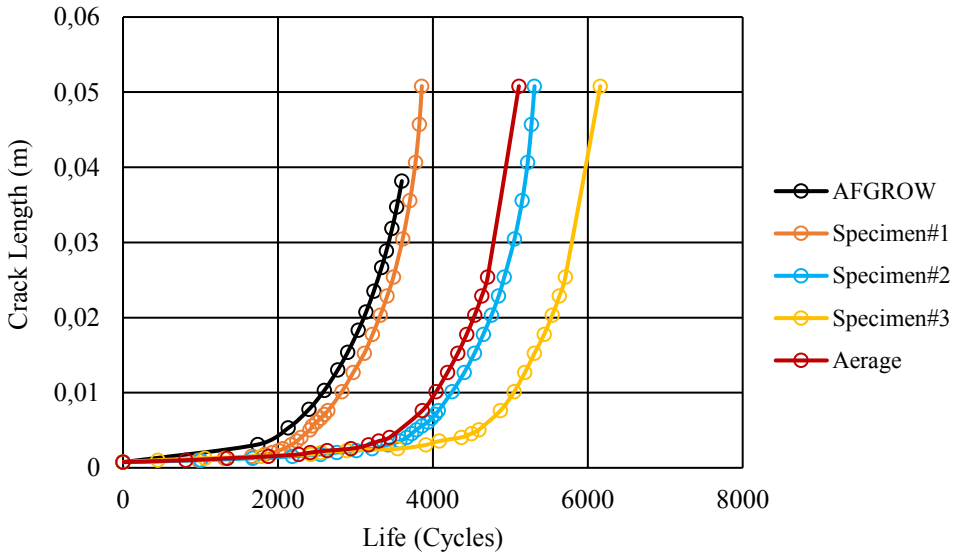

Figure 5.4. Comparison of crack length versus life (experimental tests [35] vs. AFGROW)

CHAPTER 6

FATIGUE CRACK GROWTH USING XFEM

In this chapter, the crack geometry of the understudy is modeled using XFEM. In this chapter only the results of XFEM analysis are presented.

6.1. Modelling of the DTC Problem in XFEM

In this study, XFEM analysis is conducted using the ANSYS Parametric Design Language (APDL). The geometry of the double through the thickness crack problem as presented in the experimental test campaign described in Crews' report [36] is modeled using the developed code in APDL. The developed code is capable of perfectly modelling the geometry as well as the loading and the boundary conditions and defining the required parameters for the XFEM analysis. The geometry is modeled with two different boundary conditions. As shown in Figure 6.1, two nodes at the left most and the right most in the crack plane located are fixed in the y direction to due to the symmetry of the geometry. To prevent the rigid body motion, there should exist two fixed nodes in the x direction. In the first scenario, the same nodes also fixed in the x direction. In the second scenario, two nodes at the middle of the model located in the upper and lower edges are considered as fixed nodes in the x direction. In the modeled geometry pressure loads of 115 MPa are applied to the upper and the lower (y=890 mm and y=0) boundaries of the model to simulate the fatigue loading under cyclic constant amplitude load (Figure 6.1). The load ratio (R) is also set to zero to simulate the zero based constant amplitude loading. The comparison of the results for different boundary conditions are discussed in Appendix B. Based on the study given in Appendix B, it is seen that boundary condition 2 (BC2) gives closer stress intensity factors compared to the Bowie's solution which includes the finite width correction. It should be noted that BC2 is

actually the correct boundary condition which simulates the experimental conditions. Here, results of boundary condition 1 (BC1) is also included; because original Bowie's solution without the effect of finite width correction is valid for an infinite width plate and with the boundary condition BC1 one can simulate an infinite width plate since the crack front stress would not be affected from the boundary condition at infinity. However, since the experimental specimen, thus the analysis model, has finite width, as shown in the stress plots given in Appendix B, crack front stress is affected from the x direction boundary condition applied at the nodes located at the left most and the right most in the crack plane. Hence, in the rest of the study, BC#2 is applied to simulate the crack growth. BC#2 represents near real test conditions and is in good agreement with Bowie solution with finite width correction factor for calculated stress intensity factors.

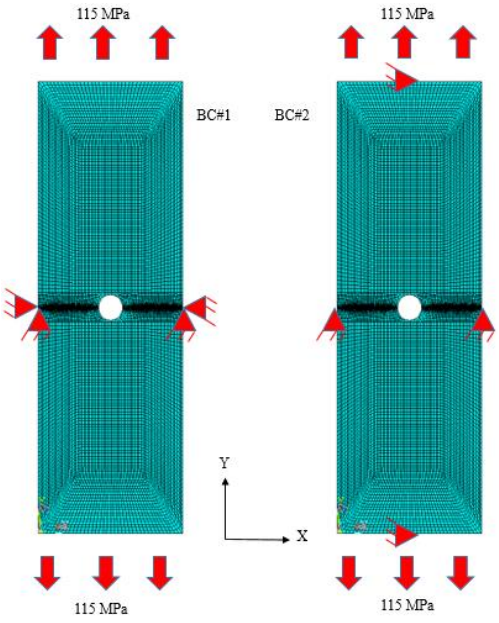

Figure 6.1. *Finite Element Model of the Open Hole Specimen with DTC*

The ΔK values and the associated contour stress intensity factors up to contour nine are the output of developed code. At the end of the analysis routine, extracted ΔKs are used to calculate the fatigue life using the Forman model and the developed integration code in MATLAB. To assure the quality and accuracy of XFEM

analyses, convergence test is conducted. The variation of stress intensity factor from the analytical method is observed by changing the mesh size along the crack surface and the enrichment region. For convergence analysis, three different mesh sizes are tested to assure the accuracy of the results. Table 6.1 shows the details of element sizing and meshing for these tests. A representing figure for meshed model and also enrichment field mesh and also initial crack definition in the model is given in Figure 6.2.

Table 6.1. *Meshing Details of the Convergence Analysis*

	Mesh#3	Mesh#2	Mesh#1
Crack Plane Element Size (mm)	0.25	0.38	0.75
Number of Elements around the Hole Circumference	108	80	44
Total number of elements	80051	43292	14427
Enrichment region element size (mm)	1.5	2	4
Out of Enrichment element size (mm)	4.5	6	8
Total Number of Nodes	80372	43538	14597
Meshing Time (s)	25	13	6

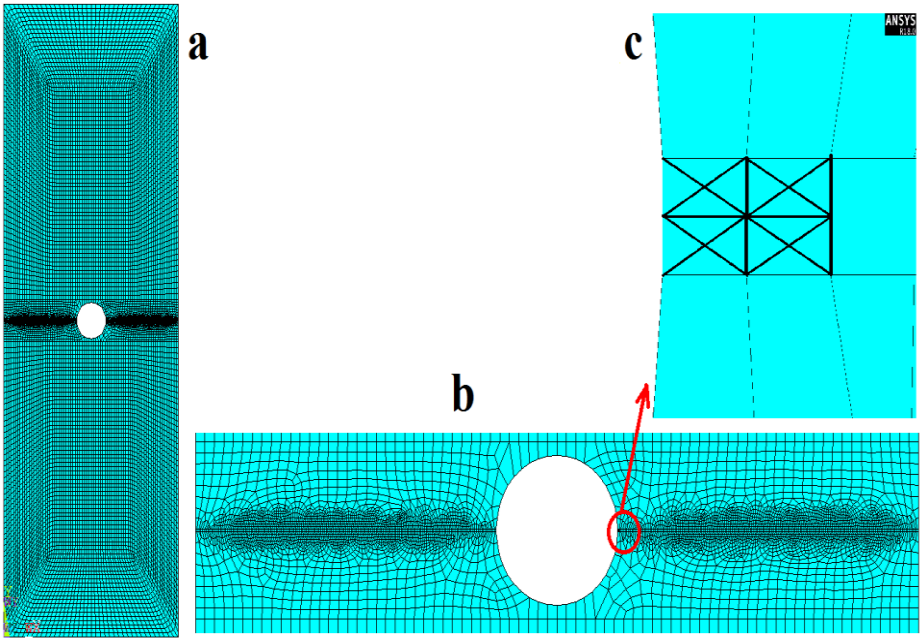

Figure 6.2. a) Meshed model using Mesh#2 b) Enrichment field c) Initial crack definition in XFEM

To compare different mesh size effect on the stress intensity factor with the analytical results, graphs of crack length versus ΔK are depicted for all mesh cases and also for the analytical method with finite width correction factor in Figure 6.3.

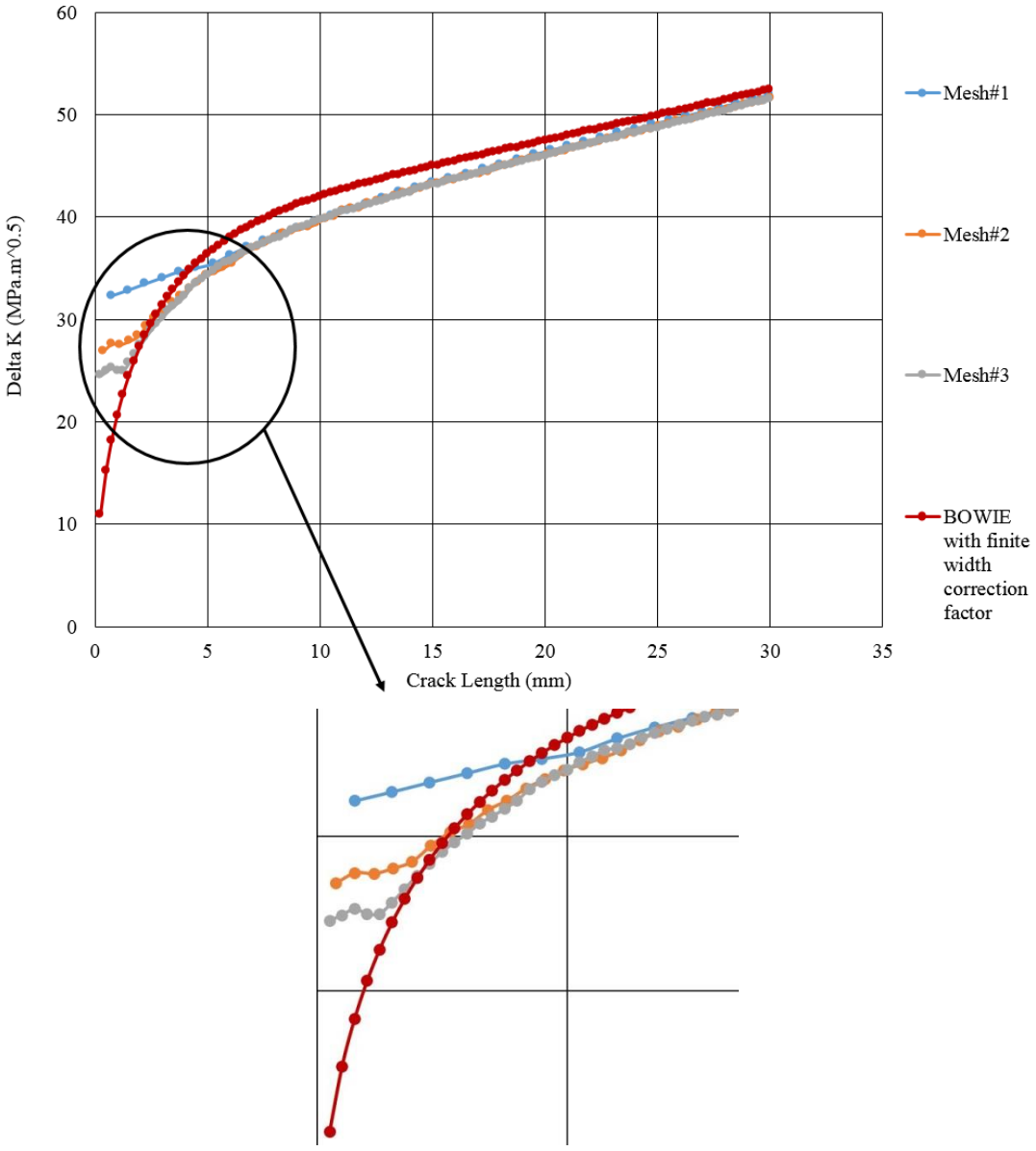

Figure 6.3. Comparison of XFEM mesh sensitivity

As can be observed from Figure 6.3 finer mesh size (mesh 3) results in closer ΔK values to the analytical results. However, this improvement is limited just for small crack lengths (up to 2.4 mm) and for longer crack lengths almost all mesh sizes coincide with each other. In short crack lengths, the effect of singularity region in the XFEM analysis increases and affects the crack tip stress intensity factor accordingly; hence, finer mesh results in better resolution as the J-integral contours of area integration are limited to a smaller region, and the singularity region shrinks. Finer mesh size than Mesh#2 does not significantly enhance the results. Hence, Mesh#2 is chosen to continue with in the present study.

Another important factor for the calculation of SIF is the stability of the calculated SIF through different contours. It should be noted that near crack-tip region is affected from the singularity zone of the crack tip and regions far away from the crack tip are out of the crack sensitivity zone. APDL calculates the average of contour three to contour n for the SIF evaluation. Nonetheless, the study of contour by contour variation of the SIF suggests that it is more beneficial to choose the average value of contour four to contour seven in the evaluation of stress intensity factors. Figure 6.4 illustrates the variation of the stress intensity factor with the contours. It is observed that the least variation in the SIFs occurs for contours from four to seven; hence this is the reason for picking the average values of SIFs of contours forth through seventh. As shown in Figure 6.4, for an specific length of the crack, more or less the magnitude of SIF remains constant for contours four to seven. Developed APDL code for the crack growth analysis is capable of calculating the J-integral up to the ninth contour. To capture the most accurate SIF, SIF values for contour four through contour seventh are averaged for each crack growth increment to calculate the fatigue life. To calculate the fatigue life, it is necessary to integrate the Forman model for each growth increment and then add up all the cycles up to a specific crack length. This calculation is done using a MATLAB code. The criterion in which crack growth ceases is explained in detail in the response surface methodology design field chapter, but for time being it should be mentioned that in

practice, amount of crack extent is limited to the distance between two consequent rivets depending on the rivet pattern applied and the crack growth is stopped at the crack length of 30 mm.

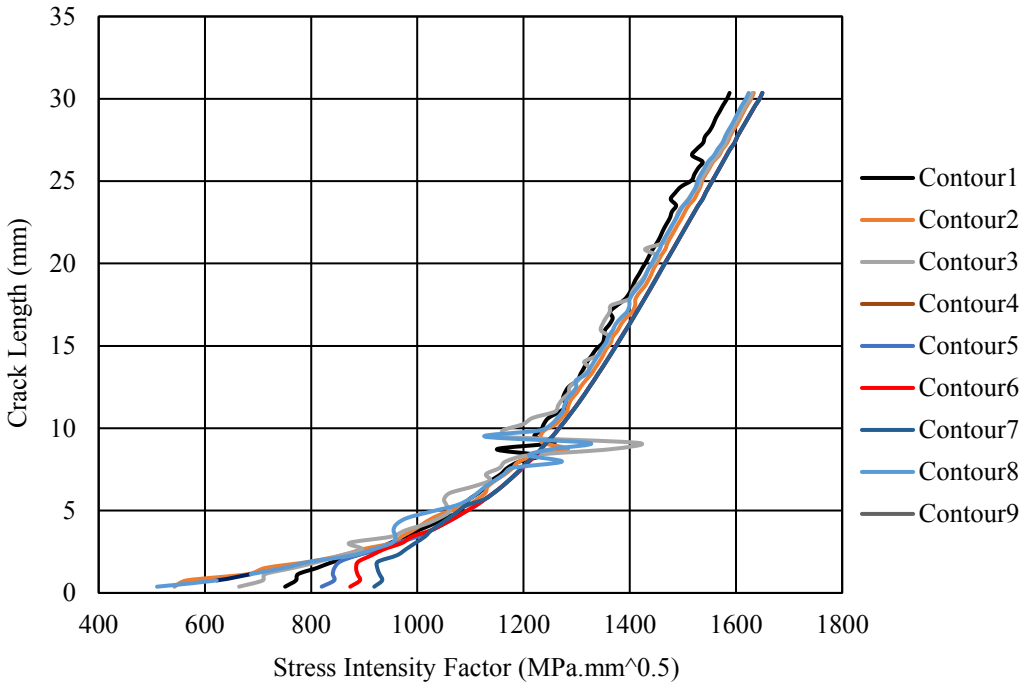

Figure 6.4. Comparison of SIF contour by contour

In a double through the thickness crack emanating from a hole, it should be assured that propagation of both cracks remain symmetric with respect to each other; otherwise, it is not a DTC problem anymore and SIFs become diverse and one of the cracks with faster growth dictates the life of the model. To assure whether the geometry is modeled correctly and both cracks are advancing symmetrically, for both cracks *SIF* ratio (K_{left}/K_{right}) versus the crack length is shown in Figure 6.5. From the Figure (6.5), a well-balanced symmetric growth of the cracks is obvious. A

maximum difference of 0.15%is observed in calculated SIF from the commencement to cessation of the left and right cracks.

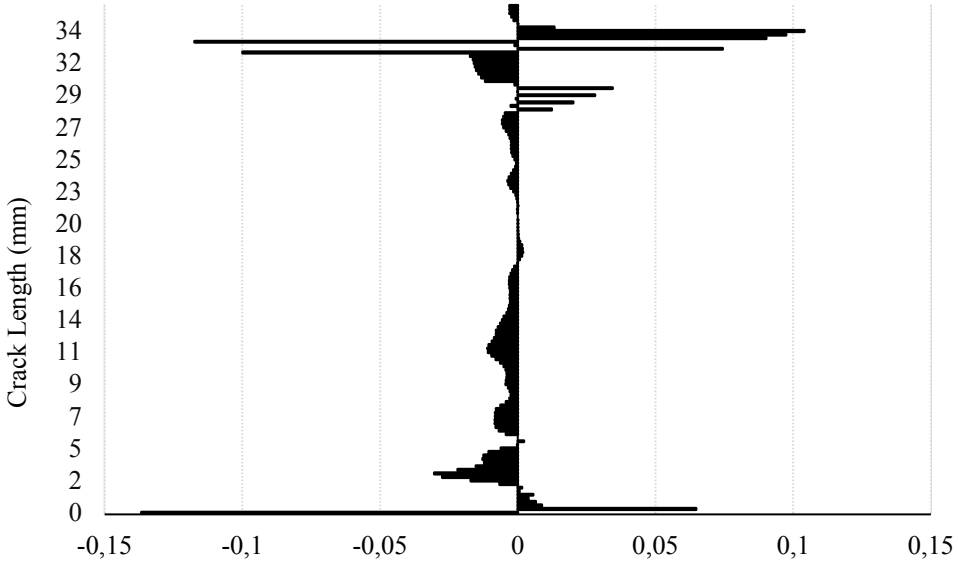

Figure 6.5. : $\frac{K_{left}}{K_{right}}$ ratio difference in percent

6.2. XFEM Life Prediction

As discussed earlier, the Forman model is utilized to model the fatigue life in this study. To this end, obtained stress intensity factors using XFEM analysis is employed to predict the fatigue life. A code is developed in MATLAB (see Appendix C) to integrate the Forman model to calculate fatigue life. Developed MATLAB code reads the SIF and crack length from the text output of the XFEM analysis and then stores the data into a matrix to feed the FORMAN model to calculate cycles for each crack length; to this end the life of two consecutive crack length are calculated and finally all cycles summed up. Under the specific test conditions of the experimental setup, the model reaches 30 mm crack growth in 3347 cycles.

6.3. Comparison of XFEM and AFGROW Results

As can be seen from Figure 6.6, a good correlation exists between AFGROW and XFEM for shorter crack lengths. The average fatigue life for specimens in experimental report is shown in Figure 6.7 together with the XFEM results. Comparison between fatigue life results of experimental tests, XFEM analyses and AFGROW results, reveals that, for longer crack lengths, XFEM gives more accurate fatigue lifes with respect to the AFGROW results..

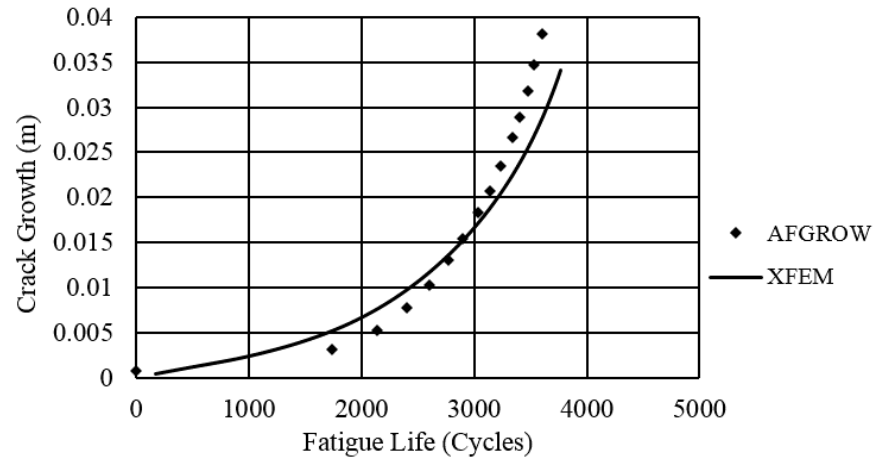

Figure 6.6. Comparison of Fatigue Lives obtained by XFEM and AFGROW

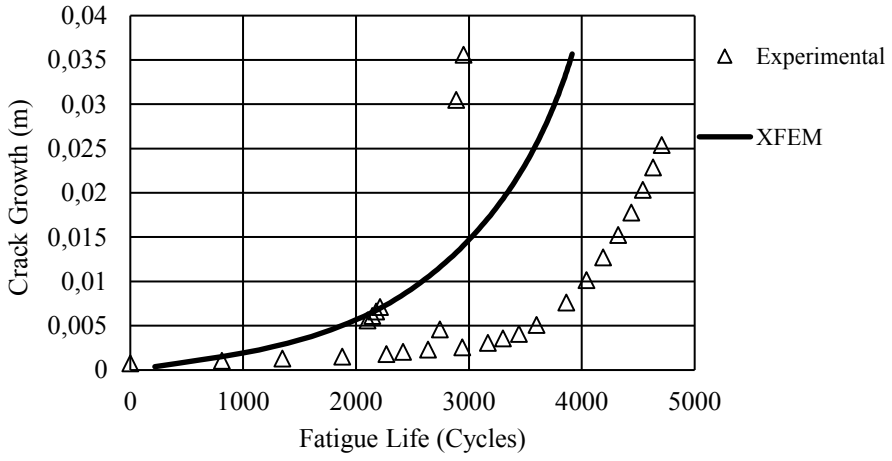

Figure 6.7. Average life for experimental specimens

CHAPTER 7

FUNDAMENTALS OF RESPONSE SURFACE METHODOLOGY

7.1. Introduction

Response surface methodology (RSM) is a set of statistical and mathematical techniques, beneficial for developing, improving, and optimizing the response of a system. This methodology is firstly introduced by George E. P. Box and K. B. Wilson in 1950s. The backbone of RSM is to utilize a series of designed experiments to reach an optimal response. RSM has important applications in the formulation, development, and design of new products, as well as in the performance improvement of the existing designs. The most widely used applications of RSM are in the industry, specifically in situations where many input parameters influence the performance or accuracy of the design. These performance quantities or accuracy of the desired behavior is called the response. Throughout this thesis, fatigue life is the desired response to establish a regression model. In most cases of RSM applications, more than one response is involved. Usually, the input variables are called independent variables, and they are the control parameters of the engineer, for the purpose of a test or an experiment.

Generally, the engineer (experimenter) is dealing with a design, or system consisting of a response (*y)* which depends on the controllable variables $\xi_1, \xi_2, \dots, \xi_k$. The input variables are also called factors or independent variables. Independent variables or factors are controlling the response in a RSM system. The fatigue life in this study is controlled by defined independent variables, namely remote tensile load (σ), radius of the hole (r) and the crack length (c).The actual relationship between the response (y) and the independent variables can be written as,

$$y = f(\xi_1, \xi_2, \dots, \xi_k) + \varepsilon \tag{7.1}$$

where the exact form of the actual response function f is not known and it can be very complicated, and ε is an error term due to uncontrollable sources of variabilities which are not considered in f. Hence, ε includes the effects like, measuring errors on the response; erroneous sources that are inherent in the system (such as noise), the effect of other (unknown) variables, etc. In this study, error term may source from several uncontrollable variabilities. In the experimental tests, uneven preparation of test specimens and inaccurate measuring devices can be mentioned; however, in XFEM analyses, variation of modeled geometry from real test condition and mesh dependency of calculated results are among probable sources of error in response term (Fatigue Life). Thus, ε is treated as a statistical error, and it has a normal distribution with mean zero and variance σ^2. By assuming that the mean of ε is zero, it can be shown that:

$$E(y) \equiv \eta = E[f(\xi_1, \xi_2, \dots, \xi_k)] + E(\varepsilon) = f(\xi_1, \xi_2, \dots, \xi_k) \tag{7.2}$$

The variables $\xi_1, \xi_2, \dots, \xi_k$ in Equation 7.2 are called the natural variables, as they are expressed in their natural units of measurement. For instance, radius of the hole (r) as an independent variable is called a natural variable if its unit mentioned in length unit (e.g. mm). It is convenient often, to transform the natural variables to coded variables such as $x_1, x_2, \dots, x_k$, which are defined to have the same spread or standard deviation and be dimensionless with a mean zero. The actual response function in equation 7.2 can be rewritten in terms of the coded variables as:

$$\eta = f(x_1, x_2, \dots, x_k) \tag{7.3}$$

Since the form of the actual response function f is unknown, it should be approximated. In fact, the successful use of RSM is critically dependent upon the engineer's ability to develop an appropriate approximation for f. Most often, a low-

order polynomial in tiny regions of independent variables exhibits an appropriate approximation. Nevertheless, usually, a first-order or a second-order model is used. In the case of two independent variables, the coded version of the first order model is as follows:

$$\eta = \beta_0 + \beta_1 x_1 + \beta_2 x_2 \tag{7.4}$$

Figure 7.1 shows a typical three-dimensional response surface for the particular case of the first-order model.

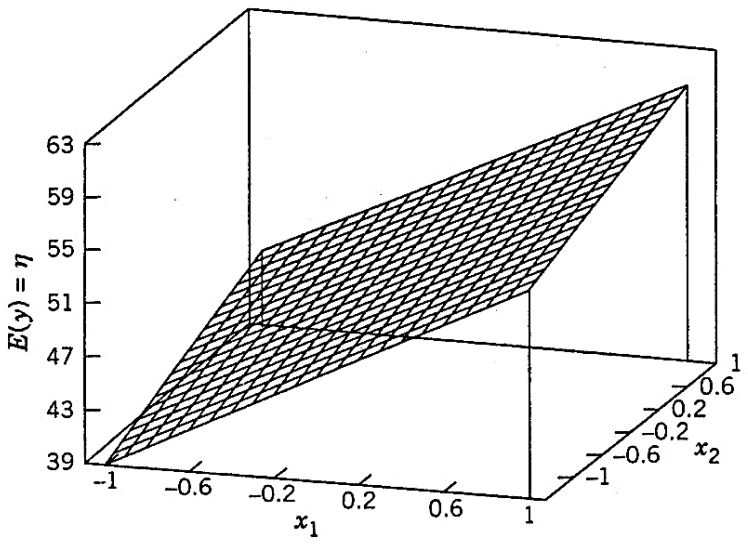

Figure 7.1. Representation of a 3D first-order response surface [57].

The contour plot for such a surface in case of the first order model represents parallel lines of the constant response in the (x_1, x_2) plane. This type of response surface (first order model) may be of interest when only a small region is to be investigated. For a larger region the curvature of the response would not be taken into account

with the first order model and the accuracy of the response would become considerably low.

For instance, application of a first order model for a tiny region around point *A* in Figure 7.2 may be suitable.

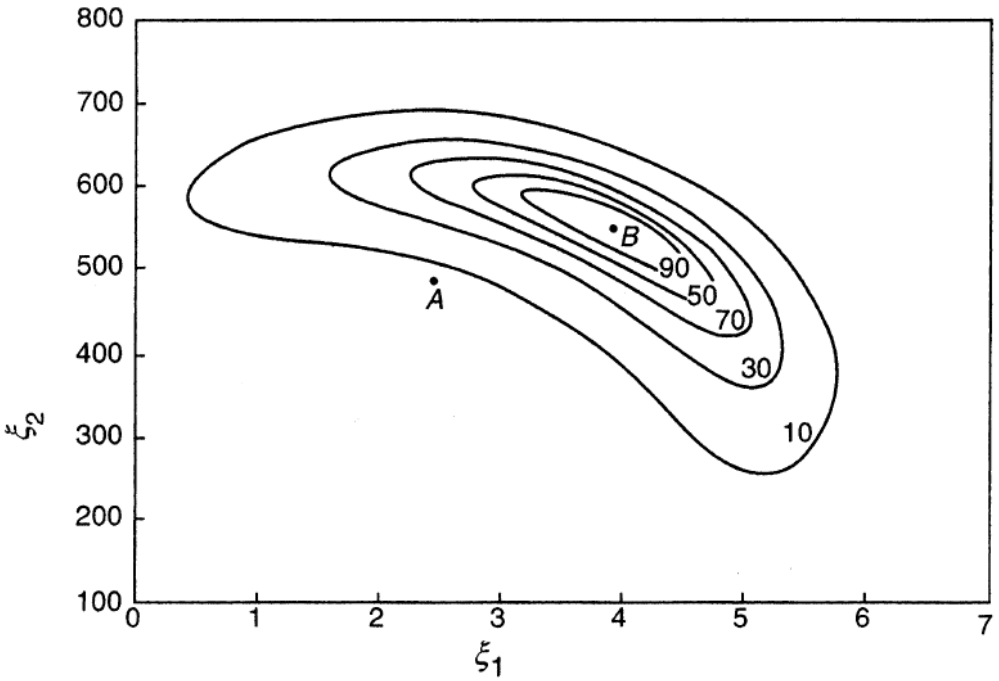

Figure 7.2. Suitability of first-order response surface for a small region around point A

The shape of the first order model, given by Eqn. 7.4, is called the main effects, because it includes only the main effects of the two variables x_1 and x_2 and the interaction between these variables is not included in the first-order model. Nonetheless, interaction terms may be included in Eqn. 7.4 as given by Eqn. 7.5.

$$\eta = \beta_0 + \beta_1 x_1 + \beta_2 x_2 + \beta_{12} x_1 x_2 \tag{7.5}$$

Equation 7.5 gives the first-order model with interaction. Figure 7.3 shows the three-dimensional response surface and the related contour plot for a typical first order with interactions.

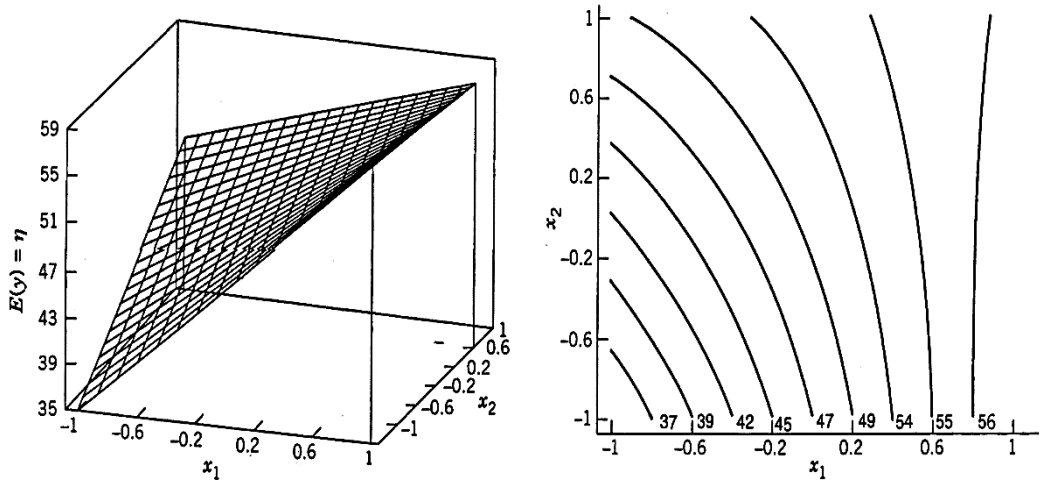

Figure 7.3. A typical first-order model with interaction terms

As can be noticed, by the addition of the interaction terms to the first order model, curvature is introduced to the response, which leads to different rate change of the response. Nevertheless, often the curvature of the response is too strong and first order model even with interactions cannot reflect the true response. In such cases it is necessary to apply a second-order model. The general form of a two variable second order model is given by Eqn. 7.6.

$$\eta = \beta_0 + \beta_1 x_1 + \beta_2 x_2 + \beta_{11} x_1^2 + x_{22} x_2^2 + \beta_{12} x_1 x_2 \tag{7.6}$$

Second order model may result in a good approximation of the response near the small region of point B in Figure 7.2, when there is significant curvature in the true response. Figure 7.4 represents a second order model in 3D space with contour plots.

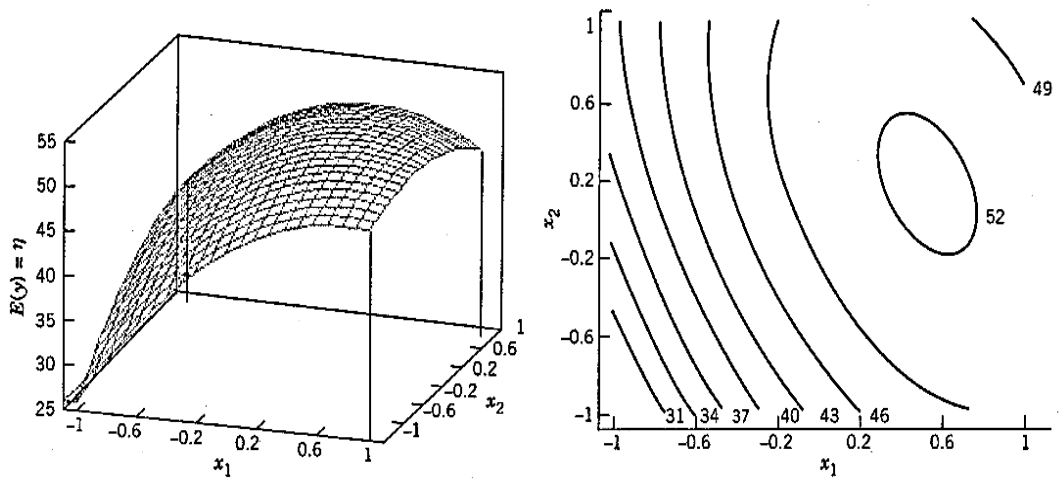

Figure 7.4. Illustration of a second-order model in 3D space with contour plots

Application of the second order model resulted in mound-like surface and also elliptic contour plots as well.

The second-order model is widely used in response surface methodology for several reasons.

1. The second-order model is very flexible. It can take on a wide variety of functional forms, so it will often work well as an approximation to the true response surface.

2. It is easy to estimate the parameters (the $\beta's$) in the second-order model. The method of least squares can be used for this purpose.

3. There is considerable practical experience indicating that second-order models work well in solving real response surface problems.

In general, the first-order model is given by,

$$\eta = \beta_0 + \beta_1 x_1 + \beta_2 x_2 + \cdots + \beta_k x_k \tag{7.7}$$

and the second-order model is given by,

$$\eta = \beta_0 + \sum_{j=1}^{k} \beta_j x_j + \sum_{j=1}^{k} \beta_{jj} x_j^2 + \sum \sum_{i<j=2}^{k} \beta_{ij} x_i x_j \qquad (7.8)$$

In some situations, approximating polynomials of order higher than two are used. The general motivation for a polynomial approximation for the true response function *f* is based on the Taylor series expansion around the point $x_{10}, x_{20}\ldots, x_{k0}$. For example, the first-order model is developed from the first-order Taylor series expansion as in Eqn. 7.9,

$$f \cong f(x_{10}, x_{20}, \ldots, x_{k0}) + \frac{\partial f}{\partial x_1}|_{x=x_0}(x_1 - x_{10}) + \frac{\partial f}{\partial x_2}|_{x=x_0}(x_2 - x_{20}) + \cdots + \frac{\partial f}{\partial x_k}|_{x=x_0}(x_k - x_{k0}) \qquad (7.9)$$

where x refers to the vector of independent variables and x_0 is the vector of independent variables at the specific point $x_{10}, x_{20}, \ldots, x_{k0}$. In Equation 7.9, only the first-order terms in the expansion are included, so if

$\beta_0 = f(x_{10}, x_{20}, \ldots, x_{k0})$, $\beta_1 = \left(\frac{\partial f}{\partial x_1}\right)|_{x=x_0}$, …, $\beta_k = \left(\frac{\partial f}{\partial x_k}\right)|_{x=x_0}$, then it becomes the first-order approximating model given by Equation 7.7. If in Equation 7.9 second-order terms are included, this would lead to the second-order approximating model given by Equation 7.8.

7.2. Variables Region of Operability

Data collection phase of the RSM should be carefully done. To this end, a specific experimental design, which is called as response surface design, is a tool in this regard. Furthermore, care should be taken that RSM designs and analyses are matched accordingly. For example, in order to analyze data from a planned experiment using a second-order model, then the selection of the design should be appropriate for such an analysis. Likewise, the different design should be selected if

the curvature is anticipated identical to what can be modeled with a second-order model. In this regard, before selecting the design for data collection care should be taken about the milestones of a specific experiment and analysis. For a specific designed experiments an operability region is defined where the model performs within some region of independent variables. It is clear that it is impossible to explore the entire region of operability with a single experiment. Alternately, a smaller region of interest or region of experimentation around a point within the larger region of operability is defined. Generally, the region of experimentation is of a cuboidal region or a spherical region, as shown around the point *A* and point *B* respectively in Figure. 7.5.

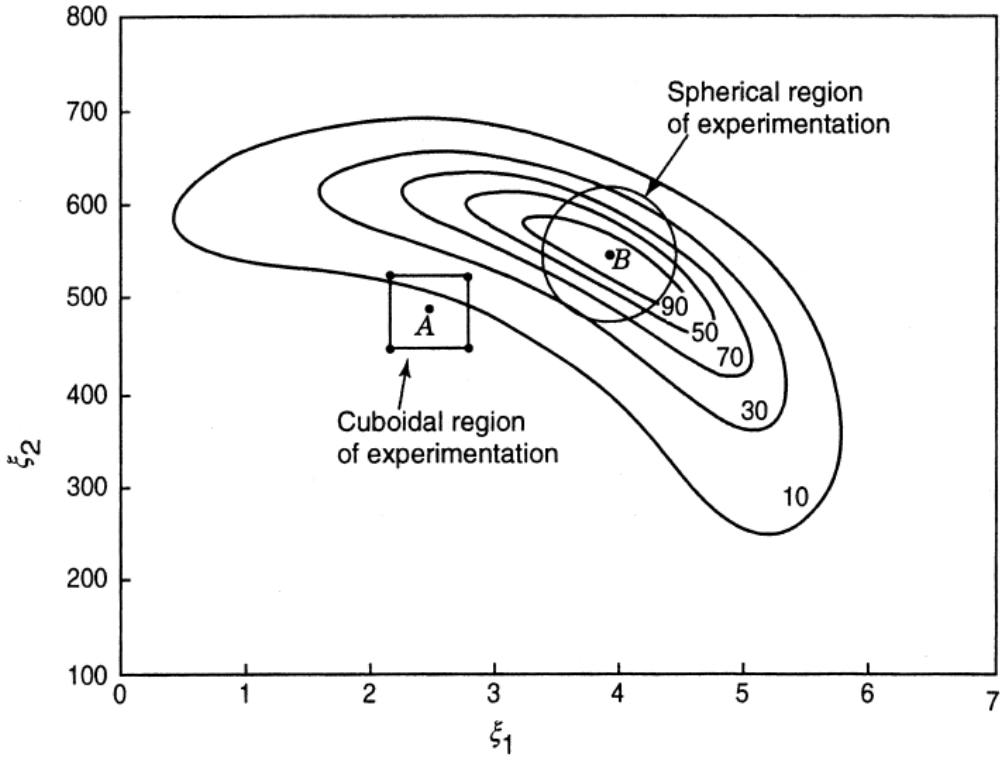

Figure 7.5. Illustration of cuboidal and spherical regions of experimentation[57]

7.3. Null Hypothesis

To assure whether a linear relationship between the response variable y and the regressor variables $(x_1, x_2, \dots, x_k)$ exists or not, the null hypothesis (H_0) is defined as follows:

$$H_0: \beta_1 = \beta_2 = \cdots = \beta_k = 0$$
$$H_1: \beta_j \neq 0 \; for \; at \; least \; one \; j \tag{7.10}$$

The null hypothesis is a general statement or default position that there is no relationship between two variables. Null hypothesis considers whether the β_js in equation 7.8, are equal to zero in a second order response model. Rejection of H_0 in Equation 7.10 implies that at least one of the regressor variables $x_1, x_2, \dots, x_k$ contributes significantly to the model. Test procedure consists of partitioning the total sum of squares $SS_T = \sum_{i=1}^{n}(y_i - \bar{y})^2$ into a model based sum of squares (regression) and a residual based sum of squares (or error). By partitioning the sums of squares we have total sums of squares as,

$$SS_T = SS_R + SS_E \tag{7.11}$$

where SS_R and SS_E are sum of squares due to the model (or regression) and a sum of squares due to residual (or error) respectively. Assuming that the null hypothesis $H_0: \beta_1 = \beta_2 = \cdots = \beta_k = 0$ is true, it can be shown that SS_E and SS_R are independent. The procedure for checking null hypothesis $(H_0: \beta_1 = \beta_2 = \cdots = \beta_k = 0)$ is to evaluate [58],

$$F_0 = \frac{SS_R/k}{SS_E/(n-k-1)} = \frac{MS_R}{MS_E} \tag{7.12}$$

where evaluation of F_0 is called F-test analysis. F-test determines how consistent results are with the null hypothesis and to calculate probabilities of observing an F_0 value that is at least as high as the value that analysis of variance (ANOVA) analysis obtained. In an ANOVA analysis reference probability is called significance level (also called P-value or α) and is chosen usually as 0.01, 0.05 or 0.1. If the p-value is less than a specified significance level (α) (usually 0.01, 0.05, or 0.1), it can be declared that the difference is statistically significant and the test's null hypothesis is rejected. In conclusion, more the P-value gets smaller, (smaller than α) , more probable to reject null hypothesis.

In almost every statistical software, this procedure is usually summarized as in Table 7.1. This kind of test is called analysis of variance, as it is based on the partitioning of the overall variability in the response (y).

Table 7.1. *Typical table of analysis of variance*

Source of Variation	Sum of Squares	Degrees of Freedom	Mean Square	F_0
Regression	SS_R	k	MS_R	MS_R/MS_E
Error or residual	SS_E	$n-k-1$	MS_E	
Total	SS_T	$n-1$		

7.4. Goodness of Fit

The coefficient of determination R^2 is defined as,

$$R^2 = \frac{SS_R}{SS_T} = 1 - \frac{SS_E}{SS_T} \tag{7.13}$$

Higher R^2 value is an indicator of a decrease in the deviation of the response, obtained by the regressor predictors $(x_1, x_2, \dots, x_k)$ in the model. R^2 lies in the $0 \leq R^2 \leq 1$ range. However, bigger R^2 does not necessarily imply that the regression

model is a satisfactory one. By adding a predictor variable to the model, R^2 always increases, regardless of whether the added predictor is statistically significant or not. Hence, it is possible for models that have large values of R^2 to yield poor predictions of new observations or estimates of the mean response, hence, it is advisable to use adjusted R^2 which statisticaly is defined as in Eqn. 7.14 [57].

$$R^2_{adj} = 1 - \frac{\frac{SS_E}{n-p}}{\frac{SS_T}{n-1}} = 1 - \frac{n-1}{n-p}(1-R^2) \tag{7.14}$$

Generally, the adjusted R^2 will not always increase as variables are added to the model. As a matter of fact, if unnecessary terms are added, R^2_{adj} often decreases.

7.5. MODEL ADEQUACY CHECKING

Adequacy of the model should always be checked. To do this, firstly, the fitted model must be examined to assure that it provides an adequate approximation to the true system and also it should be verified that none of the least squares regression assumptions are violated. Unless the model provides an adequate fit, proceeding with a fitted response surface will likely give poor or misleading results.

7.5.1. Residual Analysis

Least squares fit residuals, defined by $e_i = y_i - \hat{y}_i, i = 1,2, \dots, n$, play an important role in the evaluation of the model adequacy.

By constructing a normal probability plot of the residuals, the normality assumption of the model can be checked. The normality assumption is satisfied if the residuals plot forms an approximately a straight line. Figure 7.6 shows a normal probability plot which satisfies normality assumptions. If the normality plot indicates problems with respect to the normality assumption, the transformation of the response variable may be a remedy to this problem.

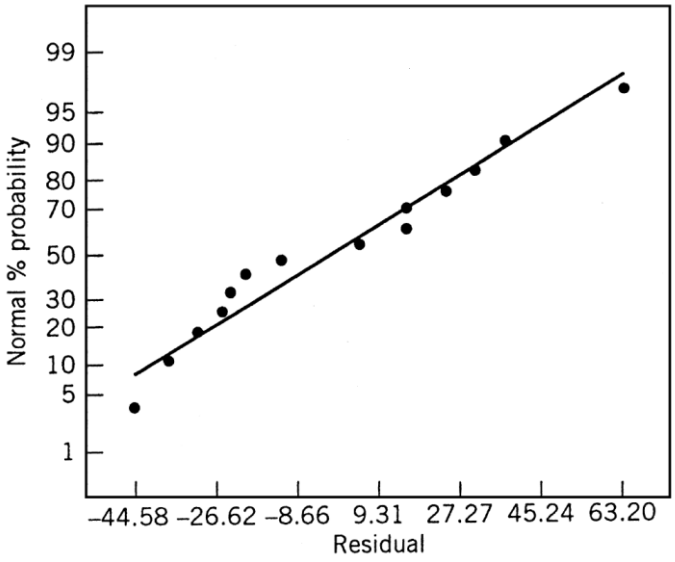

Figure 7.6. Normal probability plot which satisfies normality assumptions

7.5.2. Transformation of the Response Variable

As mentioned earlier, a data transformation may be used as a remedy when residual normality analysis fails to satisfy underlying model assumptions, such as non-normality or non-constant variance in the response variable. Often, the purposes of transformations are: 1. making the response variable more stable, 2. keeping the distribution of the response variable closer to the normal distribution and 3. enhancement of the fit of the model to the true data. Fit of the model to the true data may enhanced by the simplification of the model by canceling out higher order polynomial terms and interactions. Occasionally, using the transformation of the response variable can effectively help to accomplish more than one of the transformation objectives simultaneously.

The power family of transformations $y* = y^{\lambda}$ is very useful, where λ is the parameter of the transformation to be determined (e.g., $\lambda = 0.5$ means the use of the square root of the original response). Box and Cox (1964) [57] showed how the transformation parameter λ may be estimated simultaneously with the other model parameters (overall mean and treatment effects). The computational procedure of

their theory consists of performing a standard analysis of variance, for various values of λ, as follows:

$$y^{(\lambda)} = \begin{cases} \frac{y^{\lambda-1}}{\lambda} & \lambda \neq 0 \\ \ln y & \lambda = 0 \end{cases} \tag{7.1.5}$$

The maximum likelihood estimate of λ is defined as the value for which the error sum of squares, ($SS_E(\lambda)$) is a minimum. This value of λ is usually found by plotting a graph of $SS_E(\lambda)$ versus λ and then reading the value of λ that minimizes $SS_E(\lambda)$ from the graph. Usually, between 10 and 20 values of λ is sufficient for the estimation of the optimum value. A second iteration using a finer mesh of values can be performed if a more accurate estimate of λ is necessary.

7.6. Design for Fitting Second-Order Models

In order to fit a second-order response surface in the design variables $x_1, x_2, \ldots, x_k$. The general form of a second-order fit is given by Eqn. 7.16.

$$y = \beta_0 + \sum_{i=1}^{k} \beta_i x_i + \sum_{i=1}^{k} \beta_{ii} x_i^2 + \sum \sum_{i<j=2}^{k} \beta_{ij} x_i x_j + \varepsilon \tag{7.16}$$

In most of the practical situations, the range of the design variables are specific and strict. In other words, the region of interest and the region of operability are the same and the obvious region for the design is a square (k = 2), cube (k = 3), or hypercube ($k \geq 4$). This kind of situation occurs frequently in many areas which suggests a central composite design that eight corners of the cube are centered and scaled to ($\pm$1, $\pm$1, $\pm$1) and starpoint (α) = 1. The (0, 0, 0) at the design center indicates center runs. Figure 7.7 shows the design, often called the face-centered cube (or FCD) because the axial points occur at the centers of the faces, rather than outside the faces

as in the case of a spherical region. Alpha (α) is the distance of each axial point (also called star point) from the center in a central composite design. A value less than one puts the axial points in the cube, a value equal to one puts them on the faces of the cube and a value greater than one puts them outside the cube (Figure 7.8). Table 7.2 illustrates a three factor (K=3) FCD design of experiments in coded form.

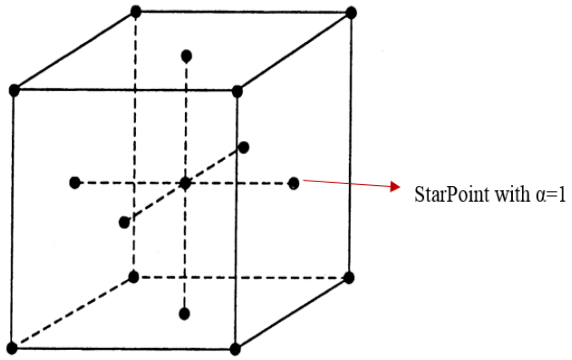

Figure 7.7. Illustration of a FCD design in cuboidal space

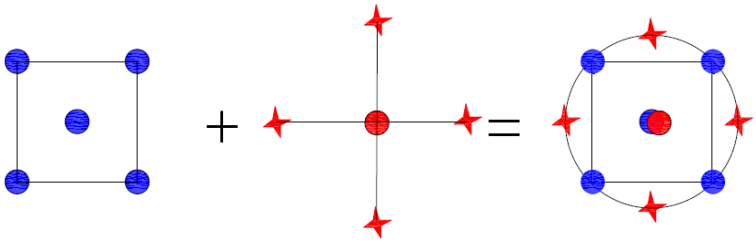

Figure 7.8. Illustration of corner, axial and star points in a composite designs

In the case of a cuboidal design region, the face-centered cube is an effective second-order design. It is important for the region to be covered in a symmetric fashion. The face-centered cube design is not rotatable. Rotatability or near-rotatability is not an important priority when the region of interest is clearly cuboidal. Rotatable designs provide constant prediction variance at all points that are

equidistant from the design center. The face-centered cube is a useful design for any number of design variables.

Table 7.2. *The coded form of a FCD design (k=3 and α= 1)*

Experiment No #	x_1	x_2	x_3
1	1	-1	-1
2	-1	1	-1
3	-1	-1	1
4	1	1	-1
5	1	-1	1
6	-1	1	1
7	1	1	1
8	-1	0	0
9	1	0	0
10	0	-1	0
11	0	1	0
12	0	0	-1
13	0	0	1
14	0	0	0

CHAPTER 8

DEVELOPMENT OF A REGRESSION MODEL FOR THE DTC PROBLEM USING XFEM ANALYSIS

8.1. Introduction

In this chapter, the development of a regression model by means of the response surface methodology is performed. As mentioned in chapter 7, in order to generate a response surface for the fatigue life of specimens with double through the thickness cracks emanating from rivet holes, it is necessary to design sequential experiments to be able to estimate the fatigue life via the regression model. There exist several methods to design experiments to predict the response behavior, however, in this study, response surface methodology (RSM) is chosen to track the fatigue life behavior. Later in this chapter, the crucial elements of the RSM design are defined; afterwards, designed experiments are analyzed using XFEM separately. Finally, calculated fatigue life results undergo ANOVA statistical analysis procedure to obtain a regression model which estimates fatigue life of specimens with double through crack emanating from rivet holes.

8.2. Definition of Independent Variables in the RSM

In order to design sequential experiments according to RSM, it is needed to define the variables which affect the response, which is fatigue life in the present study. For a specimen with double through the thickness cracks emanating from the rivet hole, the important factors which affect the fatigue life are: 1. Remote tensile load (σ) 2. Hole radius (r) 3. Load ratio (R) 4.Initial crack length (c).

8.3. Definition of Region of Operability for Independent Variables

Although independent variables are defined, yet it is necessary to define the region of operability for each variable. Each variable can take any magnitude of its unit from minus infinity to positive infinity, however, for defined variables, it would be meaningless to have such wide range. Range of each variable should be meaningful physically and permissibly.

Since the hoop stresses are about two times higher than the longitudinal stresses due to the cabin pressurization, hoop stress is the primary loading to be considered in riveted joints. Therefore, in almost all of the theoretical and experimental studies uniaxial tensile loading with near zero positive load ratio is considered [59]. Hence, the influence of the load ratio (R) is neglected in this study. The nominal maximum stress in fuselage skins is normally between 80 and 120 MPa [60], nevertheless, somewhat higher load levels than the expected load levels are used in the present study (60MPa-150MPa). Permissible rivet size diameter for load carrying structures should not be below 3/32 (2.38 mm) inches and should not exceed 1/4 (6.35mm) inches according to the FAA advisory circular (14 CFR) [61], Hence, the selected range for the rivet hole radius in this study is considered to be between 1 and 5 mm. Pre-crack length is considered to be as low as 1 mm and maximum of 5 mm. To determine the maximum length of grown crack to stop simulations in XFEM analysis, the spacing between the rivets in a pattern of riveted joints is considered as the limiting growable crack size. As can be seen from Figure 8.1, FAA suggests a rivet spacing which is three times the rivet diameter [61]. Thus in this study the biggest diameter used for the rivet hole is picked to decide on the maximum crack growth (3x10 =30 mm).

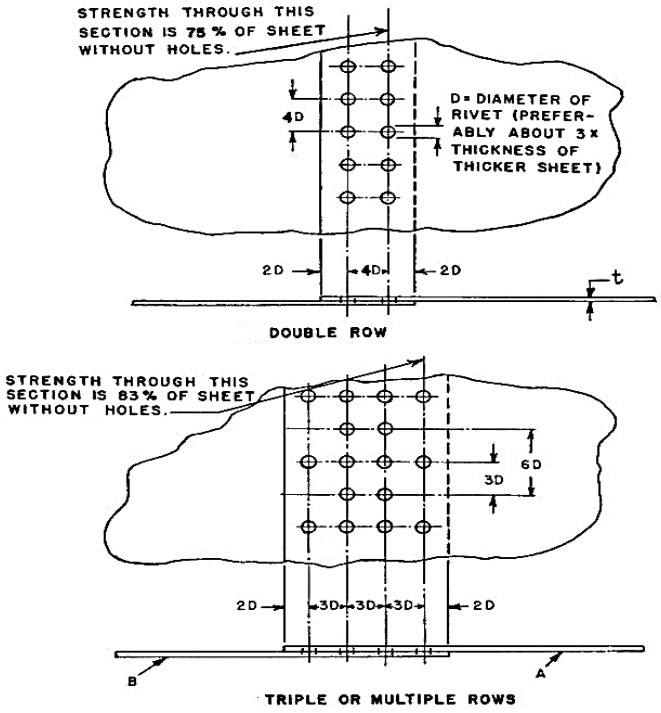

Figure 8.1. FAA recommendation on rivet spacing

8.4. FCD Design of Experiments

The general characteristics of central composite designs are discussed in chapter 7. Here, a closer look to this type of designs is given. A Box-Wilson central composite design, which is called central composite design (CCD), is often used for developing a second-order polynomial for the response variables in response surface methodology without using a whole set of full factorial design of experiments. To obtain the coefficients of a polynomial with quadratic terms, the experimental design must have at least three levels of each independent variables. There are three different points in a CCD design, namely axial points, factorial points and central points. Factorial points are corners points of an n-dimensional cube, coming from the full or fractional factorial design where the factor levels are coded to –1, + 1. Center of the design space is called “Central” point. Axial points are symmetrically located on the axes of the coordinate system with respect to the central point at a distance α

from the design space center. There exist two main types of Central Composite Designs, namely face-centered CCD (FCD) and rotatable CCD. In FCD, a k factor three-level experimental design requires 2^k + 2 k + C experiments, where k is the number of factors, 2^k points are in the corners of the cube representing the experimental domain, 2k axial points are in the center of each face of the cube [(± α, 0,…0), (0, ± α,...0),… (0, 0,… ± α)] and C points are the replicates in the center of the cube that are necessary to estimate the variability of the experimental measurements. Center points test the lack-of-fit or curvature for the model. Figure 8.2 illustrates the three-level three-factor FCD design. In this Figure, black points are factorial points located at the vertices of the cube, red point is central point of the design space, and the blue points are the axial points located symmetrically with respect to the coordinate system and stand at a length of unity (α =1) from the center of the design space. In this FCD design with three-factors, there exist eight factorial points and six center runs, six axial points (2 × 3) which in total it necessitates a total of twenty runs.

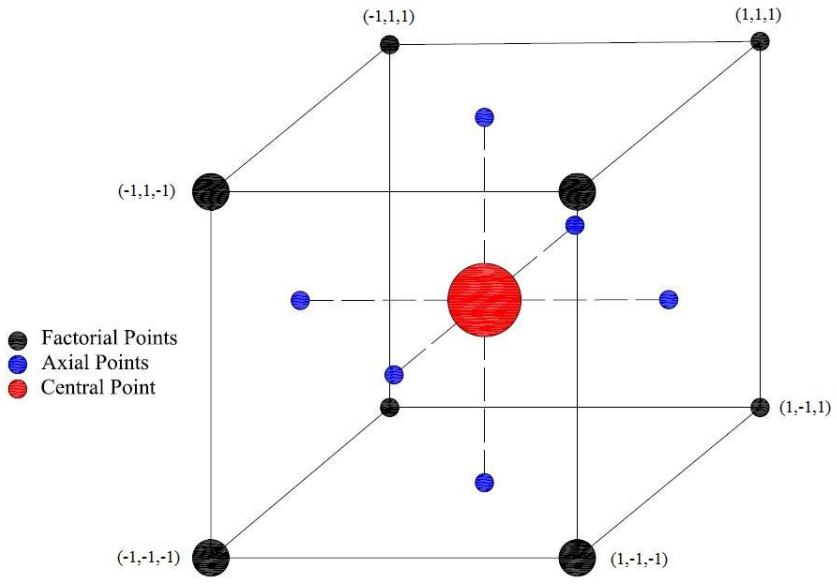

Figure 8.2. Illustration of a three factor FCD design of experiments with coded factors

For the DTC problem, Table 8.1 shows the region of operability for independent factors and their extremes in coded and un-coded formats.

Table 8.1. *Three factor FCD design with coded extremes*

Factors	-1	0	+1
Tensile Load (σ) (MPa)	60	105	150
Rivet Hole Radius (r) (mm)	1	3	5
Crack Length (c) (mm)	1	3	5

Table 8.2. *FCD experiments by using MINITAB*

Experiment ID	σ	c	r
1	60	1	1
2	105	5	3
3	105	3	3
4	150	3	3
5	105	3	3
6	150	1	5
7	105	1	3
8	105	3	1
9	60	3	3
10	150	5	1
11	60	5	5
12	105	3	3
13	105	3	3
14	150	5	5
15	60	1	5
16	60	5	1
17	150	1	1
18	105	3	5
19	105	3	3
20	105	3	3

Since the hoop stress in pressurized cabins of aircraft rarely exceeds 150 MPa and drops below 60 MPa, in this study tensile stress range has been chosen between 60 MPa and 150 MPa. The rivet hole radius is chosen between 1 mm and 5 mm as mentioned in the FAR maintenance and repair handbook. Rivet joint pattern dictates the spacing between two rivets. Hence, maximum crack propagation length is taken as 30 mm. In order to design and analyze the sequential FCD experiments to obtain the regression model for prediction of fatigue life for the double through the thickness crack problem, MINITAB statistical package [62] is employed. Table 8.2, shows the designed experiments by MINITAB.

Experiments 3, 5, 12, 13, 19 and 20 are identical as they are center points. Moreover, experiments 2, 4, 7, 8, 9 and 18 are located at the face centers of cuboidal design field as axial points and finally, experiments 1, 6, 10, 11, 14, 15, 16 and 17 are located at the vertices of cuboidal design field and belong to factorial points.

8.5. XFEM Analysis of the Designed Experiments

In this section, XFEM based analyses results of twenty experiments discussed in the previous section are presented. Fundamentals of XFEM analysis and also fatigue crack growth using XFEM are explained in detail in chapter four and six respectively. The general geometry for all cases of experiments are same except the independent variables which vary case by case. Figure 8.3 represents the geometry used in the XFEM analyses.

To check the convergence for the modeled finite element geometry, the smallest rivet hole radius (r=1 mm) and initial crack length (c=1 mm) in the operability region is considered. Three element sizes of 0.25mm, 0.1mm, and 0.05mm in the plane of the crack is considered to check the convergence of calculated stress intensity factors. Figure 8.4 shows the equivalent contours for different mesh sizes at the distance of 0.5 mm ahead of the crack tip. Table 8.3 gives the stress intensity factor variation for different mesh sizes at the equivalent distance of 0.5 mm ahead of the crack tip for different crack lengths. As can be seen from Table 8.3, mesh size

of 0.25 mm shows reasonable convergence and gives closer stress intensity values compared to Bowie's solution with finite width correction. Although the convergence at smaller size at the tenth contour is better, in the present study for the rest of the analyses 0.25 mm mesh size is used to reduce the computational time of the analyses.

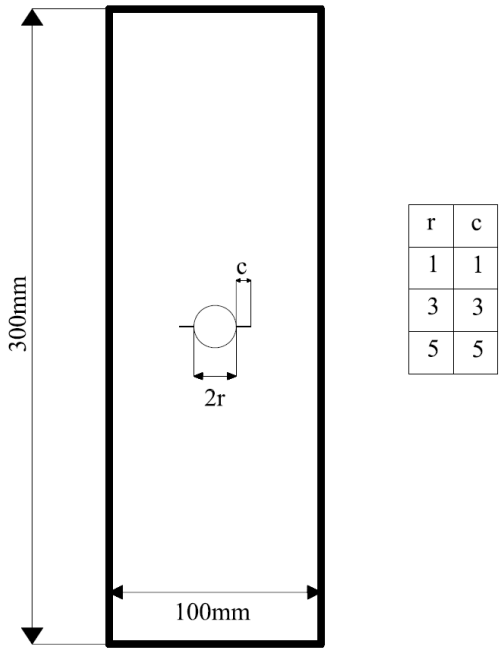

Figure 8.3. Geometry used to model in XFEM for the FCD test scenarios (only r and c are changing)

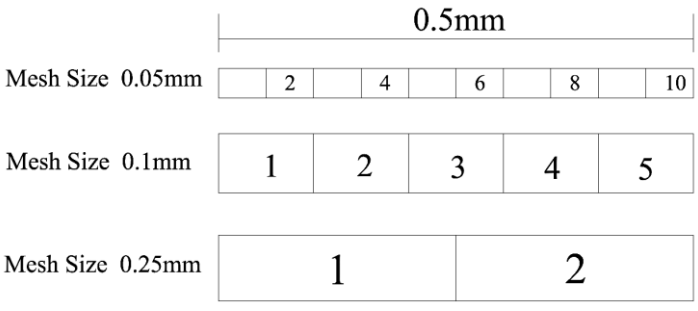

Figure 8.4. Equivalent contours for different mesh sizes at the distance of 0.5 mm ahead of the crack tip

Table 8.3. Stress intensity factor variation through different mesh sizes at the equivalent distance

Crack Length (mm)	0.05 mm mesh size SIF at contour 10	0.1 mm mesh size SIF at contour 5	0.25 mm mesh size SIF at contour 2	BOWIE with finite width correction factor
1	345	342	324	295
2	397	395	375	353
3	444	442	421	407
4	487	485	464	456
5	528	526	504	501
6	565	564	541	544
7	602	600	577	584

Figures 8.5-8.8 give the crack length versus stress intensity factor for different mesh sizes of crack plane for different contours from contour 1 to contour 9. Figure 8.8 gives the average stress intensity factor of contours 4-7 versus the crack length. From Figures 8.5-8.8, it is seen that for short crack lengths up to 7 mm, except for the first two contours, stress intensity factors calculated using contour integrations are very similar for other crack lengths. It is also observed that beyond the crack length of 6 millimeters, the contour values of stress intensity factor are more or less stable and they do not vary with respect to Bowie's solution. The difference from Bowie's solution remains constant for larger crack lengths. As a conclusion from Figures 8.5-8.8, one can infer that after contour 2, the stress intensity factors for a specific crack length remains stable. In this study, as mentioned before, the stress intensity factors of contours 4-7 are averaged to be used in life predictions. The reason for the variation of the calculated SIFs may root from the singularity region around the crack tip at very early stages of the crack growth. As mentioned earlier, an APDL code is developed for XFEM analysis (See Appendix D). Stress intensity factors are calculated by performing XFEM analysis on FCD experiments and the

fatigue life is calculated by employing a developed code in MATLAB for the integration of the Forman model. Table 8.4 shows the obtained fatigue lifes obtained for the FCD experiments.

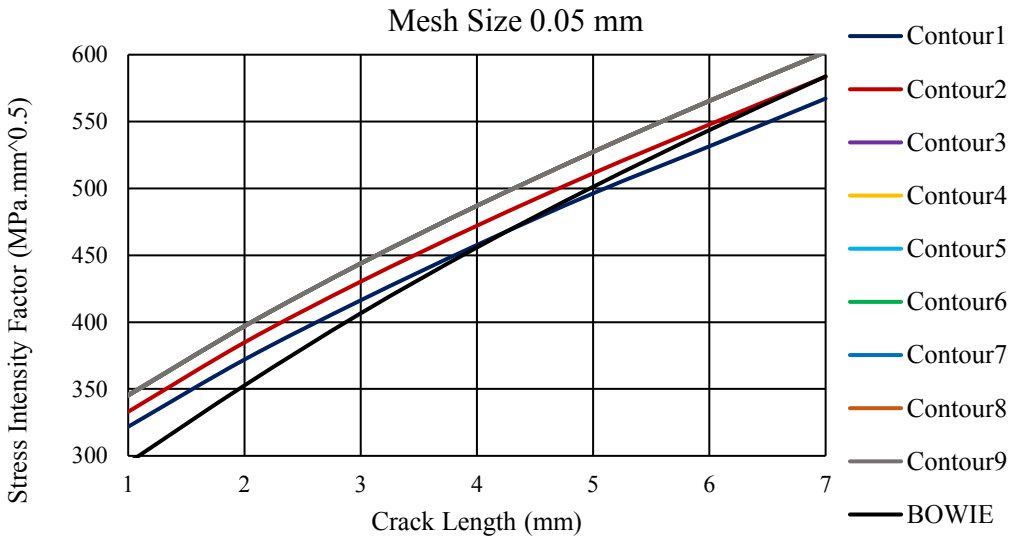

Figure 8.5. Comparison of stress intensity factor deviation from Bowie's solution with finite width correction factor for the 0.05 mm mesh size.

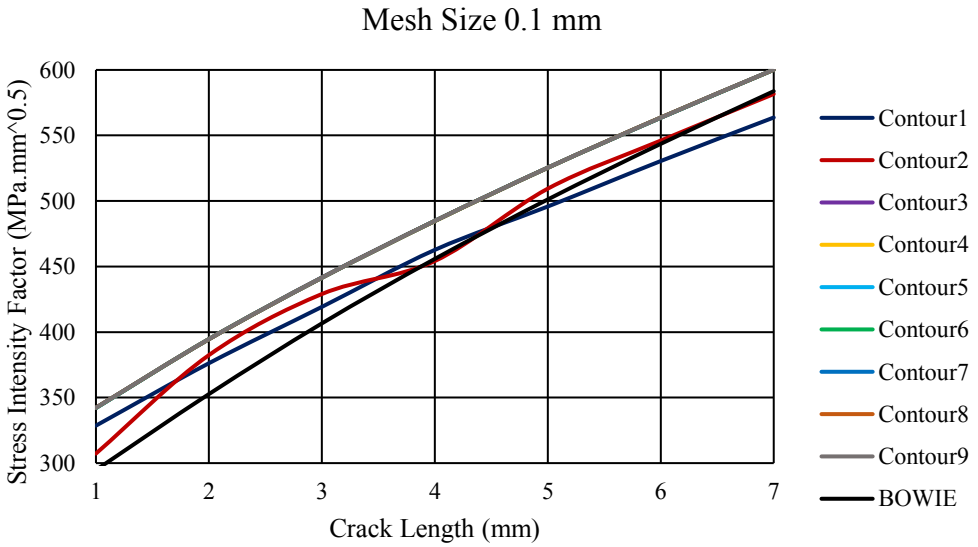

Figure 8.6.. Comparison of stress intensity factor deviation from Bowie's solution with finite width correction factor for the 0.1 mm mesh size.

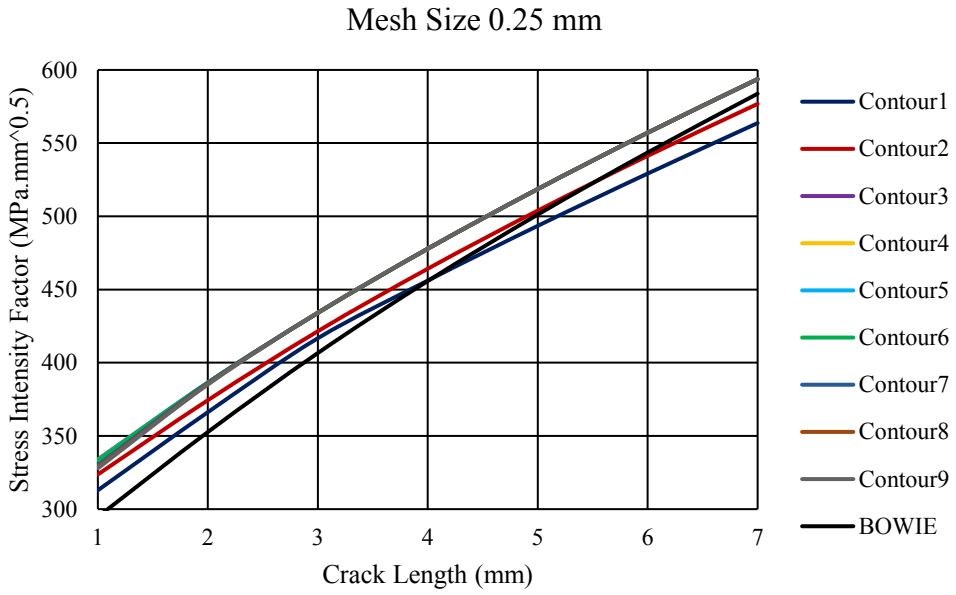

Figure 8.7. Comparison of stress intensity factor deviation from Bowie's solution with finite width correction factor for the 0.25 mm mesh size.

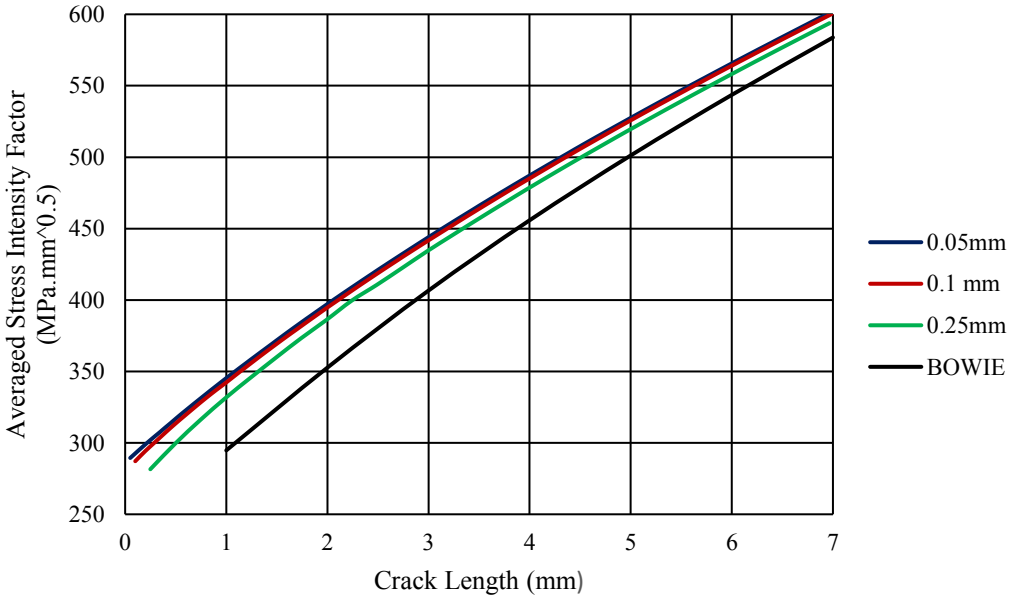

Figure 8.8. Comparison of averaged stress intensity factors (contour 4 through 7) deviation from Bowie's solution with finite width correction factor for different mesh sizes.

Table 8.4. *Calculated fatigue life using XFEM for the designed RSM experiments*

Run Order	σ (MPa)	c (mm)	r (mm)	Life (Cycles)
1	60	1	1	**1172540**
2	105	5	3	**18780**
3	105	3	3	**28417**
4	150	3	3	**6356**
5	105	3	3	**28417**
6	150	1	5	**5901**
7	105	1	3	**47868**
8	105	3	1	**53714**
9	60	3	3	**277468**
10	150	5	1	**6912**
11	60	5	5	**120307**
12	105	3	3	**28417**
13	105	3	3	**28417**
14	150	5	5	**2570**
15	60	1	5	**258723**
16	60	5	1	**258723**
17	150	1	1	**29313**
18	105	3	5	**16964**
19	105	3	3	**28417**
20	105	3	3	**28417**

As explained earlier, it should be noted that calculated fatigue life is the life corresponding to a crack length of thirty millimeters for all cases of the experiments.

8.6. ANOVA Analysis of RSM Experiments

Using the fundamentals discussed in detail in chapter 7, obtained fatigue life results of XFEM analyses are evaluated by the ANOVA analysis to develop a regression model for the fatigue life in terms of cycles. MINITAB software [62] is employed to conduct ANOVA analysis for the RSM experiments. In the first attempt to develop a

regression model, it is observed that using the original response results in a poor model; however, by transforming the original response a highly correlated model is obtained. The optimal value of λ for transforming the response data is obtained by the Equation 8.5.1 which is also mentioned in chapter 7.

$$y^{(\lambda)} = \begin{cases} \dfrac{y^{\lambda-1}}{\lambda} & \lambda \neq 0 \\ \ln y & \lambda = 0 \end{cases} \tag{8.6.1}$$

The optimal λ is obtained from ANOVA analysis conducted by MINITAB as -0.0699432. Table 8.5 gives the R^2 and R^2_{adj} of the model.

Table 8.5. *Comparison of R^2 and R^2_{adj} of the transformed response*

	$\lambda = 0.0699432$
$R^2(\%)$	99.97
$R^2_{adj}(\%)$	99.95

By choosing $\lambda = -0.0699432$ and transforming the response (Fatigue Life) analysis of variance is conducted. Afterwards, using the MINITAB software, a regression model is obtained. Table 8.6 shows the ANOVA results.

In Table 8.6, DF stands for the degree of freedom. Degrees of freedom encompasses the notion of limits on the estimation of the parameters. Typically, the degree of freedom is equal to sample size (in this study there are 20 cases) minus 1. By increasing the sample size, more information about the population will be provided and this increases the total DF. On the other hand, increasing the number of terms in the model uses more information, and this decreases the total DF available to estimate the variability of the parameter estimates. Minitab partitions the DF for the

error if two conditions are satisfied. In the first condition, there should exist terms in which the data can be fit with the data that are not included in the current model.

Table 8.6. *ANOVA results of RSM experiments*

Source	DF	Adj SS	Adj MS	F-Value	P-Value
Model	9	0.047336	0.005260	3883.17	0.000
Linear	3	0.046292	0.015431	11392.55	0.000
σ	1	0.038967	0.038967	28769.79	0.000
r	1	0.004195	0.004195	3097.32	0.000
c	1	0.003130	0.003130	2310.55	0.000
Square	3	0.000739	0.000246	181.76	0.000
σ*σ	1	0.000244	0.000244	180.10	0.000
r*r	1	0.000012	0.000012	**8.75**	**0.014**
c*c	1	0.000011	0.000011	**7.96**	**0.018**
2-Way Interaction	3	0.000306	0.000102	75.20	0.000
σ*r	1	0.000092	0.000092	68.01	0.000
σ*c	1	0.000070	0.000070	51.96	0.000
r*c	1	0.000143	0.000143	105.63	0.000
Error	10	0.000014	0.000001		
Lack-of-Fit	5	0.000014	0.000003	*	*
Pure Error	5	0.000000	0.000000		
Total	19	0.047349			

For instance, having a regressor with two or more distinct values, one may estimate a quadratic term for that predictor. If the model does not consist of any quadratic term, then there is no term to fit data in the model which results in satisfying the first condition. Existence of replicates in the data introduces the second condition. For example, if there exist three observations where value of predictors are same in all of the three observations, then those three observations are replicates. If the two conditions mentioned above are met, then DF partitions into two parts for the error

namely, the lack-of-fit and pure error. The DF for the lack-of-fit allows a test of whether the model form is adequate or not. The lack-of-fit test uses the degrees of freedom for the lack-of-fit. The more DF for pure error, the greater the power of the lack-of-fit test. Existence of the lack of fit term in the source column in Table 8.6, means that regression model fails to adequately describe some of the data. Lack of fit occurs in two cases. 1. When important terms such as interactions or quadratic terms are not included in the model. 2. If several unusually large residuals appear by fitting the model to the data. In case of existing lack of fit in ANOVA analysis, to check the accuracy of the model, P-value of individual terms of the model according to the analysis significant value (α) may be checked. If the P-value falls smaller than the significance value, then it means that the relevant term is significant. As can be seen in Table 8.6 (bold P-values), c*c and r*r terms are less significant in the regression model. Moreover, F-value is closely related to the P-value. The F-value is the statistic test used to determine whether a term in the regression model is associated with the response. Minitab uses the F-value to calculate the P-value, which helps to make a decision about the statistical significance of the terms and model. In brief, a sufficiently large F-value indicates that the term or model is significant. Generally, minimum F-value is unity and bigger F-value shows higher contribution of a term to the model. Insignificant terms according to F-value are in bold character in Table 8.6. To check the normality assumption, least square residuals plot should form an approximately straight line. Figure 8.6 and Figure 8.7 show the normal probability plot and residuals occurance histogram respectively. Figure 8.8 illustrates the residuals per each experiment.

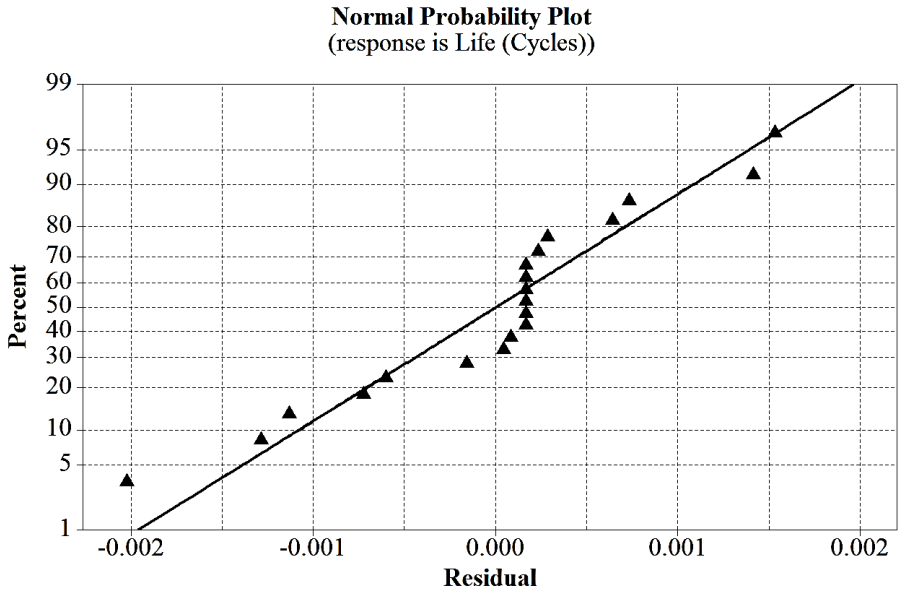

Figure 8.9. Normal Probability Plot

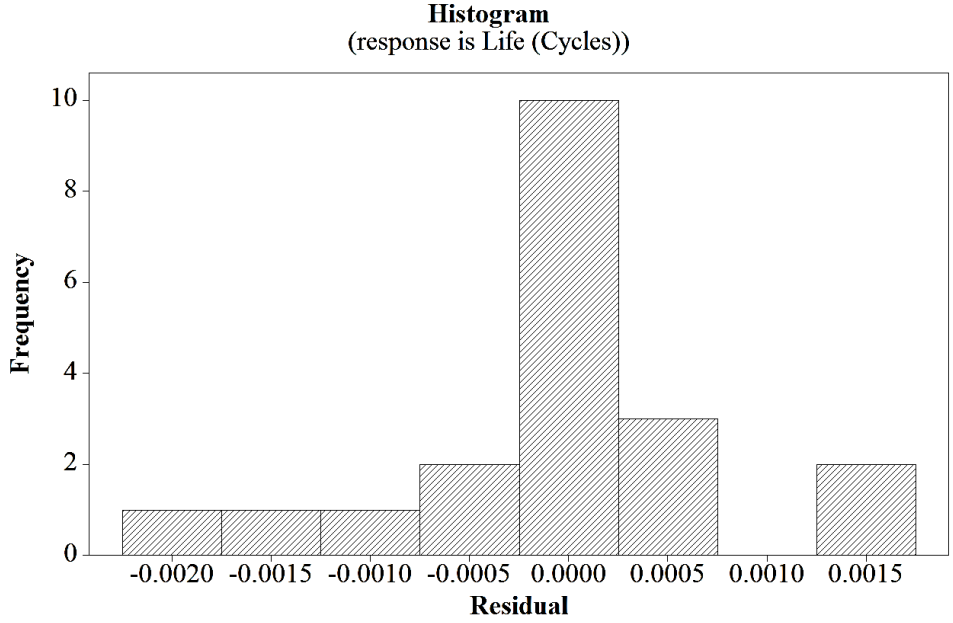

Figure 8.10. Residuals Histogram

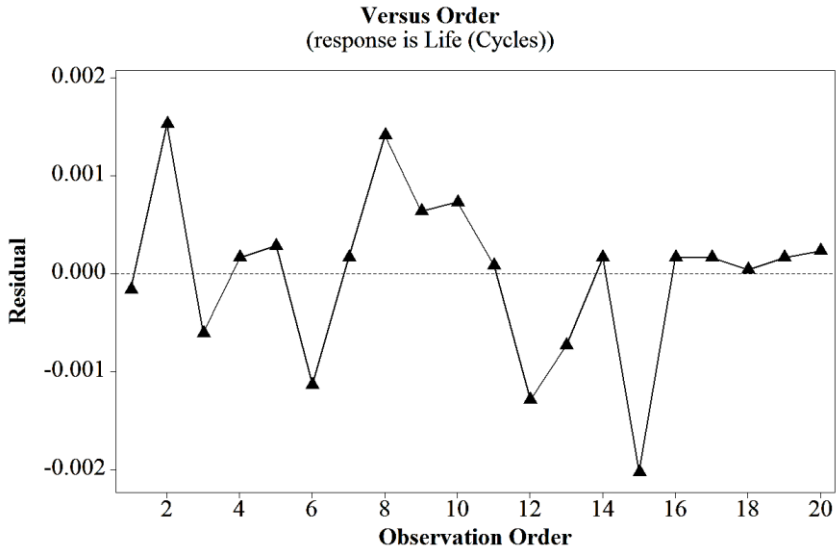

Figure 8.11 Residuals of each experiment

By considering the normal probability in Figure 8.6, it can be clearly observed that a linear distribution of residuals exists and this confirms the normality assumption of the ANOVA analysis. Furthermore, histogram of the residuals in Figure 8.7 also shows a well-balanced distribution of residuals around zero. These three graphs together are a measure for showing a well-established regression model. It should be noted that there are three outliers in the residual plot which belongs to experiments 8 11 and 17. These three outliers introduce lack of fit to the model. Table 8.7 shows the related experiments in which lack of fit arises and Table 8.8 shows the residual characteristics of unusual observations.

Table 8.7. *Unusual Observation in the fitted data*

Experiment #	Life (Cycles)	Fit	$\left[1-\frac{Fit}{XFEM}\right]*100$
17	29313	28124	4.0
11	120307	125445	-4.2
8	47868	50911	-6.35

Table 8.8. *Residual characteristics of Unusual Observations*

Experiment #	$-Life\ (Cycles)^{-00699432}$	Fit	Residual	Std Residual
17	-0.487034	-0.488447	0.001413	2.67
11	-0.441233	-0.439945	-0.001289	-2.43
8	-0.470612	-0.468587	-0.002024	-2.44

Another check for the significance level of each term in the regression model can be made by the *Pareto* chart. The Pareto chart represents the absolute values of the standardized effects from the largest effect to the smallest effect. The standardized effects are t-statistics that test the null hypothesis that the effect is 0. The chart also plots a reference line to indicate which effects are statistically significant. By using this chart, the magnitude and the importance of the effect of each term used in the regression model can be determined. Figure 8.9 depicts the *Pareto* chart for this study.

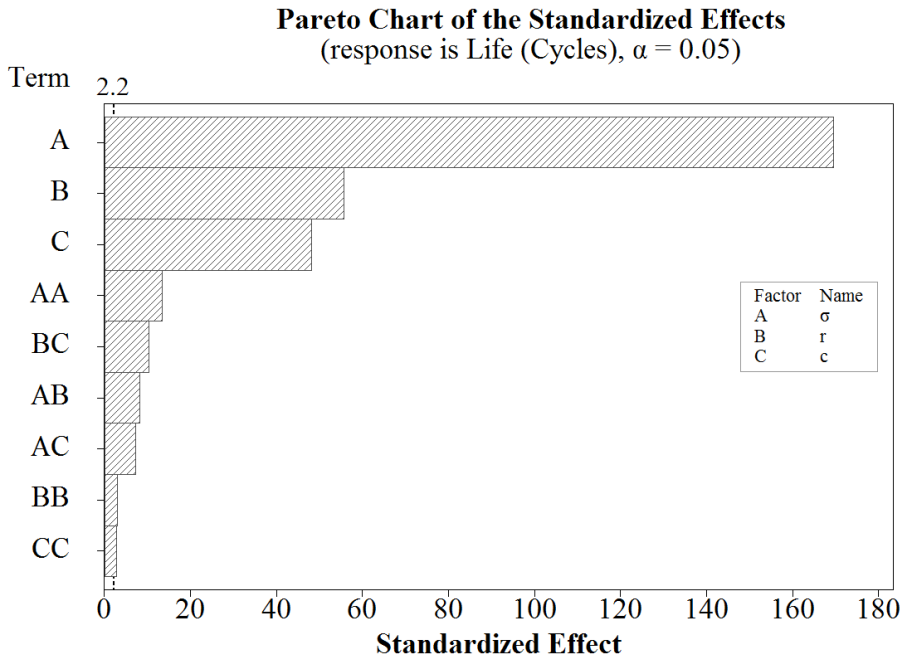

*Figure 8.*12. Pareto chart of the standardized effects

The most insignificant terms are $\sigma * c$ and $\sigma * r$. Less significance character of these terms were identified previously using the P-value and the F-value. However, σ is the most significant term in the model and c and r terms also have high significance level in the model. Developed regression model for prediction of double through the thickness cracks emanating from rivet holes under constantant amplitude loading is given by Equation 8.5.2.

$$-Life\ (Cycles)^{-0.0699432} = \begin{matrix} \text{-0.23768 - 0.002152 σ - 0.01257 r} \\ \text{- 0.01153 c + 0.000005 σ*σ} \\ \text{+ 0.000519 r*r + 0.000495 c*c -} \\ \text{0.000038 σ*r - 0.000033 σ*c} \\ \text{+ 0.001057 r*c} \end{matrix} \quad (8.6.2)$$

Fatigue lifes are transformed using the optimum λ prior to ANOVA analysis and finally the developed regression model given in Equation 8.5.2 is obtained. In order to check the accuracy of the model, some random configurations from the region of operability of the variables are selected to compare with the fatigue life results obtained by XFEM analysis of SIFs and fatigue life evaluation via Forman's equation. Table 8.9 shows the comparison of the regression model with the XFEM based analysis.

From Table 8.9, selected verification points form designed experiments represent a maximum of 2.67 percent difference from XFEM based results. Moreover, other points are selected randomly from design field to verify the model with XFEM results. Table 8.10 represents the response of developed model to ten different randomly selected points in the design space.

Table 8.9. Verification of the regression model with selected designed experiments

Verification case#	σ (MPa)	r (mm)	c (mm)	Model (Cycles)	XFEM (Cycles)	Difference (%) $(1-\frac{Model}{XFEM})100$
1	105	5	3	16861	16964	0.60
2	150	3	3	6409	6356	-0.83
3	150	1	5	7023	6912	-1.60
4	60	3	3	275255	277468	0.79
5	150	5	1	5925	5901	-0.40
6	60	5	5	121445	120307	-0.94
7	150	5	5	2564	2570	0.23
8	60	1	5	296823	299747	0.97
9	60	5	1	257879	258723	0.32
10	150	1	1	29189	29313	0.43

Table 8.10. Verification of the regression model with randomly selected points on the design field

Verification case#	σ (MPa)	c (mm)	r (mm)	Model (Cycles)	XFEM (Cycles)	Difference (%) $(1-\frac{Model}{XFEM})100$
1	65	2	1.5	464459	457600	-1.49
2	85	2.5	1.75	120801	119000	-1.51
3	105	3	2	38890	38707	-0.47
4	125	3.5	2.5	13791	13953	1.16
5	145	4	3	5724	5888	2.78
6	75	2	1.5	263526	262840	-0.26
7	100	2.5	1.75	60989	61123	0.21
8	95	3	2	59440	58738	-1.19
9	115	3.5	2.5	19592	19447	-0.74
10	135	4	3	7647	7711	0.83

Developed response surface plots by holding one of the variables constant are plotted separately in Figure 8.10 through Figure 8.12. In these figures the curvature of the response surface is depicted. Variation of surface curvature by varying two factors and keeping the third factor constant, shows how the model behaves in the boundaries of the design field.

In Figure 8.10, Figure 8.11 and Figure 8.12 the logical expectations are easily observable. Minimum *r* and minimum c (Figure 8.10), maximum σ and minimum *c* (Figure 8.11) and maximum σ and minimum *r* (Figure 8.12) result in highest fatigue life.

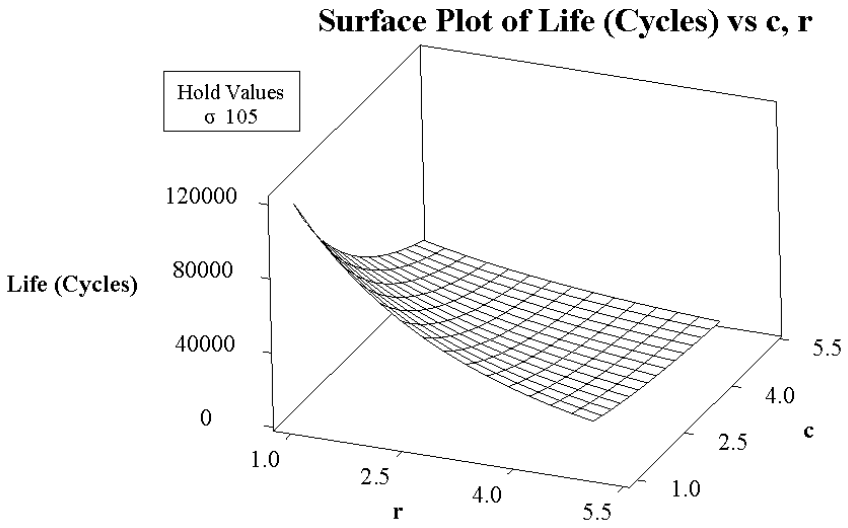

Figure 8.13. Fatigue life Surface plot for σ=105

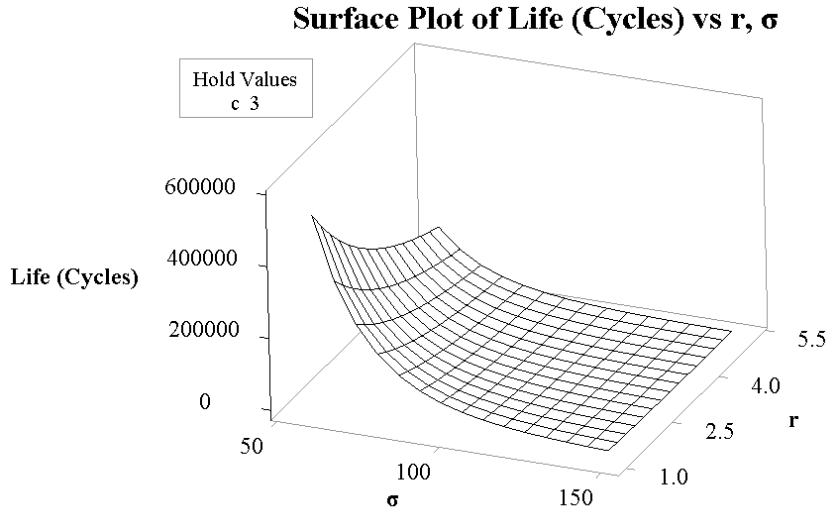

Figure 8.14. Fatigue life Surface plot for c=3

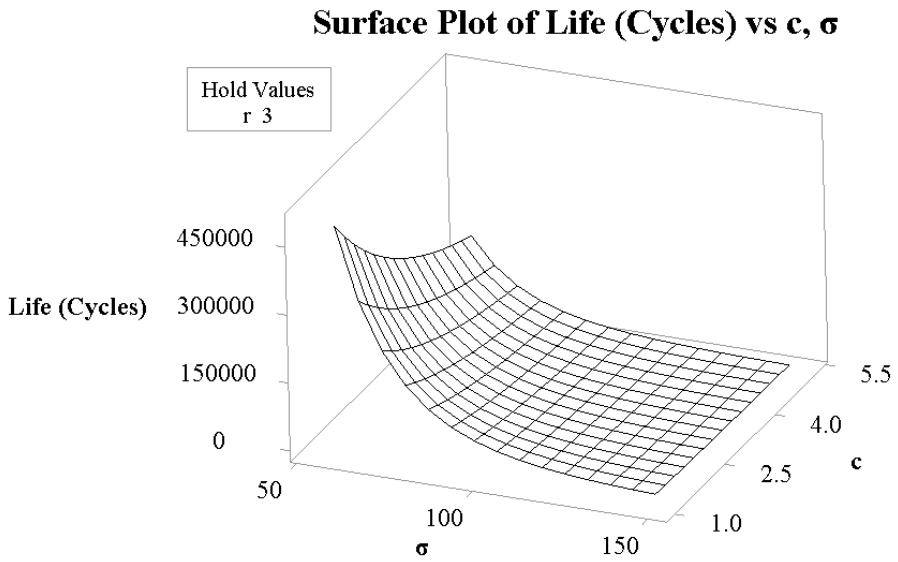

Figure 8.15. Fatigue life Surface plot for r=3

CHAPTER 9

CONCLUSION AND FUTURE WORK

In this thesis, experimental test data of DTC specimens are employed to extract necessary parameters for fatigue crack growth model to predict life of open-hole specimens. Numerical and analytical methods are used for the calculation of stress intensity factors in the open-hole specimens with the double through the thickness crack geometry. XFEM is applied in the numerical part of the study to model the geometry and obtain the SIFs through the crack growth using the Ansys Parametric Design Language. In XFEM, the need for re-meshing the model after every crack interval is not needed thanks to its integrated virtual nodes which give extra freedom to compensate kinks and jumps due to the created new crack surfaces after the crack growth. This advantage enhances the mesh quality during crack advancement, improves the accuracy of the calculated SIFs and reduces the processing time to solve the problem. In traditional finite element method, it is impossible to solve a crack growth problem in one shot. Results of XFEM are verified using the AFGROW program which is a Damage Tolerance Analysis tool developed in United States Air Force laboratories. This tool is well-known in the fracture mechanics field and especially in the Aerospace industry. AFGROW uses the analytical methods to calculate SIFs and grow the defined crack for specific crack configurations available in its library. Comparisons are made between AFGROW and XFEM and a good correlation is observed. Finally, a regression model is developed using Response Surface Methodology. Obtained regression model is verified with XFEM results with good agreement.

This work is dedicated to one of the on demand problems of fatigue crack growth in the aerospace industry; specifically to indigenous approaches to investigate different damage scenarios to establish new models and predictive tools that result in the enhancement and acceleration of on-demand design and revisions in the industry.

Another outcome of this work is concerned with maintenance and repair routines of the fleet. By employing the results of this work, it is conveniently possible to predict the remaining life of the damaged panels with DTC emanating from the rivet holes. Nevertheless, extension of this work to cover more damage cases is of crucial importance for the widespread use of the predictive models. Through this study, XFEM method is used for the crack growth analysis to determine the stress intensity factors. It is shown that the XFEM results are in good correlation with analytical results of Bowie for the DTC problem. Moreover, it is also shown that XFEM is roughly twenty percent more conservative than experimental studies due to plasticity effect which retards crack growth in the experiments.

The developed regression model using the response surface methodology at the end of this study shows an acceptable agreement with XFEM results. This model is advantageous as it eliminates the tedious task of model preparation and solving of the problem using FEA software for different configurations of the same problem.

In future, it is intended to establish damage prediction tool with a wide range of damage cases consisting of metallic and composite materials library with a user interface to allow design engineers or maintenance technicians to evaluate the probable damage life and service life of damaged parts in an aircraft. This tool will considerably save time and money and it is a good alternative to numerous costly and tedious tasks of experimental setups or finite element model preparation and analyses.

REFERENCES

[1] Brian Cotterell, "Fracture and Life," *Imperial College Press*, vol. 469, no. 1, pp. 21-38, 2010.

[2] T. Dalgleish *et al.*, "Aviation Maintenance Technician Handbook," *FAA*, vol. 136, no. 1, pp. 23–42, 2008.

[3] A. A. Griffith, "The Phenomena of Rupture and Flow in Solids," *Philos. Trans., R. Soc. Lond.*, vol. 221, p. 163, 1920.

[4] C. E. Inglis, "Stresses in a Plate due to the Presence of Cracks and Sharp Comers," *Proc. Inst. Nav. Archit.*, 1913.

[5] G. R. Irwin, "Analysis of Stresses and Strains Near the End of a Crack Traversing a Plate," *Trans. ASME, J. Appl. Mech.*, vol. 24, p. 361, 1957.

[6] A. . Griffith, "The Phenomena of Rupture and Flow in Solids," *Philos. Trans. R. Soc. London*, vol. 221, pp. 163–198, 1921.

[7] G. R. Irwin, "Fracture Dynamics," *Fract. Met. ASM*, pp. 147–166, 1948.

[8] E. Orowan, "Fracture and Strength of Solids," *Rep. Prog. Phys.*, vol. 12, pp. 185–232, 1949.

[9] P. C. Paris, M. P. Gomez, and W. E. Anderson, "A Rational Analytic Theory of Fatigue," *Trend Engin., Univ. Wash*, pp. 9–14, 1961.

[10] P. C. Paris, "The Fracture Mechanics Approach to Fatigue," *Syracuse Univ. Press*, pp. 107–132, 1964.

[11] O. L. Bowie, "Analysis of an infinite plate containing radial cracks originating at the boundary of an internal circular hole," *J. Math. Physic.*, pp. 60–71, 1956.

[12] P. C. Paris and G. C. Sih, "Stress analysis of cracks," *ASTM STP*, pp. 30–83, 1965.

[13] N. J. Forman R G, Shivakumar V, "Development of the NASA/FLAGRO computer program for analysis of airframe structures," *Advanced Structural Integrity Methods for Airframe Durability and Damage Tolerance, Part 2*, 1994, pp. 277–288.

[14] J. J. C. Newman, "A Crack Opening Stress Equation for Fatigue Crack Growth," *Int.J. Fract*, vol. 24, no. 3, pp. R131–R135, 1984.

[15] J. Harter and A. Litvinov, "About AFGROW," 2015. [Online]. Available: www.afgrow.net.

[16] J. C. Newman, E. L. Anagnostou, and D. Rusk, “Fatigue and crack-growth analyses on 7075-T651 aluminum alloy coupons under constant- and variable-amplitude loading,” *Int. J. Fatigue*, no. 62, pp. 133–143, 2014.

[17] P. C.J, A. R.R, and W. P, “A Modern Family of Crack Tip Elements for MSC/NASTRAN,” in *MSC/NASTRAN User’s Conference*, 1986.

[18] D. Swenson and M. James, “FRANC2D/L: A Crack Propagation Simulator for Plane Layered Structures,” 1997.

[19] “Franc 2D/L and Casca: A Crack Propagation Simulator and Pre-processor program, Cornell Version.” [Online]. Available: http://www.cfg.cornell.edu/index.htm.

[20] M. B. SAYAR, “Determination of Stress Intensity Factors In Cracked Panels Reinforced With Rivetted Stiffeners,” 2012.

[21] N. Moes, J. Dolbow, and T. Belytschko, “A finite element method for crack growth without re-meshing,” *Int. J. Numer. Methods Eng.*, vol. 46, no. 1, pp. 131–150, 1999.

[22] A. Hansbo and P. Hansbo, “A finite element method for the simulation of strong and weak discontinuities in solid mechanics,” *Comput. Methods Appl. Mech. Eng.*, vol. 193, no. 33–35, pp. 3523–3540, 2004.

[23] E. Giner, N. Sukumar, J. Tarancon, and F. Fuenmayor, “An Abaqus implementation of the extended finite element method,” *Eng. Fract. Mech.*, vol. 76, no. 3, pp. 347–368, 2009.

[24] J. Melenk and I. Babuska, “The Partition of Unity Finite Element Method: Basic Theory and Applications,” *Comput. Methods Appl. Mech. Eng.*, no. 39, pp. 289–314, 1996.

[25] J. J. Remmers, R. de Borst, and A. Needleman, “The Simulation of Dynamic Crack Propagation using the Cohesive Segments Method,” *J. Mech. Phys. Solids*, no. 56, pp. 70–92, 2008.

[26] J. H. Song, P. M. A. Areias, and T. Belytschko, “A Method for Dynamic Crack and Shear Band Propagation with Phantom Nodes,” *Int. J. Numer. Methods Eng.*, no. 67, pp. 868–893, 2006.

[27] Q. Duan, J.-H. Song, T. Menouillard, and T. Belytschko, “Element-local Level Set Method for Three-Dimensional Dynamic Crack Growth,” *Int. J. Numer. Methods Eng.*, no. 80, pp. 1520–1543, 2009.

[28] A. Bergara, J. I. Dorado, A. Martín-Meizoso and J. M. Martínez-Esnaola, “Fatigue crack propagation at aeronautic engine vane guides using the extended finite element method (XFEM),” *Mechanics of Advanced Materials and Structures,* 2019.

[29] J. B. Marques, S.M.O. Tavares, and P.M.S.T. de Castro, “Analysis of Mode II and Mixed Mode I-II in Fracture and Fatigue: A Numerical and Experimental Study,” *Material Design and Applications,* pp.403-423, 2018.

[30] H. Dirik and T, Yalçinkaya, “Crack path and life prediction under mixed mode cyclic variable amplitude loading through XFEM,” *Int. J. Fatigue*, no. 114, pp. 34-50, 2018.

[31] G. Kastratovića, M. Aldarwishb, A. Grbovićb and N. Vidanovića, “Stress intensity factor for multiple cracks on curved panels,” *Procedial Structural Integrity*, no.13, pp. 469-474, 2018.

[32] H. Dirik and T, Yalçinkaya, “Fatigue Crack Growth Under Variable Amplitude Loading Through XFEM,” *Procedial Structural Integrity*, no.2, pp. 3073-3080, 2016.

[33] A. Skorupa and M. Skorupa, *Riveted Lap Joints in Aircraft Fuselage: Design, Analysis and Properties*. Dordrecht, Heidelberg, New York, London: Springe, 2012.

[34] M. Skorupa, T. Machniewicz, A. Skorupa, and A. Korbel, “Fatigue strength reduction factors at rivet holes for aircraft fuselage lap joints,” *Int. J. Fatigue*, no. 80, pp. 417–425, 2015.

[35] D. Broek, *Elementary engineering fracture mechanics*. Kluwer, 1982.

[36] J. H. Crews and N. H. White, “Fatigue crack growth from a circular hole with and without high prior loading,” *NASA (Langley Res. Center)*, no. September 1972, 1972.

[37] F. A. Schijve, J.; and Jacobs, “Fatigue Crack Propagation in Unnotched and Notched Aluminum Alloy Specimens,” *Nat. Aero-Astronaut. Res. Inst*, 1964.

[38] P. C. P. and G. R. I. Hiroshi Tada, *Stress Analysis of Cracks Handbook Third Edition*, 3rd ed. ASME Press.

[39] J. C. Newman and I. S. Raju, “Stress Intensity Factor Equations For Cracks in Three-Dimensional Finite Bodies Subjected to Tension and Bending Loads,” 1984.

[40] M. Forman, R, G.;Kearney, V, E. And Eagle, R, “Numerical Analysis of Crack Propagation in Cyclic-Loaded Structures,” *Trans. ASME, Ser. D J. Basic Eng.*, vol. 89, no. 3, 1967.

[41] James A. HARTER, “AFGROW users guide and technical manual.” *Air Vehicles Directorate; Airforce Research Laboratory*, 1999.

[42] American Society for Testing and Materials., *1996 Annual book of ASTM standards. section 3 : Metals test methods and analytical procedures.* American Society for Testing and Materials, 1996.

[43] J. E. S. William F. Brown, *Plane Strain Crack Toughness Testing of High Strength Metallic Materials*. Philadelphia: ASTM, 1966.

[44] T. Belytschko and T. Black, "Elastic Crack Growth in Finite Elements with Minimal Remeshing," *Int. J. Numer. Methods Eng.*, no. 45, pp. 601–620, 1999.

[45] J. Melenk and I. Babuska, "The Partition of Unity Finite Element Method: Basic Theory and Applications.," *Comput. Methods Appl. Mech. Eng.*, no. 39, pp. 289–314, 1996.

[46] J. J. C. R. de B. Remmers and A. Needleman, "The Simulation of Dynamic Crack Propagation using the Cohesive Segments Method.," *J. Mech. Phys. Solids*, no. 56, pp. 70–92, 2008.

[47] P. M. Song, J. H., A. Areias, and T. Belytschko, "A Method for Dynamic Crack and Shear Band Propagation with Phantom Nodes.," *Int. J. Numer. Methods Eng.*, no. 67, pp. 868–893, 2006.

[48] Q. Duan, J.-H. Song, T. Menouillard, and T. Belytschko, "Element-local Level Set Method for Three-Dimensional Dynamic Crack Growth," *Int. J. Numer. Methods Eng.*, no. 80, pp. 1520–1543, 2009.

[49] J. Mergheim, E. Kuhl, and P. Steinmann, "A Finite Element Method for the Computational Modeling of Cohesive Cracks," *Int. J. Numer. Methods Eng.*, no. 63, pp. 276–289, 2005.

[50] A. Hansbo and P. Hansbo, "A Finite Element Method for the Simulation of Strong and Weak discontinuities in Elasticity," *Comput. Methods Appl. Mech. Eng.*, no. 191, pp. 3523–3540, 2004.

[51] S. Osher and J. A. Sethian, "Fronts Propagating with Curvature-Dependent Speed: Algorithms based on Hamilton-Jacobi formulations," *J. Comput. Phys.*, no. 79, pp. 12–49, 1988.

[52] M. Stolarska, N. M. DL Chopp, and T. Belytschko, "Modeling Crack Growth by Level Sets in the Extended Finite Element Method," *Int. J. Numer. Methods Eng.*, no. 51, pp. 943–960, 2001.

[53] G. P. Cherepanov, "The propagation of cracks in a continuous medium," *J. Appl. Math. Mech.*, no. 31, pp. 503–512, 1967.

[54] J. R. Rice, "A Path Independent Integral and the Approximate Analysis of Strain Concentration by Notches and Cracks," *J. Appl. Mech.*, no. 35, pp. 379–386, 1968.

[55] R. F. Lee and J. A. Donovan, "J-integral and crack opening displacement as crack initiation criteria in natural rubber in pure shear and tensile specimens," *Rubber Chem. Technol.*, no. 60, pp. 674–688, 1987.

[56] M. Yoda, “The J-integral fracture toughness for Mode II,” *Int. J. Fract.*, no. 16, pp. 175–178, 1980.

[57] C. F. Shih, B. Moran, and T. Nakamura, “Energy Release Rate Along a Three-Dimensional Crack Front in a Thermally Stressed Body,” *Int. J. Fract.*, no. 30(2), pp. 79–102, 1986.

[58] R. H. Myers, D. C. Montgomery, and C. M. Anderson.Cook, *Response Surface Methodology*, Third, 3rd. New Jersey: John Wiley & Sons, Inc., 2009.

[59] A. Skorupa and M. Skorupa, *Riveted Lap Joints in Aircraft Fuselage: Design, Analysis and Properties*. Springer, 2012.

[60] M. Skorupa, T. Machniewicz, A. Skorupa, and A. Korbel, “Fatigue strength reduction factors at rivet holes for aircraft fuselage lap joints,” *Int. J. Fatigue*, no. 80, pp. 417–425, 2015.

[61] Acceptable methods, techniques, and practices-aircraft inspection and repair. Federal Aviation Administration, 1998.

[62] “MINITAB Statistical Software.” .

APPENDICES

A. Forman Constants Calculation Example

Forman model for crack growth is shown below:

$$\frac{da}{dN} = \frac{C\Delta K^m}{((1-R)K_c - \Delta K)} \qquad (A1)$$

In order to calculate Forman constants C and m from experimental test data Forman model by assuming load ratio (R=0) can be rewritten as:

$$\frac{da}{dN}(K_c - \Delta K) = C\Delta K^m \qquad (A2)$$

$$Log(\frac{da}{dN}(K_c - \Delta K)) = Log(C\Delta K^m) \qquad (A3)$$

$$Log\left(\frac{da}{dN}(K_c - \Delta K)\right) = Log(C) + m\ Log(\Delta K) \qquad (A4)$$

Firstly, $\frac{da}{dN}(K_c - \Delta K)$ term from equation A2 is evaluated and then it is plotted versus ΔK. Finally, the linear equation of the plot is assessed in excel. As can be seen from equation A4, the line equation of the plot can be related to C and m using inverse Log function.

B. Comparison of the results by applying different Boundary Conditions in the XFEM model

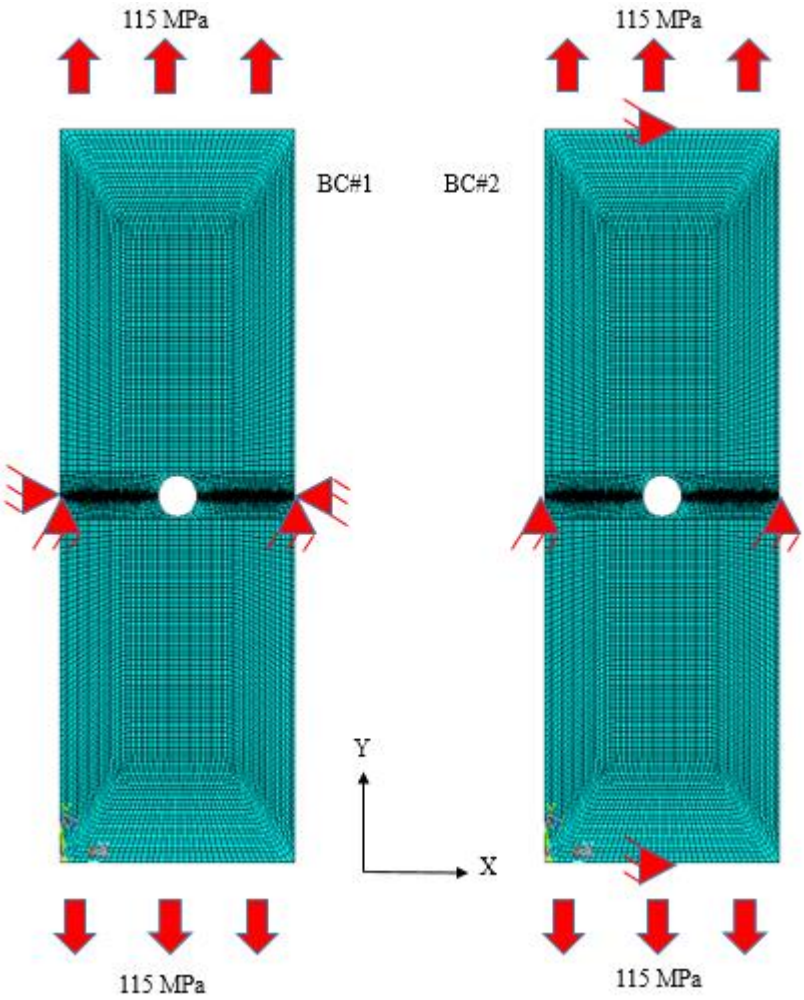

Figure B1. Applied boundary conditions

As discussed earlier in chapter 6, two different boundary conditions are assumed to model the geometry in the XFEM solution. Figure B1, represents the boundary conditions. For different crack lengths the calculated stress intensity factor for each boundary condition is compared with the Bowie's solution in Figure B2. From Figure B.2, for short crack lengths (shorter than 5 mm) there exists significant

variation from Bowie solution. Beyond the crack length of 5 mm, variation vanishes and a fixed difference exists through the end of the crack growth. Figure B3 shows a good correlation of the BC#2 results with analytical calculations and BC#1 differs a constant amount of 5% from analytical solution.

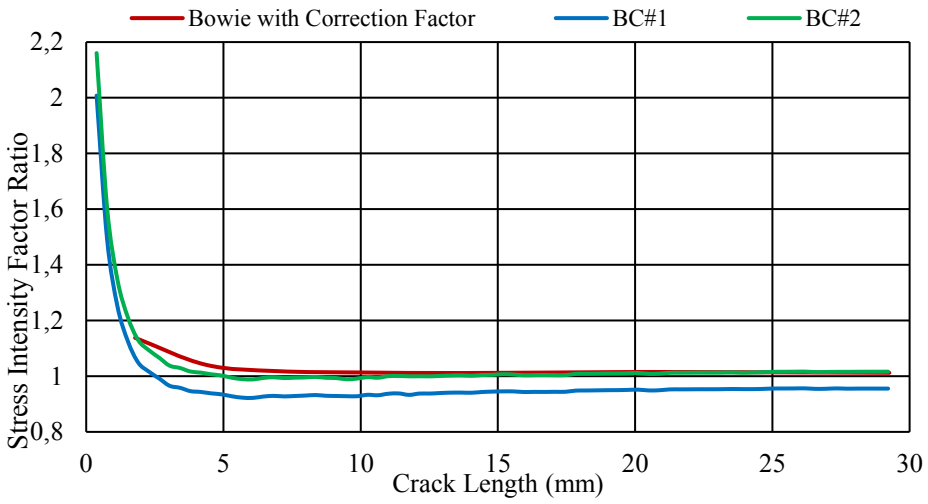

Figure B2. Comparison of SIFs for each boundary condition with the Bowie's solution

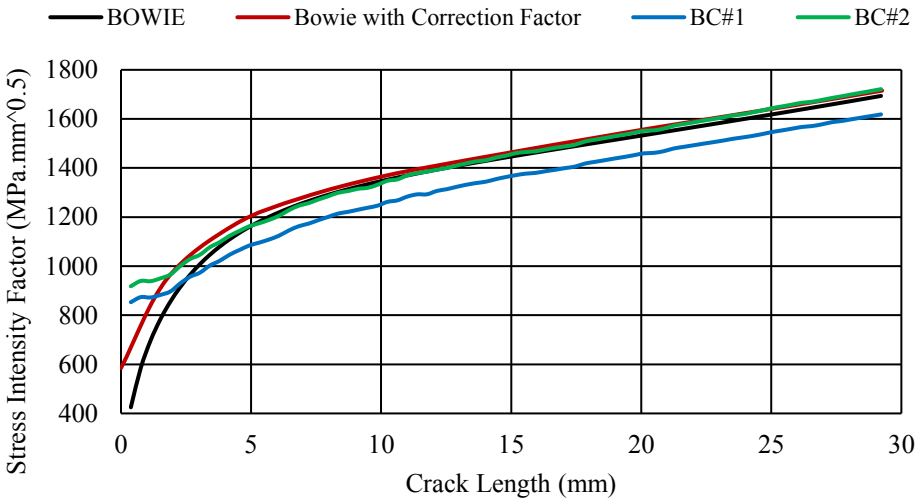

Figure B3. Comparison of SIFs for each boundary condition with Bowie solution

In Figure B4, colored stress intensity factor contours for both boundary conditions is depicted. As can be seen, in BC#2 affected zone is larger than BC#1. Also, stress intensity factor magnitude at the same region of the same crack length is greater than of BC#1.

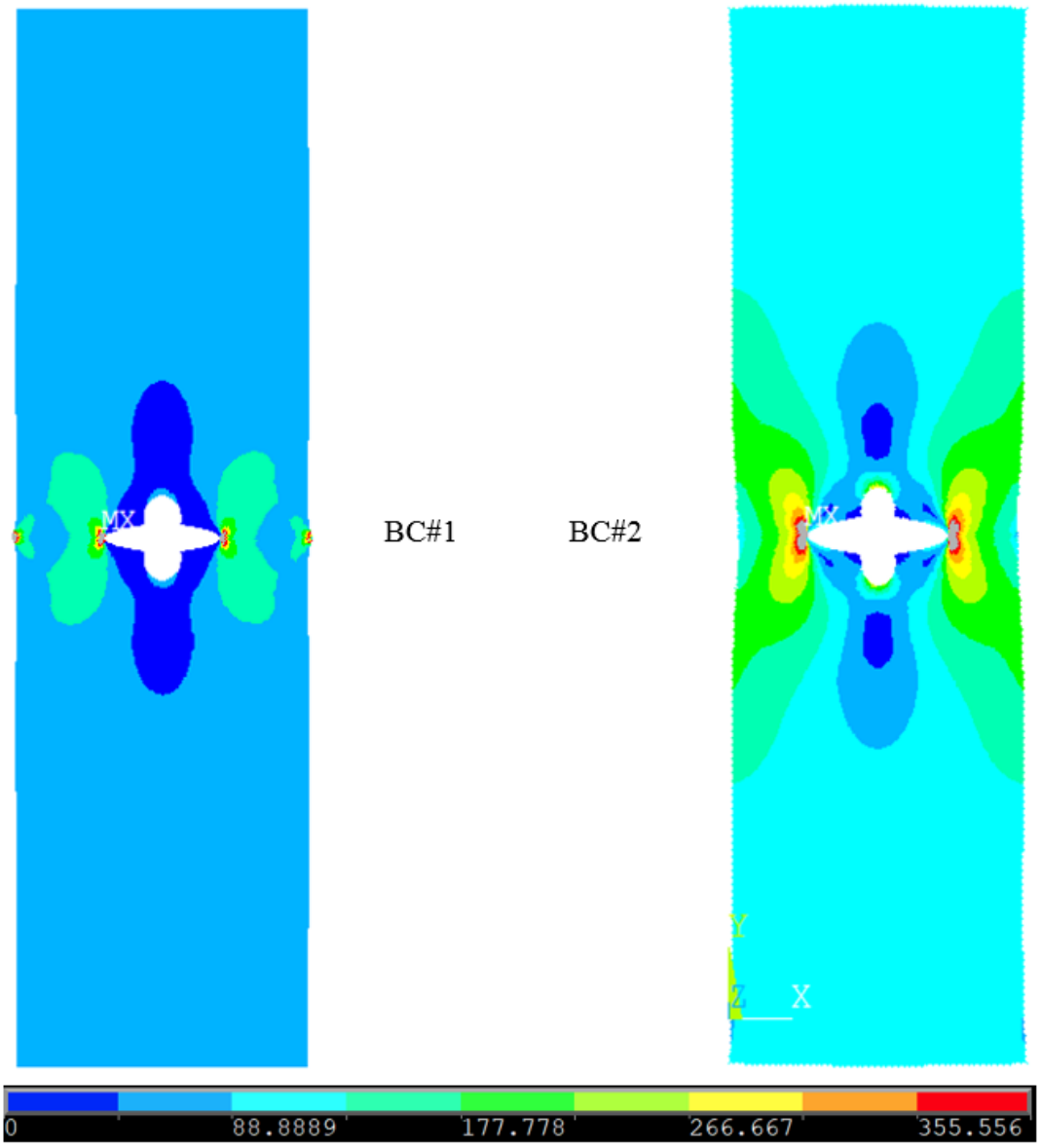

Figure B4. Stress intensity factor colored map for BC#1 and BC#2 at the crack length of 30 mm

The Y- component of the stress (σ_y) is also compared for both boundary conditions BC1 and BC2. Figure B5, Figure B6 and Figure B7 shown below, give the Y-component of the stress at different crack lengths (6.18mm, 19mm and 30mm) for both boundary conditions. To clearly see and compare the effect of the boundary conditions on the stress distribution, the same range is used for the color scale in Figures B5-B7. It is clearly seen that BC1 affects the Y- component of the stress along the crack front more than BC2 for the three crack lengths considered. Hence, it can be concluded that for the finite width specimen, BC1 can not simulate the infinite width plate and the width of the specimen is not wide enough to consider it as infinite width plate. Hence, BC2 which is actually the correct boundary condition is used in the rest of the study in this thesis.

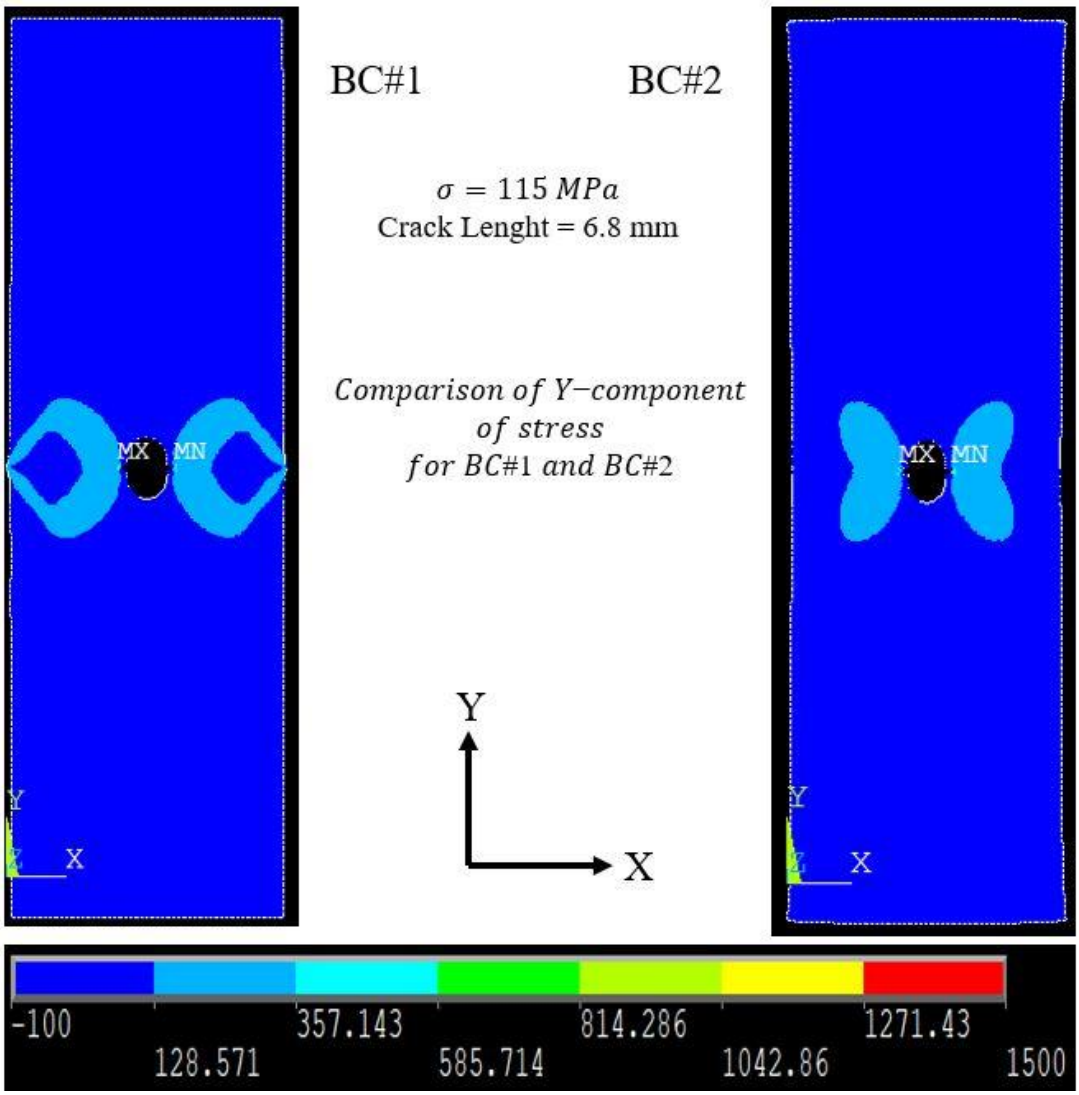

Figure B5. Comparison of Y-component stress at the crack length of 6.18 mm for different boundary conditions

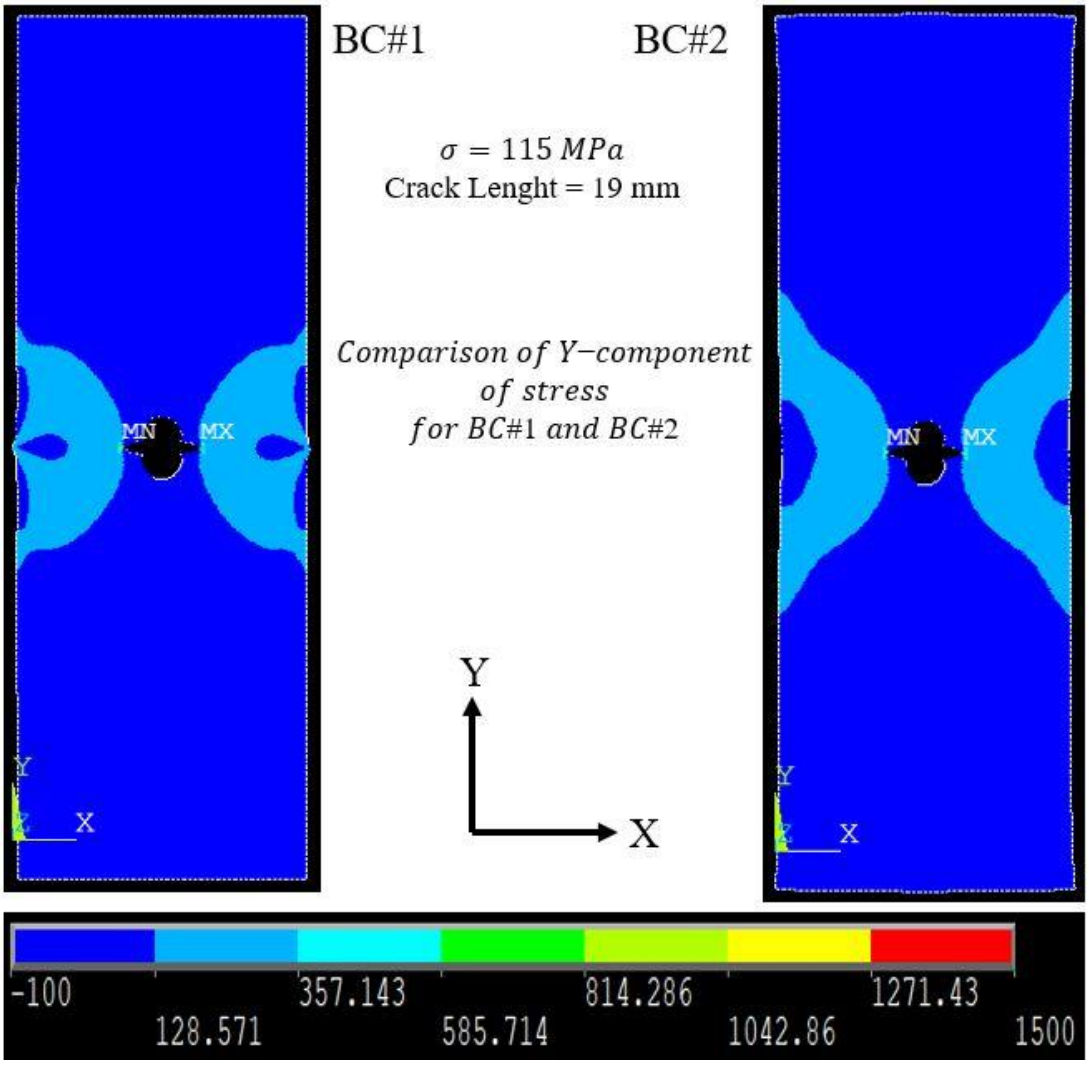

Figure B6. Comparison of Y-component stress at the crack length of 19 mm for different boundary conditions

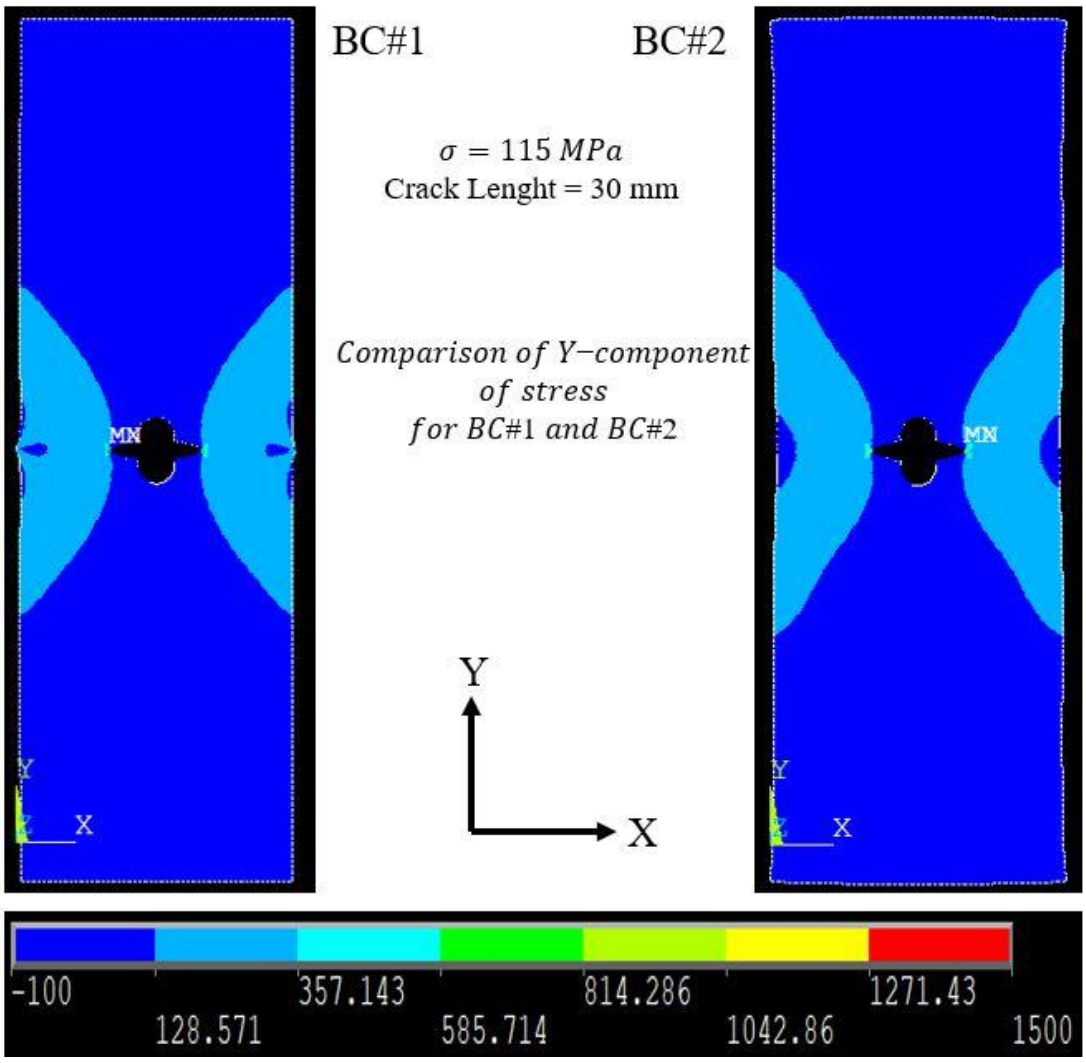

Figure B7. Comparison of Y-component stress at the crack length of 30 mm for different boundary conditions

C. MATLAB Fatigue Life Cycle Counter Code

A code developed in MATLAB to calculate fatigue life according to Forman model. In this code the extracted ΔK versus Δa data from XFEM results is read from directory and form the *dk* and da matrices respectively. Forman model constants *C* and *m* obtained in chapter two are identified as constants in the program at the beginning. Then, amount of crack growth is calculated by subtracting two consecutive crack lengths. Amount of crack growth for each ΔK is then put into *da* matrix. Afterward, using Equation C1, the left hand side of the equation is calculated and form the *delta* matrix.

$$\frac{da}{dN}(K_c - \Delta K) = C\Delta K^m \qquad (C1)$$

Finally, for each crack growth iteration Equation C2 is calculated

$$da(K_c - \Delta K) = dN * C\Delta K^m \qquad (C2)$$

By interchanging terms of Equation C3, dN for each crack growth interval is obtained and stored in L4 matrix. Eventually, by summing up all entries of L4 matrix, the total cycles of fatigue life (30 mm) is obtained.

$$dN = da(K_c - \Delta K)/C\Delta K^m \qquad (C3)$$

MATLAB code for the calculation of the fatigue life using XFEM analysis results is given below.

```
clear
clc
filename = 'rst.txt';
format LONG
A = importdata(filename);
C=3.838e-10;
m=3.94;
kc=110;
[r,con]=size(A);
L=0;
for f=2:r
    da(1,1)=A(1,1);
    da(f,1)=A(f,1)-A(f-1,1);
    dk(1,1)=A(1,2);
    dk(f,1)=A(f,2);
    delta(1,1)=(kc-dk(1,1));
    delta(f,1)=(kc-dk(f,1));
    L1(1,1)=da(1,1).*(kc-dk(1,1));
    L1(f,1)=da(f,1).*(kc-dk(f,1));
    L2(1,1)=dk(1,1).^m;
    L2(f,1)=dk(f,1).^m;
    L3(1,1)=C.*(abs(L2(1,1)));
    L3(f,1)=C.*(abs(L2(f,1)));
    L4(1,1)=L1(1,1)./L3(1,1);
    L4(f,1)=L1(f,1)./L3(f,1);
end
L=sum(L4,1)
```

D. Developed Fatigue Crack Growth Code for DTC problem in APDL

Developed code in ANSYS MECHANICAL of XFEM analysis for Double Through the Thickness Problem.

```
finish
/clear
/prep7


! Material model
E=73100                  !--- YOUNG MODULUS
NU=0.33                  !--- POISSON'S RATIO
RO=1.0                   !--- DENSITY
PRES=-115           !CAL
!********
et,1,182
!********mat prop
mp,ex,1,E
mp,prxy,1,NU
mp,dens,1,RO
!********Fatigue crack growth Law Specification
tb, cgcr, 2, , ,

!*******keypoints
k,1, 0    ,    0
k,2, 302  ,    0
k,3, 302  ,    415
```

```
k,4, 0    ,    415
k,5, 302  ,    444.81
k,6, 0    ,    444.81
k,7, 302  ,    445.19
k,8, 0    ,    445.19
k,9, 302  ,    475
k,10,     0    ,    475
k,11,     302  ,    890
k,12,     0    ,    890
!********areas
a,   1,2,3,4
a,   4,3,5,6
a,   6,5,7,8
a,   8,7,9,10
a,   10,9,11,12
cyl4,151,445,25.4   ! Area #6
asba,all,6
NUMCMP,area
NUMCMP,line
LCOMB, 21, 22, 0
LCOMB, 17, 18, 0
!********meshing
lsel,s,line,,17,21,4
LESIZE,all, , ,1, , , , ,1
type,1
mat,1
MSHMID, 2
esize,0.38
```

```
amesh,3,4
esize,2
amesh,5,6
esize,6
amesh,1,2
!Element component required for XFENRICH command
esel, s, cent, y, 415,475
esel, r, cent, x, 0,302
cm, testcmp, elem
allsel
!
! define enrichment identification
!
xfenrich, ENRICH1, testcmp, , SING,1.52,0.0001
allsel
/com
*************************************************************
*****
/com
/com                    INITIAL CRACK DATA
/com
/com
*************************************************************
*****
YC1 =445
XC1 =177.158206041
YC2 =445
XC2 = 124.841793959
esel, s, cent, x,   176.4 , XC1
esel, r, cent, y, YC1-0.0001, YC1+0.0001
```

```
cm, cenelem, elem
nelem = 10000
iel = 0
Phi = 0.0
Psi = 0.0
*do, i, 1, nelem, 1
 iel = elnext(iel)
 *if, iel, ne, 0, then
  *do, j, 1, 4, 1
    nd = nelem(iel,j)
    Phi = ny(nd) - YC1
    Psi = nx(nd) - XC1
    xfdata, ENRICH1, LSM, iel, nd, Phi, Psi
  *enddo
 *endif
*enddo
ALLSEL,ALL
esel, s, cent, x,   XC2  , 125.6
esel, r, cent, y, YC2-0.0001, YC2+0.0001
cm, cenelem, elem
nelem = 10000
iel = 0
Phi = 0.0
Psi = 0.0
*do, i, 1, nelem, 1
 iel = elnext(iel)
 *if, iel, ne, 0, then
  *do, j, 1, 4, 1
```

```
    nd = nelem(iel,j)
    Phi = ny(nd) - YC2
    Psi = nx(nd) - XC2
    xfdata, ENRICH1, LSM, iel, nd, Phi, Psi
  *enddo
 *endif
*enddo
xflist
ALLSEL,ALL
! Crack-tip element
esel,s,elem,,2
cm, crktipelem1, elem        ! Element set component for
CINT command
allsel,all
esel,s,elem,,333
cm, crktipelem2, elem        ! Element set component for
CINT command
allsel,all
! Loading
nsel,s,loc, Y, 890
sf, all, pres, PRES
allsel
nsel,s,loc, Y, 0
sf, all, pres, PRES
allsel
! B.C
nsel,s,loc, Y, 445.19
nsel,r,loc, x, 302
d, all, uy,0.0
```

```
d, all, uX,0.0
allsel
nsel,s,loc, Y, 445.19
nsel,r,loc, x, 0
d, all, uy,0.0
d, all, uX,0.0
allsel
finish
/solu
antype,0
time, 1.0
deltim, 0.01, 0.01, 0.01
outres,all, all
! CINT calculations
CINT, NEW, 1
CINT, TYPE, SIFS
CINT, CXFE, crktipelem1
CINT, NCON, 9
CINT, NORM, 0, 1
CINT, NEW, 2
CINT, TYPE, SIFS
CINT, CXFE, crktipelem2
CINT, NCON, 9
CINT, NORM, 0, 1
!CINT, PLOT, 1, 1
! CGROW calculations
cgrow, new, 1
cgrow, cid, 1
```

```
cgrow, method, xfem
cgrow, fcoption, mtab, 2
CGROW, STOP, CEMX, 45                    !CRK CONTROL
! Fatigue-related data
CGROW, FCG, METH, LC                     !life-cycle
method
CGROW, FCG, SRAT,0                       ! stress-ratio-R
cgrow, new, 2
cgrow, cid, 2
cgrow, method, xfem
cgrow, fcoption, mtab, 2
CGROW, STOP, CEMX, 45                    !CRK CONTROL
! Fatigue-related data
CGROW, FCG, METH, LC                     !life-cycle
method
CGROW, FCG, SRAT,0                       ! stress-ratio-R
kbc, 1  ! loads are stepped for fatigue analysis
solve
finish
/post1
! Get the # of data sets on the results file
set,last,last
*get, ndatasets, active, 0, set, nset
! Define table if *VPLOT is used
*DIM,DN,table,ndatasets,2
*DIM,DA,table,ndatasets,2
*DIM,DK,table,ndatasets,2
*DIM,KI1,table,ndatasets,2
*DIM,KI2,table,ndatasets,2
```

```
*DIM,KI3,table,ndatasets,2
*DIM,KI4,table,ndatasets,2
*DIM,KI5,table,ndatasets,2
*DIM,KI6,table,ndatasets,2
*DIM,KI7,table,ndatasets,2
*DIM,KI8,table,ndatasets,2
*DIM,KI9,table,ndatasets,2
*DIM,KI10,table,ndatasets,2
*DIM,DNL,table,ndatasets,2
*DIM,DAL,table,ndatasets,2
*DIM,DKL,table,ndatasets,2
*DIM,KI1L,table,ndatasets,2
*DIM,KI2L,table,ndatasets,2
*DIM,KI3L,table,ndatasets,2
*DIM,KI4L,table,ndatasets,2
*DIM,KI5L,table,ndatasets,2
*DIM,KI6L,table,ndatasets,2
*DIM,KI7L,table,ndatasets,2
*DIM,KI8L,table,ndatasets,2
*DIM,KI9L,table,ndatasets,2
*DIM,KI10L,table,ndatasets,2
! Loop on data sets and store results
*do,i,1,ndatasets
 set, , , , , , , i ! read the data set
 *GET,NODEID_RIGHT,CINT,1,NODE,1
 *get,                                                  pval,
CINT,1,CTIP,NODEID_RIGHT,CONTOUR,1,DTYPE,totn
 *VFILL,DN(i,1),DATA,pval
```

```
 *get,                                                  pval,
CINT,1,CTIP,NODEID_RIGHT,CONTOUR,1,DTYPE,tota

 *VFILL,DA(i,1),DATA,pval

 *get,                                                  pval,
CINT,1,CTIP,NODEID_RIGHT,CONTOUR,1,DTYPE,dltk

 *VFILL,DK(i,1),DATA,pval

 *GET,NODEID_L,CINT,2,NODE,1

 *get, pval, CINT,2,CTIP,NODEID_L,CONTOUR,1,DTYPE,totn

 *VFILL,DNL(i,1),DATA,pval

 *get,                                                  pval,
CINT,2,CTIP,NODEID_RIGHT,CONTOUR,1,DTYPE,tota

 *VFILL,DAL(i,1),DATA,pval

 *get,                                                  pval,
CINT,2,CTIP,NODEID_RIGHT,CONTOUR,1,DTYPE,dltk

 *VFILL,DKL(i,1),DATA,pval

 *GET,   resultVal1,   CINT,   1,   CTIP,   NODEID_RIGHT,
CONTOUR,1 ,DTYPE, k1

 *VFILL,KI1(i,1),DATA,resultVal1

 *GET,   resultVal2,   CINT,   1,   CTIP,   NODEID_RIGHT,
CONTOUR,2 ,DTYPE, k1

 *VFILL,KI2(i,1),DATA,resultVal2

 *GET,   resultVal3,   CINT,   1,   CTIP,   NODEID_RIGHT,
CONTOUR,3 ,DTYPE, k1

 *VFILL,KI3(i,1),DATA,resultVal3

 *GET,   resultVal4,   CINT,   1,   CTIP,   NODEID_RIGHT,
CONTOUR,4 ,DTYPE, k1

 *VFILL,KI4(i,1),DATA,resultVal4

 *GET,   resultVal5,   CINT,   1,   CTIP,   NODEID_RIGHT,
CONTOUR,5 ,DTYPE, k1

 *VFILL,KI5(i,1),DATA,resultVal5
```

```
 *GET,   resultVal6,   CINT,   1,   CTIP,   NODEID_RIGHT,
CONTOUR,6 ,DTYPE, k1

 *VFILL,KI6(i,1),DATA,resultVal6

 *GET,   resultVal7,   CINT,   1,   CTIP,   NODEID_RIGHT,
CONTOUR,7 ,DTYPE, k1

 *VFILL,KI7(i,1),DATA,resultVal7

 *GET,   resultVal8,   CINT,   1,   CTIP,   NODEID_RIGHT,
CONTOUR,8 ,DTYPE, k1

 *VFILL,KI8(i,1),DATA,resultVal8

 *GET,   resultVal9,   CINT,   1,   CTIP,   NODEID_RIGHT,
CONTOUR,9 ,DTYPE, k1

 *VFILL,KI9(i,1),DATA,resultVal9

 *GET,   resultVal10,   CINT,   1,   CTIP,   NODEID_RIGHT,
CONTOUR,10 ,DTYPE, k1

 *VFILL,KI10(i,1),DATA,resultVal10

 *GET, resultVal1L, CINT, 2, CTIP, NODEID_L, CONTOUR,1
,DTYPE, k1

 *VFILL,KI1L(i,1),DATA,resultVal1L

 *GET, resultVal2L, CINT, 2, CTIP, NODEID_L, CONTOUR,2
,DTYPE, k1

 *VFILL,KI2L(i,1),DATA,resultVal2L

 *GET, resultVal3L, CINT, 2, CTIP, NODEID_L, CONTOUR,3
,DTYPE, k1

 *VFILL,KI3L(i,1),DATA,resultVal3L

 *GET, resultVal4L, CINT, 2, CTIP, NODEID_L, CONTOUR,4
,DTYPE, k1

 *VFILL,KI4L(i,1),DATA,resultVal4L

 *GET, resultVal5L, CINT, 2, CTIP, NODEID_L, CONTOUR,5
,DTYPE, k1

 *VFILL,KI5L(i,1),DATA,resultVal5L

 *GET, resultVal6L, CINT, 2, CTIP, NODEID_L, CONTOUR,6
,DTYPE, k1

 *VFILL,KI6L(i,1),DATA,resultVal6L
```

```
 *GET, resultVal7L, CINT, 2, CTIP, NODEID_L, CONTOUR,7
,DTYPE, k1

 *VFILL,KI7L(i,1),DATA,resultVal7L

 *GET, resultVal8L, CINT, 2, CTIP, NODEID_L, CONTOUR,8
,DTYPE, k1

 *VFILL,KI8L(i,1),DATA,resultVal8L

 *GET, resultVal9L, CINT, 2, CTIP, NODEID_L, CONTOUR,9
,DTYPE, k1

 *VFILL,KI9L(i,1),DATA,resultVal9L

*enddo

*cfopen,CRKDATA-0.38.txt

*vwrite, 'DN: ',DN(1,1),'     DA: ',DA(1,1), '    DK:
',DK(1,1)

(A6,f12.3,' ',A6,f12.3,' ',A6,f12.3)     !(fortan format
- integer with three decimal places)

*cfclos

*cfopen,CRKDATA-0.38L.txt

*vwrite, 'DN: ',DNL(1,1),'    DA: ',DAL(1,1), '   DK:
',DKL(1,1)

(A6,f12.3,' ',A6,f12.3,' ',A6,f12.3)     !(fortan format
- integer with three decimal places)

*cfclos

*cfopen,SIF-0.38.txt

*vwrite,                 'KI1:',KI1(1,1),'KI2:',KI2(1,1),
'KI3:',KI3(1,1),'KI4:',KI4(1,1),         'KI5:',KI5(1,1),
'KI6:',KI6(1,1),     'KI7:',KI7(1,1),     'KI8:',KI8(1,1),
'KI9:',KI9(1,1), 'KI10:',KI10(1,1)

(A12,f8.1,A12,f8.1,A12,f8.1,A12,f8.1,A12,f8.1,A12,f8.1,A
12,f8.1,A12,f8.1,A12,f8.1,A12,f8.1)

!(fortan format - integer with three decimal places)

*cfclos

*cfopen,SIF-0.38L.txt

*vwrite,
```

```
'KI1:',KI1L(1,1),'KI2:',KI2L(1,1),
'KI3:',KI3L(1,1),'KI4:',KI4L(1,1),

'KI5:',KI5L(1,1), 'KI6:',KI6L(1,1),

'KI7:',KI7L(1,1), 'KI8:',KI8L(1,1), 'KI9:',KI9L(1,1)

(A12,f8.1,A12,f8.1,A12,f8.1,A12,f8.1,A12,f8.1,A12,f8.1,A
12,f8.1,A12,f8.1,A12,f8.1)     !(Fortran format - integer
with three decimal places)

*cfclos

Finish
```